

Elsevier Editorial System(tm) for Journal of Wind Engineering & Industrial
Aerodynamics
Manuscript Draft

Manuscript Number: INDAER-D-14-00133R2

Title: BRIDGE DECK FLUTTER DERIVATIVES: EFFICIENT NUMERICAL EVALUATION EXPLOITING
THEIR INTERDEPENDENCE.

Article Type: Full Length Article

Keywords: Computational fluid dynamics; bluff body aerodynamics; flutter derivatives; rectangular
cylinder; streamlined deck sections.

Corresponding Author: Dr. Felix Nieto, Ph.D.

Corresponding Author's Institution: University of La Corunna

First Author: Felix Nieto, Ph.D.

Order of Authors: Felix Nieto, Ph.D.; John S Owen, Ph.D.; David M Hargreaves, Ph.D.; Santiago
Hernández, Ph.D.

Highlights:

- An efficient CFD approach for the computation of flutter derivatives is presented.
- Relationships between flutter derivatives allow halving the number of simulations.
- Successfully applied at a ratio 4.9:1 rectangular cylinder and the G1 box section.
- Great potential in industrial applications and shape optimal design problems.

BRIDGE DECK FLUTTER DERIVATIVES: EFFICIENT NUMERICAL EVALUATION EXPLOITING THEIR INTERDEPENDENCE.

F. Nieto^a, J.S. Owen^b, D.M. Hargreaves^b & S. Hernández^a

^a School of Civil Engineering, University of A Coruña, Spain

^b Faculty of Engineering, University of Nottingham, UK

ABSTRACT

Increasing the efficiency in the process to numerically compute the flutter derivatives of bridge deck sections is desirable to advance the application of CFD based aerodynamic design in industrial projects. In this paper, a 2D unsteady Reynolds-averaged Navier-Stokes (URANS) approach adopting Menter's SST $k-\omega$ turbulence model is employed for computing the flutter derivatives and the static aerodynamic characteristics of two well known examples: a rectangular cylinder showing a completely reattached flow and the generic G1 section representative of streamlined deck sections. The analytical relationships between flutter derivatives reported in the literature are applied with the purpose of halving the number of required numerical simulations for computing the flutter derivatives. The solver of choice has been the open source code OpenFOAM. It has been found that the proposed methodology offers results which agree well with the experimental data and the accuracy of the estimated flutter derivatives is similar to the results reported in the literature where the complete set of numerical simulations has been performed for both heave and pitch degrees of freedom.

KEYWORDS: Computational fluid dynamics, bluff body aerodynamics, flutter derivatives, rectangular cylinder, streamlined deck sections.

1. INTRODUCTION

Long span bridges are prone to aeroelastic phenomena such as vortex induced vibrations, flutter or buffeting. In fact, safety against flutter instability is one of the fundamental requirements in long span bridge design. If the wind speed exceeds the critical flutter speed of the structure, self-excited oscillations of the deck would rapidly amplify causing the collapse of the bridge.

The most widely used method for the identification of the flutter critical wind speed is Scanlan's approach, developed in the 1970s (Scanlan and Tomko, 1971), where a set of semi-empirical functions, named flutter derivatives, must be identified in order to define the motion-induced aerodynamic load acting on the bridge deck (Bartoli and Mannini, 2008). Traditionally, the identification of flutter derivatives has been conducted by means of wind tunnel tests of sectional models of bridge decks. The application in recent years of numerical methods in the identification of flutter derivatives aims at avoiding expensive and cumbersome experimental campaigns which are the standard approach in industrial applications currently.

In Computational Fluid Dynamics (CFD) modeling the flutter derivatives identification can be done following two different approaches (Fransos and Bruno, 2006). The first one requires the simulation of the forced harmonic oscillations in pitch and heave degrees of freedom. Then, the flutter derivatives are identified from the amplitude and phase relationships between the imposed displacement and the induced aeroelastic forces. The second method, based on indicial theory,

43 requires simulating an abrupt displacement of the body immersed in the flow, which causes non-
44 stationary forces. The flutter derivatives can then be computed from the ratio between the Fourier
45 transforms of the step-response non-stationary forces and the prescribed step-input displacement.
46 The methodology, based on the simulation of forced oscillations, has been, by far, more widely
47 used than the one based on the indicial approach despite the apparent efficiency of the indicial
48 function approach.

49 Focusing on applications of the harmonic forced oscillations approach, the trend in the 1990's and
50 early 2000's has been developing in-house CFD solvers based on the finite-difference, finite
51 element, finite volume or discrete vortex methods. The references in the literature are numerous
52 and some examples, without intending to be exhaustive are: Mendes and Branco (1998), Larsen
53 and Walther (1998), Morgenthal and McRobie (2002), Xiang and Ge (2002), Vairo (2003), Jeong
54 and Kwon (2003), Frandsen (2004), Zhu et al. (2007) and Zhu et al. (2009). Developing in-house
55 software has obviously been a barrier for the application of numerical methods in industrial bridge
56 design problems due to its scientific complexity and the required labor and financial resources.
57 Therefore more recently the focus has been put on applying general purpose commercial finite
58 volume solvers in bridge aerodynamics problems. An early application was authored by Bruno et
59 al. (2001) who used FLUENT for studying the aerodynamic response of a static box deck and the
60 effect of section details such as fairings and barriers. Fluid-structure interaction problems have
61 been addressed more recently. In Ge and Xiang (2008) both in-house solvers and the commercial
62 code FLUENT are applied, depending on the chosen approach for turbulence modeling. Sarwar et
63 al. (2008) obtained the flutter derivatives of a bridge deck section and high aspect ratio rectangular
64 cylinders by means of 3D Large Eddy Simulation (LES) using FLUENT. Huang et al. (2009) also
65 used FLUENT to compute the flutter derivatives of the Great Belt Bridge and the Sutong Yangtze
66 cable-stayed bridge. Starossek et al. (2009) employed the commercial software COMET to obtain
67 the flutter derivatives of 31 different bridge sections, including experimental validation for a subset
68 of 9 sections tested in a water tunnel. Bai et al. (2010) used a combination of in-house code and
69 ANSYS-CFX commercial software for computing force coefficients and flutter derivatives of
70 various 3D deck sections. Huang and Liao (2011) used FLUENT to simulate forced oscillations of
71 a flat plate and a bridge deck containing a linear combination of a set of frequencies. Also, Brusiani
72 et al. (2013) employed FLUENT to compute the flutter derivatives of the Great Belt Bridge using a
73 different turbulence model than Huang and co-workers. Of particular interest is the growing use of
74 open source general CFD solvers. In Sarkic et al. (2012), the open source code OpenFOAM is
75 applied to numerically replicate the wind tunnel test for identifying the force coefficients and flutter
76 derivatives of a box deck cross-section. A more recent application by some of the authors of the
77 former reference can be found in Sarkic and Höffer (2013) where the LES turbulence model is
78 applied to the same box deck.

79 CFD applications based on indicial functions are scarce in spite of its potential. In Bruno and
80 Fransos (2008) it has been remarked that in this method just a single simulation for each degree of
81 freedom is required to identify the complete set of flutter derivatives and that only the transient
82 flow needs to be simulated. Thus, this approach is less demanding in computational resources than
83 the classical forced oscillation based method. On the other hand, the problem is particularly
84 challenging from the CFD simulation perspective. Early applications are Lesieutre et al. (1994)
85 who simulated the motion of a wing in the frame of an application to aircraft manoeuvres and Brar
86 et al. (1996) who applied the Finite Element Method to obtain the flutter derivatives of an airfoil
87 and a rectangular cylinder. A modified smoothed indicial approach was further developed in
88 Fransos and Bruno (2006) and Bruno and Fransos (2008) who used FLUENT to obtain the flutter

89 derivatives of a flat plate of finite thickness and studied also the effect of the Reynolds number on
1 90 the flutter derivatives. The indicial approach has also been applied in the frame of a probabilistic
2 91 study of the aerodynamic and aeroelastic responses of a flat plate (Bruno et al, 2009). More
3 92 recently Zhu and Gu (2014) have presented a method to extract the flutter derivatives of
4 93 streamlined bridge decks, even if the application of the modified indicial approach to bluff bodies
5 94 remains questionable.
6
7
8 95 From the previous review of the state of the art regarding applications of CFD in the design of long
9 96 span bridges, the main reasons why numerical simulations are not being generally applied in bridge
10 97 design in the industry to complement wind tunnel tests need to be discussed. Developing and
11 98 upgrading in-house software is a complex task and requires highly skilled personnel and substantial
12 99 funding. Consequently it can only be achieved by a small number of organizations in the world.
13
14 100 The increasing use of commercial software in recent years is making it easier to access the required
15 101 technology. However, the cost of licenses, particularly for running massively parallel simulations,
16 102 in many cases prevents the extensive use of CFD in design problems. This circumstance has made
17 103 particularly appealing the use of open source solvers for both industry and academia, and open
18 104 source software has already been applied in bridge design problems. Besides this, the increasing
19 105 number of published successful simulations in bridge related problems means that CFD techniques
20 106 are nowadays more mature and therefore more robust and reliable.
21
22
23
24 107 In spite of the dramatic improvements in computational power and access to cluster technology of
25 108 recent years, the computer power demands linked with modeling complex fluid-structure
26 109 interaction problems remains a key issue. In this respect, any method or technique which allows
27 110 decreasing computational demands would facilitate incorporating CFD based design in bridge
28 111 engineering design. A number of researchers have proposed explicit relationships between flutter
29 112 derivatives which have proved to be reliable for streamlined bridge decks such as Matsumoto
30 113 (1996), Scanlan et al. (1997), Chen and Kareem (2002) or Tubino (2005). The application of these
31 114 formulae allows the number of computer simulations for obtaining the flutter derivatives to be
32 115 reduced to just half of the number required following the standard approach based on forced
33 116 harmonic vibrations in heave and pitch degrees of freedom. To the authors' knowledge the
34 117 aforementioned approach has not been applied in CFD-based studies to date.
35
36
37
38
39 118 The aim of the current piece of research is to propose a cost effective, and therefore efficient,
40 119 computer based approach for obtaining force coefficients and flutter derivatives of bridge deck box
41 120 sections which could be used in industrial applications where the shape of different bridge deck
42 121 designs could be numerically optimized. Consequently, a 2D URANS strategy is proposed, using
43 122 the general purpose open source CFD solver OpenFOAM v2.1.1 in combination with the explicit
44 123 relationships between flutter derivatives mentioned above. The more demanding 3D Detached
45 124 Eddy Simulation (DES) or LES approaches, in spite of their superior accuracy, have not been
46 125 considered in this work since they would pose additional challenges in terms of higher computer
47 126 power demands and model setup.
48
49
50
51
52 127 A rectangular cylinder showing a separated and reattached time-averaged flow pattern has been
53 128 selected as one of the case studies for the computation of the flutter derivatives. In particular, a
54 129 ratio $B/H=4.9$ rectangular cylinder (B is the prism width and H is the height) was chosen in order to
55 130 replicate an existing sectional model at the wind tunnel of the University of Nottingham. In the
56 131 literature, the number of published references, both experimental and computational, dealing with
57 132 the response of $B/H=5$ rectangular cylinders is plentiful, to a great extent thanks to the BARC
58 133 initiative (Bruno et al. 2014). Taking into account the expected minimal differences between the
59
60
61
62
63
64
65

134 aerodynamic response of $B/H=4.9$ and $B/H=5$ rectangular cylinders, for the sake of the efficiency
 135 of means in research, the authors have considered that the existing literature on 5:1 rectangular
 136 cylinders is adequate for the validation of the force coefficients and the flutter derivatives of the
 137 $B/H=4.9$ rectangular cylinder at 0° angle of attack. However, in the case that additional numerical
 138 studies would require validation against experimental data outside the range found in the literature,
 139 further wind tunnel tests could readily be conducted using the existing $B/H=4.9$ sectional model.

140 The second application case has been the G1 generic box section described in Scanlan and Tomko
 141 (1971) and Larsen and Walther (1998). The modern practice in long span bridge design has
 142 incorporated box deck cross-sections as the most common choice for these challenging structures.
 143 There are several reasons for this: a good aerodynamic and aeroelastic response characteristic of
 144 streamlined cross-sections, high torsional stiffness, construction economy and, in many cases,
 145 superior aesthetic value compared to truss girders. Recent examples of applications comprising box
 146 decks are the Forth Replacement Crossing in the United Kingdom, the Normandy Bridge and
 147 Millau Viaduct, in France, the Sutong Bridge in China or the Russky Bridge in Russia, amongst
 148 many others.

149 In the first part of this paper, the fundamental formulation and the numerical approach adopted,
 150 along with the computational models, for simulating the aerodynamic response of the bridge decks
 151 are explained. Then, the results of the study of the sensitivity of the solution to the spatial and
 152 temporal discretisations for the G1 generic section are summarized. Next the aerodynamic
 153 characteristics of the static $B/H=4.9$ rectangular cylinder are analyzed based on the values of the
 154 Strouhal number, force coefficients and the distribution of the averaged pressure coefficient and its
 155 standard deviation. Then the flutter derivatives of the rectangular cylinder, where the relationships
 156 between flutter derivatives have been applied, are reported and compared with wind tunnel data. It
 157 follows the analysis of the characteristics of the static G1 section based on force coefficients and
 158 the distribution of the averaged pressure coefficient. The results section ends with the report of the
 159 flutter derivatives of the G1 section and the corresponding comparison with experimental and other
 160 numerical data in the literature. Finally, conclusions are drawn from the work reported herein.

161 2. NUMERICAL FORMULATION

162 The flow around the bluff bodies of interest is modeled by means of the unsteady Reynolds-
 163 averaged Navier-Stokes equations considering incompressible flow. A 2D URANS approach has
 164 been preferred which, according to Brusiani et al. (2013), is equivalent to imposing the perfect
 165 correlation of the flow structures in the span-wise direction.

166 The time averaging of the equations for conservation of mass and momentum gives the Reynolds
 167 averaged equations of motion in conservative form. According to Wilcox (2006):

168

$$\frac{\partial U_i}{\partial x_i} = 0 \quad (1.a)$$

$$\rho \frac{\partial U_i}{\partial t} + \rho U_j \frac{\partial U_i}{\partial x_j} = - \frac{\partial P}{\partial x_i} + \frac{\partial}{\partial x_j} (2\mu S_{ij} - \rho \overline{u'_i u'_j}) \quad (1.b)$$

169

170 where U_i is the mean velocity vector, x_i is the position vector, t is the time, ρ is the fluid density,
 171 assumed constant, u'_i is the fluctuating velocity and the overbar represents the time average, P is

172 the mean pressure, μ is the fluid viscosity and S_{ij} is the mean strain-rate tensor. From the above
 173 equation, the specific Reynolds stress tensor is defined as:

$$\tau_{ij} = -\overline{u_i u_j} \quad (2)$$

174
 175 which is an additional unknown to be modeled based on the Boussinesq assumption for one and
 176 two equation turbulence models (Wilcox, 2006).

$$\tau_{ij} = 2\nu_T S_{ij} - \frac{2}{3}k\delta_{ij} \quad (3)$$

177
 178 where ν_T is the kinematic eddy viscosity, S_{ij} is the mean strain-rate tensor and k is the turbulent
 179 kinetic energy per unit mass.

180 In this work the closure problem is solved applying Menter's $k-\omega$ SST model for incompressible
 181 flows, reported in Menter and Esch (2001).

182 For the simulations where forced oscillations of the bluff body have been imposed, the Arbitrary
 183 Lagrangian Eulerian (ALE) formulation has been applied for allowing movements of the mesh
 184 inside the computational domain. The conservation of mass and momentum equations are written
 185 as follows (Bai et al., 2010, Sarkic et al., 2012):

$$\frac{\partial(U_i - U_{gi})}{\partial x_i} = 0 \quad (4.a)$$

$$\rho \frac{\partial U_i}{\partial t} + \rho U_j \frac{\partial(U_i - U_{gi})}{\partial x_j} = -\frac{\partial P}{\partial x_i} + \frac{\partial}{\partial x_j} (2\mu S_{ij} - \rho \overline{u_i u_j}) \quad (4.b)$$

186
 187 where U_{gi} is the grid velocity in the i -th direction.

188 3. FORCE COEFFICIENTS AND FLUTTER DERIVATIVES COMPUTATION BY 189 MEANS OF FORCED OSCILLATION SIMULATIONS

190 The definition of the force coefficients considered in this study is given in (5):

$$C_d = \frac{D}{\frac{1}{2}\rho U^2 B} \quad C_l = \frac{L}{\frac{1}{2}\rho U^2 B} \quad C_m = \frac{M}{\frac{1}{2}\rho U^2 B^2} \quad (5)$$

191
 192 In the former expressions D is the drag force per span length, positive in the windward direction, L
 193 is the lift force per span length, positive upwards, and M is the pitching moment per span length,
 194 positive clockwise, ρ is the fluid density, U is the flow speed and B is the bluff body width.

195 Flutter derivatives are semi-empirical parameters which relate motion-induced forces ~~and~~ with the
 196 displacements of the structure and their time derivative. These parameters have traditionally been
 197 identified using wind tunnel tests, but more recently, numerical based simulations have been
 198 applied.

199 According to Simiu and Scanlan (1996), the aeroelastic forces on a bridge deck, considering two
 200 degrees of freedom (heave and pitch), can be written as follows:

$$L_{ae} = \frac{1}{2}\rho U^2 B \left[KH_1^* \frac{\dot{h}}{U} + KH_2^* \frac{B\dot{\alpha}}{U} + K^2 H_3^* \alpha + K^2 H_4^* \frac{h}{B} \right] \quad (6.a)$$

$$M_{ae} = \frac{1}{2}\rho U^2 B^2 \left[KA_1^* \frac{\dot{h}}{U} + KA_2^* \frac{B\dot{\alpha}}{U} + K^2 A_3^* \alpha + K^2 A_4^* \frac{h}{B} \right] \quad (6.b)$$

201

202 where L_{ae} is the aeroelastic force per unit of span length, M_{ae} is the aeroelastic moment per unit of
 203 span length, ρ is the fluid density, U is the flow speed, $K = (B\omega)/U$ is the reduced frequency, B is
 204 the deck width, ω the circular frequency of oscillation, h is the heave displacement, α is the
 205 torsional rotation, \dot{h} and $\dot{\alpha}$ are the time derivatives and H_i^* and A_i^* ($i = 1, \dots, 4$) are the flutter
 206 derivatives.

207 Assuming prescribed harmonic forced oscillations $h = h_0 e^{i\omega t}$ and $\alpha = \alpha_0 e^{i\omega t}$, where h_0 and α_0
 208 are the amplitudes of the oscillations, and also that motion-induced forces are linear functions of
 209 the movement; after some manipulation, the following expressions are obtained for the
 210 identification of the flutter derivatives:

$$H_1^* = -\left(\frac{U}{Bf}\right)^2 \frac{C_l \sin \varphi_{L-h}}{(2\pi)^2 h_0/B} \quad (7.a)$$

$$A_1^* = -\left(\frac{U}{Bf}\right)^2 \frac{C_m \sin \varphi_{M-h}}{(2\pi)^2 h_0/B} \quad (7.e)$$

$$H_2^* = -\left(\frac{U}{Bf}\right)^2 \frac{C_l \sin \varphi_{L-\alpha}}{(2\pi)^2 \alpha_0} \quad (7.b)$$

$$A_2^* = -\left(\frac{U}{Bf}\right)^2 \frac{C_m \sin \varphi_{M-\alpha}}{(2\pi)^2 \alpha_0} \quad (7.f)$$

$$H_3^* = \left(\frac{U}{Bf}\right)^2 \frac{C_l \cos \varphi_{L-\alpha}}{(2\pi)^2 \alpha_0} \quad (7.c)$$

$$A_3^* = \left(\frac{U}{Bf}\right)^2 \frac{C_m \cos \varphi_{M-\alpha}}{(2\pi)^2 \alpha_0} \quad (7.g)$$

$$H_4^* = \left(\frac{U}{Bf}\right)^2 \frac{C_l \cos \varphi_{L-h}}{(2\pi)^2 h_0/B} \quad (7.d)$$

$$A_4^* = \left(\frac{U}{Bf}\right)^2 \frac{C_m \cos \varphi_{M-h}}{(2\pi)^2 h_0/B} \quad (7.h)$$

211

212 where φ_{L-h} , $\varphi_{L-\alpha}$, φ_{M-h} and $\varphi_{M-\alpha}$ are the phase lags of the fluctuating aeroelastic lift and
 213 moment with respect to the heave and pitch harmonic oscillations and C_l and C_m are the amplitudes
 214 of the non-dimensional aeroelastic lift and moment.

215 It must be borne in mind that in Larsen and Walther (1998), whose results are used later for
 216 validation, the flutter derivatives are computed dividing equations (7.a) to (7h.) by 2.

217 4. RELATIONSHIPS BETWEEN FLUTTER DERIVATIVES

218 As mentioned in the introduction, a number of publications can be found in the literature reporting
 219 several relationships amongst flutter derivatives. Tubino (2005) has derived the following
 220 relationships between heave-related and pitch-related flutter derivatives assuming the linear
 221 formulation hypothesis for the self-excited forces:

$$H_1^*(K) = KH_3^*(K) - \frac{C_d}{K} \quad (8.a)$$

$$A_1^*(K) = KA_3^*(K) \quad (8.c)$$

$$H_4^*(K) = -KH_2^*(K) \quad (8.b)$$

$$A_4^*(K) = -KA_2^*(K) \quad (8.d)$$

222 The above equations are similar to the ones reported by Matsumoto (1996) apart from the (H_1^*, H_3^*)
223 relationship, that does not consider the term containing the drag coefficient. For streamlined
224 sections with low drag coefficient its contribution is nearly negligible.

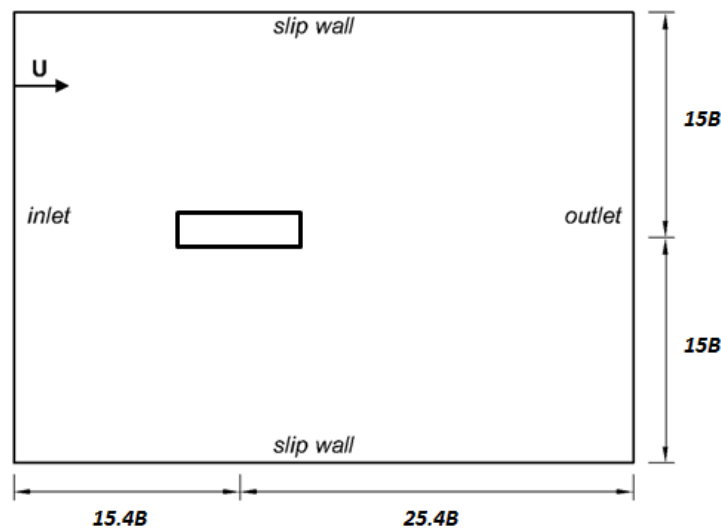
225 Experimental validation of the former relationships reported in Tubino (2005), has shown that the
226 relationships between (H_1^*, H_3^*) and (A_1^*, A_3^*) were satisfied for all the cases considered while the
227 relationships between (H_2^*, H_4^*) and (A_2^*, A_4^*) were closely verified for streamlined deck cross-
228 sections, since minor discrepancies are identified between experimental realizations and the
229 approximated values. In Matsumoto (1996), the reported relationships between flutter derivatives
230 are confirmed for rectangular cylinders less affected by vortex generation, proposing as a reference
231 lower bound a 5:1 ratio.

232 5. GEOMETRY AND COMPUTER MODELING

233 Two different geometries have been considered as case studies in the present work: a $B/H=4.9$
234 rectangular cylinder (H is the section depth or height), and the generic G1 deck section, described
235 in Larsen and Walther (1998), representative of streamlined box decks.

236 5.1. $B/H=4.9$ rectangular cylinder

237 Figure 1 shows the layout of the flow domain and boundary conditions employed in the rectangular
238 cylinder simulations. The flow domain considered for the rectangular cylinder case is $40.8B$ by $30B$
239 similar to the size employed in successful simulations by other researchers such as Fransos and
240 Bruno (2010).



241

242 Figure 1. Flow domain definition and boundary conditions for the $B/H=4.9$ rectangular cylinder
243 (not to scale).

244 A constant velocity inlet has been set at the upwind boundary (the left side in the figure) of the
245 computational domain. The incoming flow has a turbulence intensity of 1 % along with a $0.1B$
246 turbulent length scale as per Ribeiro (2011). A pressure outlet at atmospheric pressure has been
247 imposed at the right side (see figure 1). The upper and lower boundaries have been defined as slip
248 walls. The corners of the prism have been modeled as sharp and its walls are defined as non-slip.
249 When the rectangular cylinder is forced to oscillate the resultant velocity field around the

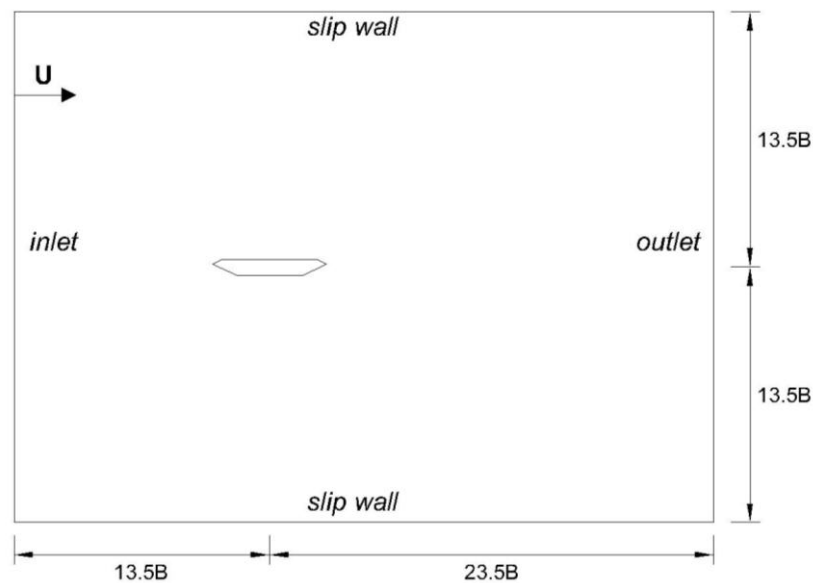
250 rectangular cylinder wall is corrected, so that the velocity of the flow at the moving boundary is
251 equal to the mesh velocity and therefore no flux across the wall takes place.

252 The numerical schemes adopted in the simulations reported herein are summarized next. The
253 interpolation of values from the cell centers to face centers is done using a linear scheme. The
254 gradient terms are discretised using the Gauss scheme with a linear interpolation scheme. For the
255 divergence terms, the Gauss scheme is also selected, adopting linear upwind and limited linear
256 interpolation schemes. For the Laplacian terms the choice has been the Gauss scheme with a linear
257 interpolation scheme and a limited surface normal gradient scheme. The Euler first order bounded
258 implicit scheme was set for the first time derivative terms.

259 A block structured mesh with a topology similar to the one in Braun and Awruch (2003), has been
260 generated. The total number of cells is 148320, and the number of cells around the walls of the
261 rectangular cylinder is 460. For the first layer of cells, the height to width ratio is $\delta_1/B = 5.11 \times$
262 10^{-4} , for which the mean value of the non-dimensional height ($y^+ = (\delta_1 u_*)/\nu$, where δ_1 is the
263 height of the first prismatic grid layer around the deck and u_* is the friction velocity) is about 1.8
264 and the maximum value is close to 8 at $Re = 1.01 \times 10^5$. These bounds are ~~the~~ similar to those
265 reported in Sarkic et al. (2012), and in this model, the number of cells with $y^+ > 4$ is about 5% of
266 the total number of cells around the rectangular cylinder and they are located mainly in the
267 windward corners. In both static and forced harmonic oscillations a maximum Courant number of 1
268 has been imposed, which produces for the static prism at the Reynolds number of reference a mean
269 non-dimensional time step $\overline{\Delta s} = \overline{\Delta t}U/B = 6.7 \times 10^{-4}$. The abundant literature reporting
270 numerical studies on rectangular cylinders means verification studies concerning mesh size and
271 time step refinements for the rectangular cylinder case can be avoided, since the authors have used
272 common mesh topologies and have adopted mesh characteristics and a time step more demanding
273 than other successful simulations.

274 5.2. G1 generic deck cross-section

275 The detailed geometry of the G1 generic cross-section is depicted in figure 8. The flow domain size
276 in this case is $37B$ by $27B$ (B is the deck width), similar to the size employed in the rectangular
277 cylinder case. The boundary conditions are the same as in the rectangular cylinder case.



278

279 Figure 2. Flow domain definition and boundary conditions for the G1 section (not to scale).

280 To verify the spatial discretisation, for the streamlined G1 deck section three different grids, with
 281 different mesh densities, have been considered for the static deck case with a 0° angle of attack.
 282 The meshes are identified as Coarse, Medium and Fine grids. In all the cases, a 2D block structured
 283 regular mesh has been used. A high density mesh has been defined around the deck cross-section,
 284 the so-called boundary layer mesh, taking special care in order to obtain maximum values for the
 285 first grid non-dimensional height y^+ below 4, which is a more demanding bound than the one set
 286 by Sarkic et al. (2012) for a similar problem. In this manner, no wall functions are required and the
 287 turbulence model equations are integrated along the viscous sublayer. The thickness of this layer is
 288 $B/25$. The Coarse mesh comprises 25 rows of elements in this zone and the height of the first
 289 element around the cross-section is defined as $\delta_1/B = 2.08 \times 10^{-4}$, while the expansion ratio
 290 between the end cell and the start cell is 25. For the Medium (Figure 3) and Fine meshes the
 291 boundary layer definition was identical: 50 rows considering an expansion ratio of 10, which gives
 292 a first cell non-dimensional height $\delta_1/B = 2.03 \times 10^{-4}$, very close to the Coarse mesh case in
 293 order to be able to drive conclusions from the verification analyses since the y^+ values are
 294 comparable for the three cases. For a Reynolds number $Re = 1.07 \times 10^5$, these mesh arrangements
 295 offer a mean value of the y^+ around the deck close to 1, with a very limited number of cells with
 296 $y^+ > 2$ located at the windward corners of the deck. The maximum value of y^+ for the three cases
 297 is about 3.7.

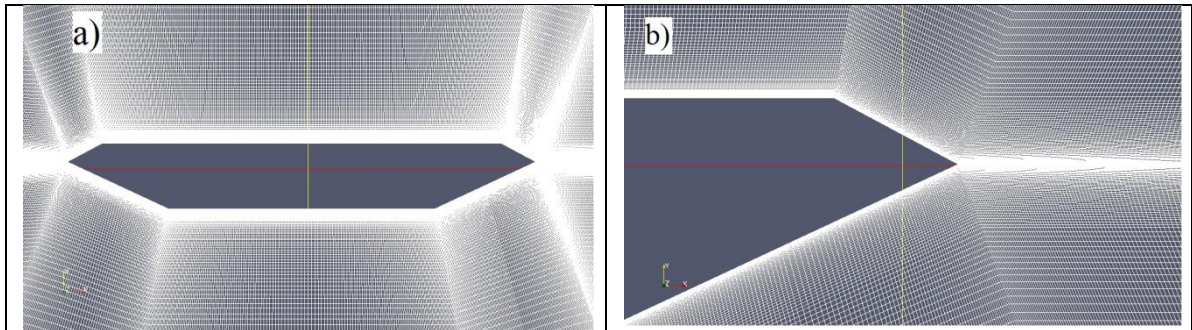
298 In table 1 the total number of cells, the number of cells around the deck section and the integral
 299 aerodynamic parameters are reported along with the standard deviation (prime symbol) values of
 300 the force coefficients for each mesh.

Table 1. Properties and results of the grid-refinement study for the G1 section.

| Grid | Total cells | Cells around deck | S_t | C_d | C_l | C_m | C'_d | C'_l | C'_m |
|--------|-------------|-------------------|-------|-------|--------|-------|--------|--------|--------|
| Coarse | 149600 | 640 | 0.20 | 0.056 | -0.026 | 0.035 | 0.0003 | 0.010 | 0.0022 |
| Medium | 268150 | 770 | 0.19 | 0.057 | -0.033 | 0.034 | 0.0006 | 0.022 | 0.0047 |
| Fine | 363300 | 770 | 0.19 | 0.057 | -0.034 | 0.034 | 0.0006 | 0.022 | 0.0047 |

301

302



303 Figure 3. G1 section block structured grid: a) close-up of the deck and b) detail around the lee-ward
 304 corner of the deck.

305 The main discrepancies found have been the lower values in the standard deviation of the force
 306 coefficients and the slight underestimation of the lift coefficient when the coarse mesh has been

1
2
3
4
5
6
7
8
9
10
11
12
13
14
15
16
17
18
19
20
21
22
23
24
25
26
27
28
29
30
31
32
33
34
35
36
37
38
39
40
41
42
43
44
45
46
47
48
49
50
51
52
53
54
55
56
57
58
59
60
61
62
63
64
65

307 used. Consequently the Coarse mesh has been disregarded and Medium mesh is adopted hereafter
 308 since the results are similar to the ones obtained using the Fine mesh at a lower computational cost.

309 Regarding the analysis of the sensitivity of the solution depending on the chosen time step, two
 310 different maximum Courant numbers equal to 1 and 0.5 have been considered in order to check the
 311 influence of the temporal discretisation (Mannini et al., 2010). In table 2, where the non-
 312 dimensional time step is defined as $\overline{\Delta s} = \overline{\Delta t}U/B$, the numerical results obtained are reported,
 313 finding that they offer very close figures; therefore the higher maximum Courant number is
 314 retained for the remaining simulations.

Table 2. Results of the time-refinement study for the G1 section.

| Max. Co. numb. | $\overline{\Delta s}$ | S_t | C_d | C_l | C_m | C'_d | C'_l | C'_m |
|----------------|-----------------------|-------|-------|--------|-------|--------|--------|--------|
| 1 | 3.5e-4 | 0.19 | 0.057 | -0.033 | 0.034 | 0.0006 | 0.022 | 0.0047 |
| 0.5 | 1.8e-4 | 0.20 | 0.058 | -0.037 | 0.034 | 0.0006 | 0.019 | 0.0040 |

315

316 5.3. Grid movement strategy

317 The computer implementation of the ALE formulation requires a mesh-update method that assigns
 318 mesh-node velocities or displacements at each calculation time step (Donea et al., 2004).

319 In the simulations conducted in this research the boundary motion is defined by the prescribed
 320 forced oscillations of the bluff body, which follows a sinusoidal law with given frequency and
 321 amplitude. On the other hand, the exterior boundaries of the fluid domain are fixed along the
 322 simulations. The whole mesh is allowed to deform between the moving and fixed boundaries.

323 Amongst the available mesh movement algorithms a Laplacian smoothing technique for each
 324 component of the node-mesh position has been chosen (Oliver, 2009). According to Jasak and
 325 Rusche (2009), the Laplace equation can be expressed as:

$$\nabla \cdot k \nabla \mathbf{u} = 0 \quad (9)$$

326 where \mathbf{u} is the node-mesh displacement vector and k is the diffusion coefficient.

327 In this work the mesh control is achieved by computing the motion of the grid points solving the
 328 Laplace equation with variable diffusivity using a method based on the quadratic inverse distance
 329 from the oscillating boundary. This prevents the distortion of the smallest elements around the
 330 rectangular cylinder (Löhner, 2008).

331 5.4. Forced oscillations characteristics and application of relationships between flutter 332 derivatives

333 With the aim of limiting the computational cost of obtaining the set of 8 flutter derivatives, the
 334 relationships between flutter derivatives (8.a–8.d) reported in Tubino (2005) are applied. As a
 335 consequence, only half of the simulations are required, which represents a substantial reduction in
 336 the computational demands of the problem. The pitch degree of freedom has been chosen as the
 337 one for carrying out the numerical simulations; therefore the H_2^* , H_3^* , A_2^* and A_3^* flutter derivatives
 338 are computed by means of the CFD simulations, while the H_1^* , H_4^* , A_1^* and A_4^* flutter derivatives are
 339 estimated using equations (8.a) to (8.d). The amplitude of the forced oscillations in the present
 340 work is $\alpha_0 = 1^\circ$ for the two considered application examples. The sign convention adopted herein

341 has been the same as in Sarkar et al. (2009): heave and aeroelastic lift force positive downward,
 342 while the aeroelastic moment and rotation have been considered positive for a nose-up rotation.

343

344 6. RESULTS AND DISCUSSION

345 6.1 $B/H=4.9$ rectangular cylinder

346 6.1.1 Flow simulation around the static $B/H=4.9$ rectangular cylinder

347 In table 3 the Strouhal number, the mean drag coefficient and the standard deviation of the lift and
 348 drag coefficients at $Re = 1.01 \times 10^5$ are presented along with experimental data from Schewe
 349 (2009) and the numerical data computed using two different 2D URANS approaches. The URANS
 350 references which have been considered for comparison are: Ribeiro (2011) who reports, amongst
 351 others, the results of a Reynolds Stress Model (RSM) simulation and Mannini et al. (2011) where
 352 the Linearised Explicit Algebraic (LEA) version of the Explicit Algebraic Reynolds Stress Model
 353 (EARSM) coupled with the standard $k-\omega$ turbulence model is employed. It must be borne in mind
 354 that in the references used for validation the ratio of the rectangular cylinder is $B/H=5$. In table 3,
 355 the reference dimension for drag coefficient and the standard deviations is B , therefore the data in
 356 Mannini et al. (2011), Ribeiro (2011) and Schewe (2009) which are based on H , have been
 357 modified for comparison. For the simulation of the $B/H=4.9$ static rectangular cylinder the
 358 simulated length has been about 100 non-dimensional time units and the reported results in table 3
 359 have been averaged along a non-dimensional time $s = tU/B = 74$.

Table 3. $B/H=4.9$ rectangular cylinder: Strouhal number and force coefficients.

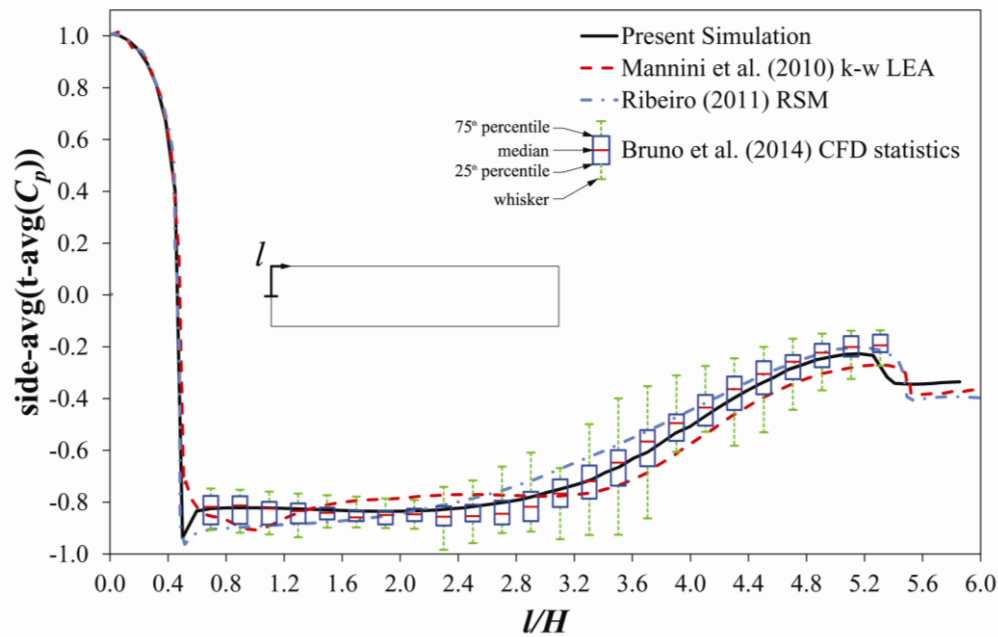
| | S_f | C_d | C'_d | C'_l |
|--|-------|-------|--------|----------------|
| Present simulation | 0.123 | 0.227 | 0.0049 | 0.193 |
| Mannini et al. (2011) – LEA $k-\omega$ | 0.094 | 0.212 | 0.0038 | 0.215 |
| Ribeiro (2011) - RSM | 0.073 | 0.234 | | 0.18 |
| Schewe, (2009) – EXP. | 0.111 | 0.206 | | ≈ 0.08 |

360

361 Table 3 shows a good agreement with the experimental and numerical data, particularly taking into
 362 account that, since the aspect ratio of the rectangular cylinder considered in the simulation is lower
 363 than 5, it must show slightly higher values for both Strouhal number and drag force coefficients
 364 according with the trend in drag coefficient and Strouhal number for rectangular cylinders with
 365 aspect ratios between 4 and 6, reported in Shimada and Ishihara (2012). It is notable how Menter's
 366 $k-\omega$ SST turbulence model considered in this simulation offers results comparable with the
 367 sophisticated LEA approach in Mannini et al. (2011). The proximity of the Strouhal number in this
 368 simulation to the experimental value obtained in Schewe (2009) should also be highlighted and
 369 therefore a better prediction of this parameter than in Ribeiro (2011) has been obtained.

370 As a further validation of the reported simulations, in figure 4 the side-averaged (between the upper
 371 and lower half perimeters) and time-averaged distribution of the pressure coefficient C_p of the
 372 static ratio $B/H=4.9$ rectangular cylinder are reported along with the results in Mannini et al. (2010)
 373 for the $k-\omega$ LEA turbulence model, Ribeiro (2011) for the RSM and the statistics for the CFD
 374 realizations reported in Bruno et al. (2014). The side-averaged and time-averaged pressure
 375 coefficient of the ratio 4.9 rectangular cylinder is very close to the median values on the long side
 376 of the rectangular cylinder (l/H between 0.7 and 5.3, being l the length along the half of the
 377 perimeter of the rectangular cylinder, as it is described in figure 4) which indicates that the
 378 accuracy of the simulation is comparable with the CFD realizations in the frame of the BARC

379 initiative. Furthermore, the numerical results correctly reproduce the experimental data for the 5:1
 380 rectangular cylinder, bearing in mind the scatter in the wind tunnel tests available in the literature.

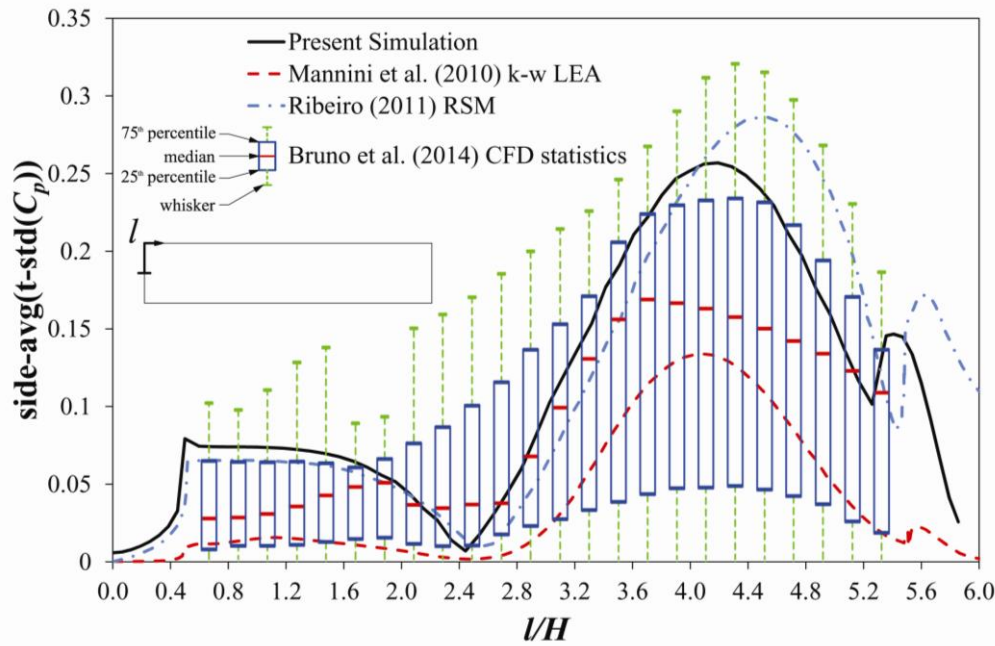


381

382 Figure 4. Side-averaged and time-averaged C_p distributions around $B/H=4.9$ and $B/H=5$
 383 rectangular cylinders.

384 In figure 5, the side-averaged distribution of the standard deviation ~~in-time~~ of the pressure
 385 coefficient is reported along with the statistical data for the CFD realizations in Bruno et al. (2014)
 386 and the simulations in Mannini et al. (2010) and Ribeiro (2011). In Bruno et al. (2014) the scatter
 387 in the distribution of the standard deviation of the pressure coefficient has been shown for both
 388 experimental and numerical realizations. The standard deviation distribution of the C_p reported for
 389 the $B/H=4.9$ rectangular cylinder is well inside the boundaries of the BARC realizations and it is
 390 particularly close to the RSM simulation in Ribeiro (2011). It has reported in Bruno et al. (2014)
 391 that RANS simulations present a minimum in the standard deviation of the pressure coefficient
 392 at about $2H$ from the windward corner. This minimum is also present in the simulation reported in
 393 this work.

1
2
3
4
5
6
7
8
9
10
11
12
13
14
15
16
17
18
19
20
21
22
23
24
25
26
27
28
29
30
31
32
33
34
35
36
37
38
39
40
41
42
43
44
45
46
47
48
49
50
51
52
53
54
55
56
57
58
59
60
61
62
63
64
65



394

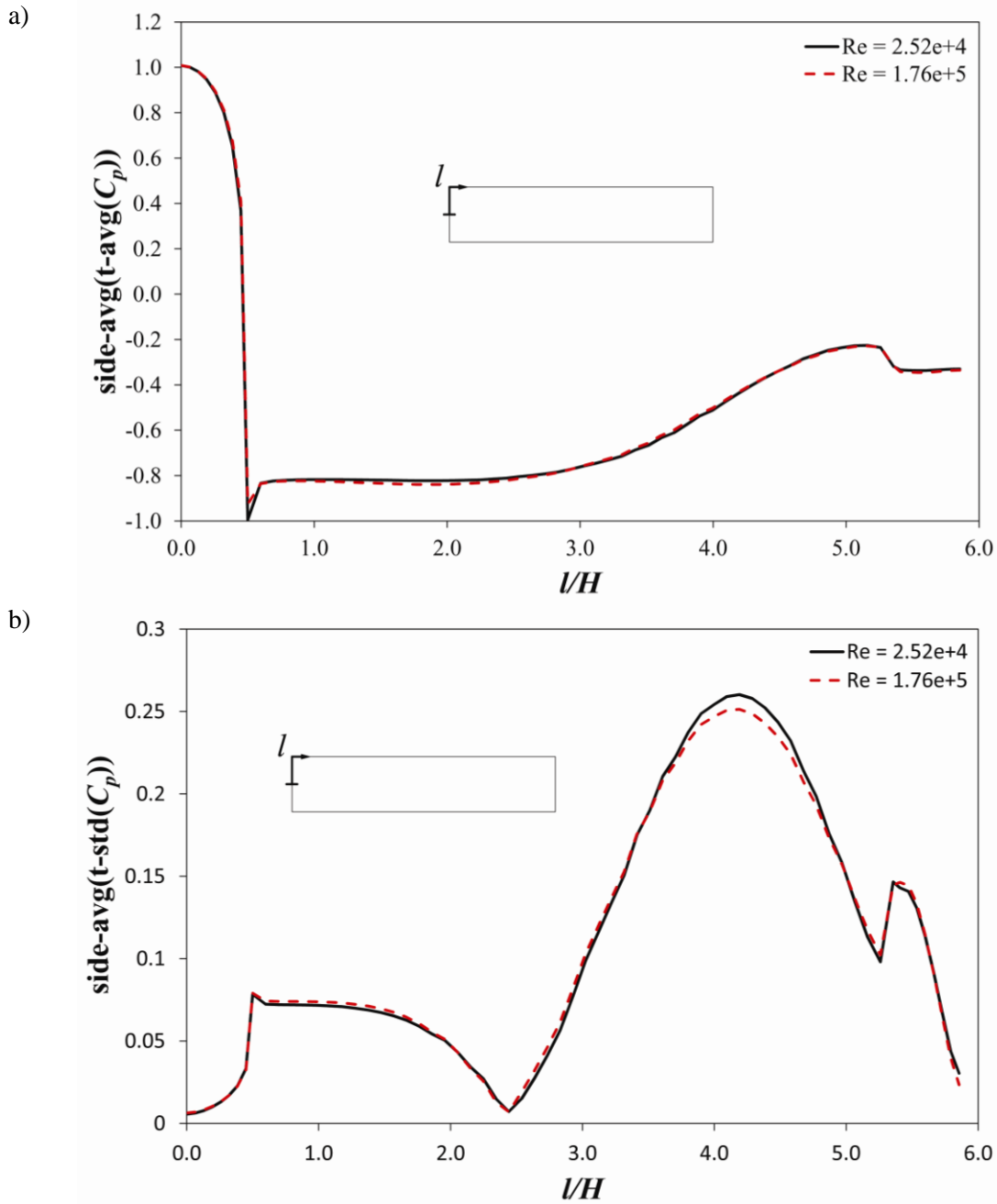
395 Figure 5. Side-averaged distributions around $B/H=4.9$ and $B/H=5$ rectangular cylinders of the
 396 standard deviation in time of C_p .

397 Based on the comparison of the drag coefficient, the standard deviation of the lift coefficient, the
 398 Strouhal number and the distribution to the time-averaged and time-standard deviation of the
 399 pressure coefficient, the agreement of the present simulation with the experimental and numerical
 400 data in the literature can be considered adequate.

401 6.1.2 Flutter derivatives of the $B/H=4.9$ rectangular cylinder

402 The flutter derivatives for the aspect ratio 4.9 rectangular cylinder have been computed over a
 403 range of reduced velocities $U_R = U/(f \cdot B) = (0.88, 26.40)$. In order to cover the whole range of
 404 reduced velocities, three frequencies of oscillation have been considered (0.5 Hz., 1 Hz. and 3 Hz.)
 405 in conjunction with flow speeds between 1 m/s and 7 m/s, which means that the range of covered
 406 Reynolds number is between 2.52×10^4 and 1.76×10^5 . In some cases ($U_R = 2.6, 5.3, 10.6$ and 15.84),
 407 the same reduced velocity has been computed with different combinations of flow velocity and
 408 frequency of oscillation in order to verify the independence of the results with the combination of
 409 both parameters.

410 Since the same mesh has been retained for all the simulations, the non-dimensional height y^+
 411 reaches a maximum value close to 11 for the maximum Reynolds number ($Re = 1.76 \times 10^5$; $U = 7$
 412 m/s), while the mean value of y^+ is about 2.7. For the minimum Reynolds number ($Re =$
 413 2.52×10^4 ; $U = 1$ m/s), the maximum y^+ reaches a value close to 3.5 and the mean value of y^+ is
 414 0.6. With the aim of ascertaining the effect of the differences in the y^+ numbers on the simulations
 415 at the lower and upper bounds of the Reynolds number, as well as the dependency of the
 416 aerodynamic characteristics with the Reynolds number, the side-averaged and time-averaged along
 417 with the side-averaged time-standard deviation distributions of the pressure coefficient are
 418 presented for $U = 1$ and $U = 7$ m/s (Figure 6).

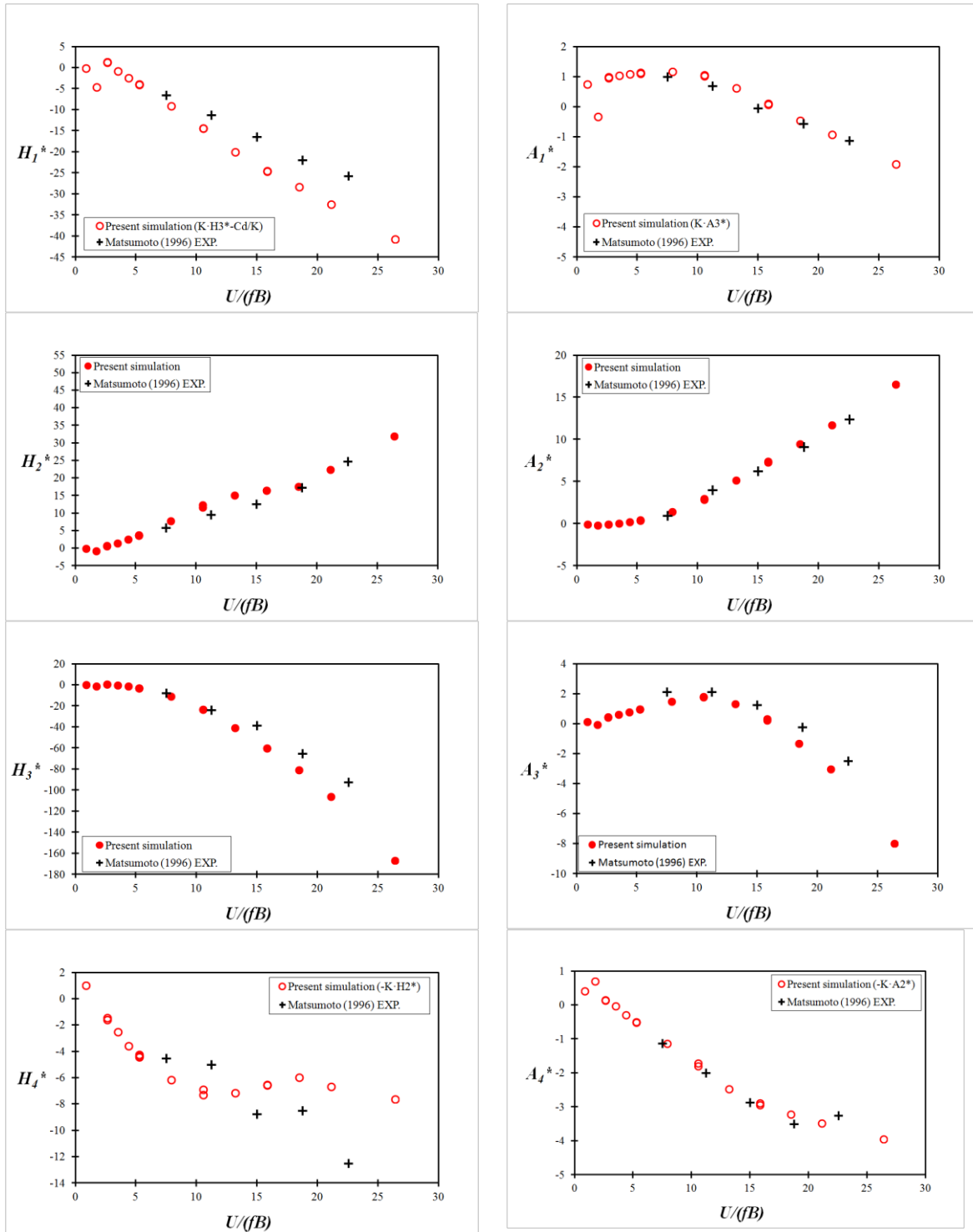


419 Figure 6. Side-averaged distributions around $B/H=4.9$ rectangular cylinder of the a) time-averaged
 420 and b) time-standard deviation of C_p for $U = 1$ and $U = 7$ m/s.

421 Figure 6 shows similar results for the side-averaged distributions of the time-averaged and the
 422 standard deviation of the pressure coefficient. Only small differences in the peak value of the
 423 distribution of the standard deviation of the pressure coefficient around the rectangular prism can
 424 be identified. Consequently, the relatively high values of the maximum y^+ at $U = 7$ m/s do not
 425 jeopardize the accuracy of the simulation. At the same time, the aerodynamic characteristics of the
 426 static sharp edged rectangular cylinder at 0° angle of attack seems to be quite insensitive to the
 427 Reynolds number, as it has been reported in Holmes (2007), citing Scruton (1981). Besides this, in
 428 the set of reduced velocities considered for the computation of the flutter derivatives, the maximum
 429 flow speed of 7 m/s is adopted for a single reduced velocity $U_R = 18.48$. In the same manner, the
 430 flow speed of 6 m/s is employed only for repeated values of $U_R = 5.3$ and $U_R = 15.84$. Therefore,

431 in the set of flutter derivatives which are presented next, the majority of the simulations have been
 432 conducted at $Re \leq 1.26 \times 10^5$.

433 In figure 7 the flutter derivatives computed from these simulations are reported along with the
 434 experimental data in Matsumoto (1996). The length of the simulations reported in the following has
 435 been between 40 and 260 non-dimensional time units, depending on the flow speed and the
 436 frequency of oscillation.



437 Figure 7. Flutter derivatives of the $B/H=4.9$ rectangular cylinder: computed flutter derivatives and
 438 comparison with experimental data in Matsumoto (1996).

439 The estimated flutter derivatives agree well with the experimental data and only the H_4^* flutter
 440 derivative shows some discrepancies with the wind tunnel values. These differences in H_4^* are
 441 comparable with the ones found in CFD simulations where forced oscillations in the heave degree
 442 of freedom have been conducted, such as in Sarwar et al. (2008) for a $B/H=20$ rectangular cylinder
 443 or Huang (2009). There are no significant differences for the repeated simulations at the same
 444 reduced velocities, which points out the relative independence of the results with the various
 445 combinations of flow speed and frequency of oscillation.

446 6.2 G1 generic deck cross-section

447 6.2.1 Flow simulation around the static G1 section

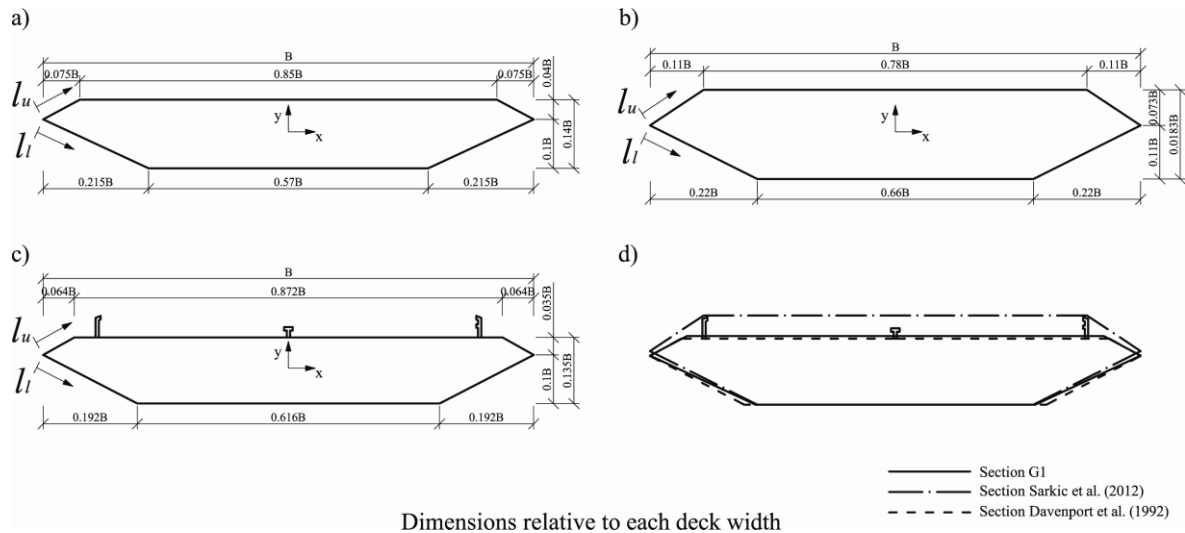
448 The drag coefficient, the root mean square of the lift coefficient time history and the Strouhal
 449 number of the G1 section for 0° angle of incidence computed in this study are compared in table 4
 450 with the numerical results reported in Larsen and Walther (1998) who applied the Discrete Vortex
 451 Method in their simulations. In this case the numerical simulation of the static G1 section has been
 452 extended along 65 non-dimensional time units. The time statistics have been obtained from the
 453 final 45 non-dimensional time units.

Table 4. Static G1 section: drag coefficient, RMS of the lift coefficient and Strouhal number.

| | C_d | C_l^{RMS} | S_t |
|---------------------------|-------|-------------|-------|
| Present simulation | 0.06 | 0.04 | 0.19 |
| Larsen and Walther (1998) | 0.08 | 0.07 | 0.17 |

454

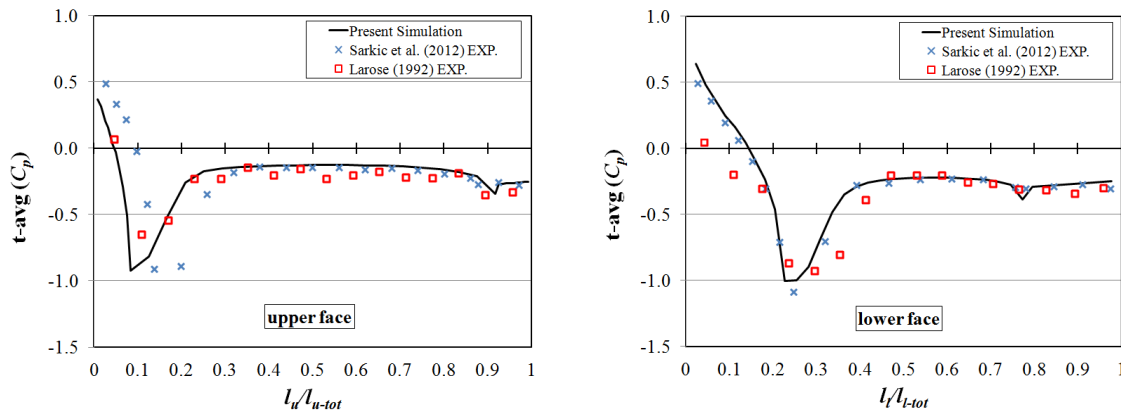
455 The agreement amongst the results for the 0° angle of attack is reasonable, however as a further
 456 validation of the numerical approach chosen by the authors, the time-averaged pressure coefficient
 457 distribution along the deck is going to be presented and compared with the experimental data
 458 reported in Sarkic et al. (2012), where the time-averaged pressure coefficient distribution along a
 459 bare box deck is provided. For further comparison, the experimental data in Bruno and Khri
 460 (2003) (taken from Larose, 1992) of the smooth flow tests of a taut strip model of the Great Belt
 461 Bridge fitted with barriers, has also been included. The geometry of the deck and the position of the
 462 pressure probes in the aforementioned reference are taken from Davenport et al. (1992). The
 463 distribution of the ~~time~~ standard deviation of the pressure coefficient is not reported since the
 464 unsteadiness of the flow was rather weak, providing values of the pressure coefficient standard
 465 deviation well below the available experimental data, particularly on the windward half of the cross
 466 section. A similar behavior is described in Sarkic et al. (2012). In figure 8, the geometry of the
 467 bridge decks considered for validation is described, while in figure 9 the time-averaged pressure
 468 coefficient distribution is shown.



Dimensions relative to each deck width

469

470 Figure 8. Geometry: a) G1 section b) section in Sarkic et al. (2012) c) section in Davenport et al.
471 (1992) d) comparison between sections.



472 Figure 9. Time-averaged pressure coefficient distribution: numerical results and comparison with
473 experimental data in Sarkic et al. (2012) and Larose (1992).

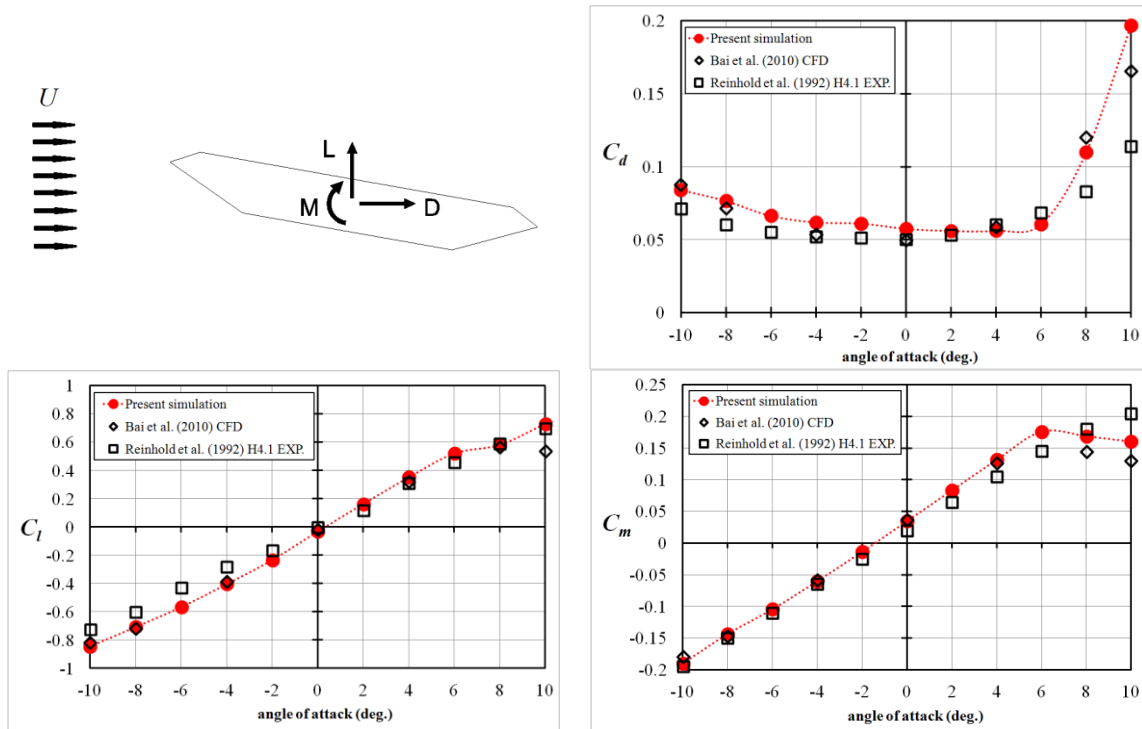
474 The agreement in the pressure coefficient distribution between the numerical simulation and the
475 wind tunnel data in Sarkic et al. (2012) is good. On the upper face, the peak values at the windward
476 corner are correctly simulated and the lateral shift is due to the differences in the geometry in the
477 upper surface (see figure 8). Also the mean pressure distribution along the horizontal and the
478 leeward plates have been accurately obtained. The agreement is even better on the lower surface,
479 since the geometry of the two sections is nearly identical. In the authors' opinion the similitude in
480 the Reynolds number ($Re \approx 1 \times 10^5$) of the numerical simulation and the wind tunnel test has
481 contributed to this close agreement.

482 When the numerical results are compared with the wind tunnel data from Larose (1992), some
483 discrepancies can be identified, which can arguably be related to the difference in the Reynolds
484 number of the wind tunnel tests ($Re = 7 \times 10^4$) as well as the presence of the barriers in the tested
485 model. Besides this, discrepancy in the moderate suction on the windward surface in the lower side
486 of the deck has already been commented in Bruno and Khris (2003).

487 In order to provide a more complete view of the aerodynamic characteristics of the static G1 cross
488 section, the force coefficients in the range of angles of attack ($-10^\circ, 10^\circ$) are computed with an
489 interval of 2° . The results are compared with the experimental data reported in Reinhold et al.

490 (1992) for the H4.1 section of the Great Belt Bridge design studies and the 2D numerical results
 491 published in Bai et al. (2010), for the G1 section.

492 Figure 10 shows the force coefficients of the G1 section. A very good agreement has been obtained
 493 between the computational results and the experimental data for the similar geometry of the H4.1
 494 box deck section. In fact, the change in the slope of the moment coefficient for angles of incidence
 495 higher than 6° has been correctly captured as well as the step increment in the drag coefficient
 496 also for angles of attack higher than 6° . The accuracy of the slopes in the vicinity of 0° for both lift
 497 and moment coefficients should also be noted.

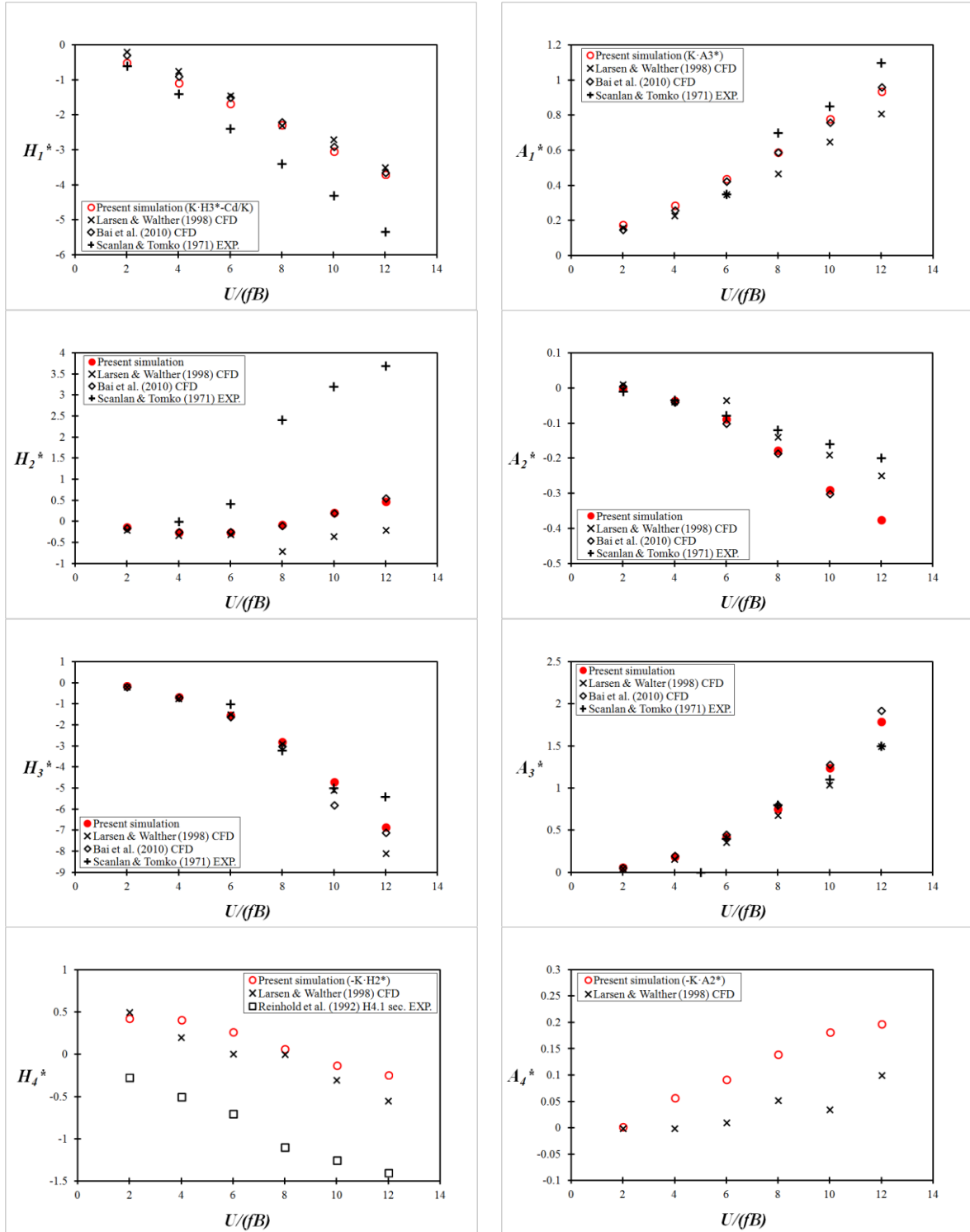


498 Figure 10. G1 section force coefficients: numerical results and comparison with experimental
 499 (Reinhold et al., 1992) and other numerical data (Bai et al., 2010).

500 6.2.2 Flutter derivatives of the G1 section

501 In order to identify by means of a computational approach the flutter derivatives of the G1 generic
 502 section, forced oscillation simulations were carried out at reduced velocities $U/(fB)$ equal to 2, 4,
 503 6, 8 10 and 12, as in Larsen and Walther (1998). Also, the formulae applied for identifying the
 504 flutter derivatives are the ones reported in Larsen and Walter (1998) and Bai et al (2010), therefore
 505 the expressions in equations (7.a) to (7h) are divided by 2. The same procedure as in the
 506 rectangular cylinder case has been applied for decreasing the computational cost. As a
 507 consequence, instead of 12 computer simulations, only 6 are required, one for each reduced
 508 velocity considered. In this case the flow velocity is the same in all the simulations and the
 509 frequency of oscillation is modified in the range (0.833, 5) Hz in order to obtain the reduced
 510 velocities of interest. The solution for the fixed G1 section has been set as the initial condition for
 511 the forced oscillation simulations. Since this allows shortening the initial transient, the
 512 computations have been extended for about 50 non-dimensional time units. For the highest value of
 513 the reduced velocity, $U_R=12$, four complete oscillation periods have been simulated, which is
 514 greater than the 2.5 periods span adopted in Larsen and Walther (1998).

515 In figure 11 the numerical results obtained for H_i^* and A_i^* ($i = 1, \dots, 3$) are compared with the
 516 experimental ones reported in Scanlan and Tomko (1971). The numerical results obtained by
 517 Larsen and Walther (1998), and Bai et al. (2010) for the same deck section are also included in the
 518 charts. Since no experimental results are available for the H_4^* and A_4^* flutter derivatives of the G1
 519 cross-section, the results for the H_4^* flutter derivative of the H4.1 section in Reinhold et al (1992)
 520 are provided. No experimental data for the A_4^* flutter derivative of the H4.1 section are available in
 521 the literature to the authors' knowledge.



522 Figure 11. Flutter derivatives of the G1 generic section: numerical results and comparison with
 523 experimental (Scanlan and Tomko, 1971; Reinhold et al., 1992) and numerical (Larsen and
 524 Walther, 1998; Bai et al., 2010) data.

525 A very good agreement has been found for the flutter derivatives related to the pitch forced
 526 oscillation: H_3^* , A_2^* and A_3^* , which have been obtained from the numerical simulations. For the H_2^*
 527 flutter derivative, similar discrepancies as in Bai et al. (2010) have been obtained. In fact, for this
 528 flutter derivative, in the case of box decks, differences between experimental data and CFD based
 529 evaluations can be found in other references in the literature, such as Jeong and Kwon (2003), Zhu
 530 et al. (2007), Ge and Xiang (2008) or Brusiani et al. (2013). For the approximated heave-related
 531 flutter derivatives H_1^* and A_1^* the obtained results agree with wind tunnel test data and their
 532 accuracy is comparable with the other CFD-based simulations. For the flutter derivatives H_4^*
 533 and A_4^* it is more difficult to properly assess the reliability of the approximated values since
 534 experimental data are not available. It has been found that for the H_4^* flutter derivative the present
 535 simulation provides values very similar to those reported by Larsen and Walther (1998). In the
 536 same manner, the slope is almost the same as for the H4.1 experimental flutter derivative and the
 537 upwards shift of the numerical results can also be found, for instance, in Brusiani et al. (2013)
 538 where the flutter derivatives of the H4.1 section were specifically computed. For the A_4^* flutter
 539 derivative the approximated values do not show important differences in value with respect to the
 540 ones in Larsen and Walther (1998).

541 In order to assess the degree of accuracy in the simulations reported in this work, in table 5 the
 542 relative errors in the value of the flutter derivatives H_1^* , H_2^* , H_3^* , A_1^* , A_2^* and A_3^* , for which
 543 experimental data are available, are reported. It must be borne in mind that the data for the lower
 544 reduced velocities cannot be identified from the charts in Scanlan and Tomko (1971) for some of
 545 the flutter derivatives.

546 The relative errors of the numerical values taking as reference the experimental values are
 547 evaluated according to the following formula:

$$e = \frac{|exp. value - num. value|}{|exp. value|} \quad (9)$$

548

549 Table 5. Relative errors in the evaluation of the flutter derivatives of the G1 section

| Flutter derivative | U_R | Present simulation | Larsen and Walther (1998) | Bai et al. (2010) |
|--------------------|-------|--------------------|---------------------------|-------------------|
| H_1^* | 2 | 0.14 | 0.67 | 0.50 |
| | 4 | 0.23 | 0.46 | 0.36 |
| | 6 | 0.30 | 0.40 | 0.38 |
| | 8 | 0.33 | 0.32 | 0.35 |
| | 10 | 0.29 | 0.37 | 0.33 |
| | 12 | 0.31 | 0.34 | 0.32 |
| H_2^* | 6 | 1.60 | 1.71 | 1.57 |
| | 8 | 1.03 | 1.29 | 1.04 |
| | 10 | 0.93 | 1.11 | 0.94 |
| | 12 | 0.87 | 1.05 | 0.85 |
| H_3^* | 6 | 0.54 | 0.50 | 0.60 |

1
2
3
4
5
6
7
8
9
10
11
12
13
14
15
16
17
18
19
20
21
22
23
24
25
26
27
28
29
30
31
32
33
34
35
36
37
38
39
40
41
42
43
44
45
46
47
48
49
50
51
52
53
54
55
56
57
58
59
60
61
62
63
64
65

| | | | | |
|---------|----|------|------|------|
| | 8 | 0.12 | 0.09 | 0.06 |
| | 10 | 0.06 | 0.02 | 0.16 |
| | 12 | 0.27 | 0.50 | 0.31 |
| A_1^* | 6 | 0.25 | 0.00 | 0.21 |
| | 8 | 0.16 | 0.33 | 0.16 |
| | 10 | 0.08 | 0.24 | 0.11 |
| | 12 | 0.15 | 0.26 | 0.13 |
| A_2^* | 2 | 0.95 | 2.00 | 1.50 |
| | 4 | 0.03 | 0.14 | 0.14 |
| | 6 | 0.09 | 0.56 | 0.25 |
| | 8 | 0.47 | 0.17 | 0.54 |
| | 10 | 0.81 | 0.19 | 0.88 |
| | 12 | 0.88 | 0.25 | |
| A_3^* | 6 | 0.04 | 0.10 | 0.13 |
| | 8 | 0.06 | 0.15 | 0.00 |
| | 10 | 0.13 | 0.05 | 0.16 |
| | 12 | 0.19 | 0.00 | 0.28 |

550

551 From table 5, it can be concluded that the accuracy of the three simulations is equivalent, being the
552 median of the relative errors 0.26 in the present simulation, and 0.33 and 0.32 in Larsen and
553 Walther (1998) and Bai et al. (2010). In this respect, it is notable how the approximated values
554 obtained using the proposed approach for the H_1^* and A_1^* flutter derivatives are comparable with the
555 values reported in Larsen and Walther (1998) and Bai et al. (2010) where the harmonic oscillations
556 in the heave degree of freedom were explicitly computed.

557 7. CONCLUDING REMARKS

558 In this article, the force coefficients and the flutter derivatives of an aspect ratio 4.9 rectangular
559 cylinder and a streamlined deck type G1 cross-section have been computed based on a 2D URANS
560 approach, applying Menter's $k-\omega$ SST turbulence model. A block structured mesh has been used
561 and the open source CFD solver OpenFOAM has been applied.

562 The static response of the rectangular cylinder at a 0° angle of attack has agreed well with the
563 experimental data in Schewe (2009), the RSM simulation in Ribeiro (2011) and sophisticated 2D
564 numerical simulations where the Boussinesq assumption is substituted by an EARSM approach
565 (Mannini et al., 2011).

566 For the G1 section, the influence of the spatial and temporal discretisations in the numerical results
567 has been studied. Since both experimental and numerical results of the force coefficients and flutter
568 derivatives are available in the literature for this particular cross-section, the current computational
569 results have been validated against the experimental ones and also the accuracy of the simulations
570 reported herein can be compared with CFD results published by other researchers.

571 The distribution of the time-averaged pressure coefficient around the G1 section agrees well with
572 experimental data available in the literature for similar geometries. The force coefficients of the
573 deck cross-section for angles of attack in the range -10° and $+10^\circ$ have been obtained. It has been

574 found that they are in good agreement with the experimental and numerical data in Reinhold et al.
575 (1992) and Bai et al. (2010).

576 A notable contribution of this work has been the application of the existing formulae relating the
577 flutter derivatives (Tubino, 2005) in a CFD based approach. This has allowed the computer
578 demands of this burdensome problem to be reduced. The pitch-related flutter derivatives have been
579 extracted from the pitch forced oscillation simulations while the heave-related ones have been
580 estimated using the expressions in the literature. For the two cases studied a very good agreement
581 with the experimental flutter derivatives has been found, and at least comparable accuracy with
582 other numerical simulations where both pitch and heave forced oscillations had been numerically
583 computed.

584 This work can be considered a step forward towards the routine use of CFD based techniques in the
585 aerodynamic and aeroelastic design of long span bridges since it has been demonstrated the
586 adequacy of the computational results using an efficient 2D approach. Furthermore it ~~but~~ is also a
587 step forward in the application of numerical optimization techniques in the shape design of bridges,
588 for which efficient, reliable and computational non-cumbersome CFD techniques are a must. In this
589 respect, a fully computational approach for the evaluation of force coefficients and flutter
590 derivatives, as the one reported herein, is required for the application of numerical optimization
591 techniques.

592 8. ACKNOWLEDGMENTS

593 This work has been mainly funded by the Spanish Ministry of Education, Culture and Sport under
594 the Human Resources National Mobility Program of the R-D+i National Program 2008-2011,
595 extended by agreement of the Cabinet Council on October 7th 2011. It has also been partially
596 financed by the Galician Government (including FEDER funding) with reference GRC2013-056
597 and by the Spanish Minister of Economy and Competitiveness (MINECO) with reference
598 DPI2013-41893-R. The authors fully acknowledge the support received.

599 The authors are grateful for access to the University of Nottingham High Performance Computing
600 Facility and the Breogán Cluster at the University of La Coruña.

601 REFERENCES

- 602 Bai, Y., Sun, D., Lin, J. (2010) Three dimensional numerical simulations of long-span bridge
603 aerodynamics using block-iterative coupling and DES. *Computers and Fluids*; 39, 1549-1561.
- 604 Bartoli, G., Mannini, C. (2008) A simplified approach to bridge deck flutter. *Journal of Wind
605 Engineering and Industrial Aerodynamics*; 96, 229-256.
- 606 Brar, P.S., Raul, R., Scanlan, R.H. (1996) Numerical calculation of flutter derivatives via indicial
607 functions. *Journal of Fluids and Structures*; 10, 337-351.
- 608 Braun, A.L., Awruch, A.M. (2003) Numerical simulation of the wind action on a long-span bridge
609 deck. *Journal of the Brazilian Society of Mechanical Sciences and Engineering*; 25(4), 352-
610 363.
- 611 Bruno, L., Canuto, C., Fransos, D. (2009) Stochastic aerodynamics and aeroelasticity of a flat plate
612 via generalized Polynomial Chaos. *Journal of Fluids and Structures*; 25, 1158-1176.
- 613 Bruno, L., Fransos, D. (2008) Evaluation of Reynolds number effects on flutter derivatives of a flat
614 plate by means of a computational approach. *Journal of Fluids and Structures*; 24, 1058-1076.
- 615 Bruno, L., Fransos, D., Coste, N., Bosco, A. (2010) 3D flow around a rectangular cylinder: a
616 computational study. *Journal of Wind Engineering and Industrial Aerodynamics*; 98, 263-276.

- 617 Bruno, L., Khris, S. (2003) The validity of 2D numerical simulations of vortical structures around a
618 bridge deck. *Mathematical and Computer Modelling*; 37, 795-828.
- 619 Bruno, L., Khris, S., Marcillat, J. (2001) Numerical simulation of the effect of section details and
620 partial streamlining on the aerodynamics of bridge decks. *Wind and Structures*; 4(4), 315-332.
- 621 Bruno, L., Salvetti, M.V., Ricciardelli, F. (2014) Benchmark on the aerodynamics of a rectangular
622 5:1 cylinder: an overview after the first four years of activity. *Journal of Wind Engineering and*
623 *Industrial Aerodynamics*; 126, 87-106.
- 624 Brusiani, F., de Miranda, S., Patruno, L., Ubertini, F., Vaona, P. (2013) On the evaluation of bridge
625 deck flutter derivatives using RANS turbulence models. *Journal of Wind Engineering and*
626 *Industrial Aerodynamics*; 119, 39-47.
- 627 Chen, X., Kareem, A. (2002) Advances in modeling of aerodynamic forces on bridge decks.
628 *Journal of Engineering Mechanics*; 128, 1193-1205.
- 629 Davenport, A.G., King, J.P.C., Larose, G.L. (1992) Taut strip model tests. In: Larsen, A. (Ed.),
630 *Proceedings of the 1st International Symposium on Aerodynamics of Large Bridges*,
631 Copenhagen, Denmark.
- 632 Donea, J., Huerta, A., Ponthot, J.Ph., Rodríguez-Ferrán, A. (2004) Arbitrary Lagrangian-Eulerian
633 methods. In *Encyclopedia of Computational Mechanics*. Vol 1: Fundamentals. Stein, E., de
634 Borst, R, Hughes, J.R. (Eds.). John Wiley & Sons, Ltd.
- 635 Frandsen, J.B. (2004) Numerical bridge deck studies using finite elements. Part I: flutter. *Journal of*
636 *Fluids and Structures*; 19, 171-191.
- 637 Fransos, D., Bruno, L. (2006) Determination of the aeroelastic transfer functions for streamlined
638 bodies by means of a Navier-Stokes solver. *Mathematical and Computer Modelling*; 43, 506-
639 529.
- 640 Fransos, D., Bruno, L. (2010) Edge degree-of-sharpness and free-stream turbulence scale effects on
641 the aerodynamics of a bridge deck. *Journal of Wind Engineering and Industrial Aerodynamics*;
642 98, 661-671.
- 643 Ge, Y.J., Xiang, H.F. (2008) Computational models and methods for aerodynamic flutter of long-
644 span bridges. *Journal of Wind Engineering and Industrial Aerodynamics*; 96, 1912-1924.
- 645 Holmes, J.D. (2007) *Wind loading of structures*. 2nd Edition. Taylor and Francis.
- 646 Huang, L., Liao, H., Wang, B., Li, Y. (2009) Numerical simulation for aerodynamic derivatives of
647 bridge deck. *Simulation Modelling Practice and Theory*; 17, 719-729.
- 648 Jasak, H, Rusche, H. (2009) Dynamic mesh handling in OpenFOAM. In: Fourth OpenFOAM
649 workshop. Montreal, Canada.
- 650 Jeong, U.Y., Kwon, S. (2003) Sequential numerical procedures for predicting flutter velocity of
651 bridge sections. *Journal of Wind Engineering and Industrial Aerodynamics*; 91, 291-305.
- 652 Larose, G.L. (1992) The response of a suspension bridge deck to turbulent wind: the taut-strip
653 model approach. M. Eng. Sc., The University of Western Ontario.
- 654 Larsen, A., Walther, J.H. (1998) Discrete vortex simulation of flow around five generic bridge deck
655 sections. *Journal of Wind Engineering and Industrial Aerodynamics*; 77-78, 591-602.
- 656 Lesieur, D., Reithel, P., Dillenius, M. (1994) A practical approach for calculating
657 aerodynamic indicial functions with Navier-Stokes solver. AIAA 94-0059.
- 658 Löhner, R. (2008) *Applied computational fluid dynamics techniques: an introduction based on*
659 *finite element methods (2^o Edition)*. John Wiley & Sons Ltd.
- 660 Mannini, C., Soda, A., Schewe, G. (2010) Unsteady RANS modeling of flow past a rectangular
661 cylinder: investigation of Reynolds number effects. *Computers and Fluids*; 30, 1609-1624.
- 662 Mannini, C., Soda, A., Schewe, G. (2011) Numerical investigation on the three-dimensional
663 unsteady flow past a 5:1 rectangular cylinder. *Journal of Wind Engineering and Industrial*
664 *Aerodynamics*; 99, 469-482.

- 665 Mannini, C., Soda, A., Voß, R., Schewe, G. (2010) Unsteady RANS simulation of flow around a
666 bridge section. *Journal of Wind Engineering and Industrial Aerodynamics*; 98, 742-753.
- 667 Matsumoto, M. (1996) Aerodynamic damping of prisms. *Journal of Wind Engineering and*
668 *Industrial Aerodynamics*; 59, 159-175.
- 669 Mendes, P.A., Branco, F.A. (1998) Numerical wind studies for the Vasco da Gama Bridge,
670 Portugal. *Structural Engineering International*; 8(2), 124-128.
- 671 Menter, F., Esch, T. (2001) Elements of industrial heat transfer prediction. 16th Brazilian Congress
672 of Mechanical Engineering.
- 673 Morgenthal, G., McRobie, A. (2002) A comparative study of numerical methods for fluid-structure
674 interaction analysis in long-span bridge design. *Wind and Structures*; 5(2-4), 101-114.
- 675 Oliver, A. (2009) Mesh motion alternatives in OpenFOAM. PhD course in CFD with OpenSource
676 software project report. http://www.tfd.chalmers.se/~hani/kurser/OS_CFD_2009/. Accessed
677 July, 18th 2014.
- 678 Reinhold, T.A., Brinch, M., Damsgaard, A. (1992) Wind tunnel tests for the Great Belt Link. In:
679 Larsen, A. (Ed.), *Proceedings of the 1st International Symposium on Aerodynamics of Large*
680 *Bridges*, Copenhagen, Denmark.
- 681 Ribeiro, A.F.P. (2011) Unsteady RANS modeling of flow past a rectangular 5:1 cylinder:
682 investigation of edge sharpness effects. In: *Proc. of the 13th International Conference on Wind*
683 *Engineering*, Amsterdam, The Netherlands.
- 684 Sarkar, P.P., Caracoglia, L., Haan Jr., F.L., Sato, H., Murakoshi, J. (2009) Comparative and
685 sensitivity study of flutter derivatives of selected bridge deck sections, Part 1: analysis of inter-
686 laboratory experimental data. *Engineering Structures*; 31, 158-169.
- 687 Sarkic, A., Fisch, R., Hoffer, R. Bletzinger, K. (2012) Bridge flutter derivatives based on
688 computed, validated pressure fields. *Journal of Wind Engineering and Industrial*
689 *Aerodynamics*; 104-106, 141-151.
- 690 Sarkic, A., Hoffer, R. (2013) Improved numerical simulation of bridge deck aeroelasticity by
691 model validation. In: *Proceedings of the Sixth European-African Conference on Wind*
692 *Engineering*. Cambridge, UK.
- 693 Sarwar, M.W., Ishihara, T., Shimada, K., Yamasaki, Y., Ikeda, T. (2008) Prediction of
694 aerodynamic characteristics of a box girder bridge section using the LES turbulence model.
695 *Journal of Wind Engineering and Industrial Aerodynamics*; 96, 1895-1911.
- 696 Scanlan, R.H., Jones, N.P., Singh, L. (1997) Inter-relations among flutter derivatives. *Journal of*
697 *Wind Engineering and Industrial Aerodynamics*; 69-71, 829-837.
- 698 Scanlan, R.H., Tomko, J.J. (1971) Airfoil and bridge deck flutter derivatives. *Journal of the*
699 *Engineering Mechanics Division*. EM6, 1717-1737.
- 700 Schewe, G. (2009) Reynolds-number-effects in flow around a rectangular cylinder with aspect ratio
701 1:5. In: Borri, C., Augusti, G., Bartoli, G., Gacchini, L. (Eds.) *Proceedings of the Fifth*
702 *European and African Conference on Wind Engineering*. Firenze University Press, Florence,
703 Italy.
- 704 Scruton, C. (1981) *An introduction to wind effects on structures*. Oxford University Press.
- 705 Shimada, K., Ishihara, T. (2012) Predictability of unsteady two-dimensional k-ε model on the
706 aerodynamic instabilities of some rectangular prisms. *Journal of Fluids and Structures*; 28, 20-
707 39.
- 708 Simiu, E., Scanlan, R.H. (1996) *Wind effects on structures*. 3rd Edition; John Wiley & Sons, Inc.
- 709 Starossek, U., Aslan, H., Thiesemann, L. (2009) Experimental and numerical identification of
710 flutter derivatives for nine bridge deck sections. *Wind and Structures*; 12, 519-540.

1 711 Tubino, F. (2005) Relationships among aerodynamic admittance functions, flutter derivatives and
2 712 static coefficients for long-span bridges. *Journal of Wind Engineering and Industrial*
3 713 *Aerodynamics*; 93, 929-950.
4 714 Vairo, G. (2003) A numerical model for wind loads simulation on long-span bridges. *Simulation*
5 715 *Modelling Practice and Theory*; 11, 315-351.
6 716 Wilcox, D.C. (2006) *Turbulence modeling for CFD*. 3rd Edition; DCW Industries, Inc.
7 717 Xiang, H., Ge, Y. (2002) Refinements on aerodynamic stability analysis of super long-span
8 718 bridges. *Journal of Wind Engineering and Industrial Aerodynamics*; 90, 1493-1515.
9 719 Zhu, Z., Gu, M. (2014) Identification of flutter derivatives of bridge decks using CFD-based
10 720 discrete-time aerodynamic models. *Wind and Structures*; 18(3), 215-233.
11 721 Zhu, Z., Chen, Z., Gu, M (2009) CFD based simulations of flutter characteristics of ideal thin
12 722 plates with and without central slot. *Wind and Structures*; 12(1), 1-19.
13 723 Zhu, Z., Gu, M., Chen, Z. (2007) Wind tunnel and CFD study on identification of flutter
14 724 derivatives of a long-span self-anchored suspension bridge. *Computer-Aided Civil and*
15 725 *Infrastructure Engineering*; 22, 514-554.
16
17
18
19
20
21
22
23
24
25
26
27
28
29
30
31
32
33
34
35
36
37
38
39
40
41
42
43
44
45
46
47
48
49
50
51
52
53
54
55
56
57
58
59
60
61
62
63
64
65

1 **BRIDGE DECK FLUTTER DERIVATIVES: EFFICIENT NUMERICAL EVALUATION**
2 **EXPLOITING THEIR INTERDEPENDENCE.**

3 F. Nieto^a, J.S. Owen^b, D.M. Hargreaves^b & S. Hernández^a

4 ^a *School of Civil Engineering, University of A Coruña, Spain*

5 ^b *Faculty of Engineering, University of Nottingham, UK*

6
7 **ABSTRACT**

8 Increasing the efficiency in the process to numerically compute the flutter derivatives of bridge
9 deck sections is desirable to advance the application of CFD based aerodynamic design in
10 industrial projects. In this paper, a 2D unsteady Reynolds-averaged Navier-Stokes (URANS)
11 approach adopting Menter's SST $k-\omega$ turbulence model is employed for computing the flutter
12 derivatives and the static aerodynamic characteristics of two well known examples: a rectangular
13 cylinder showing a completely reattached flow and the generic G1 section representative of
14 streamlined deck sections. The analytical relationships between flutter derivatives reported in the
15 literature are applied with the purpose of halving the number of required numerical simulations for
16 computing the flutter derivatives. The solver of choice has been the open source code OpenFOAM.
17 It has been found that the proposed methodology offers results which agree well with the
18 experimental data and the accuracy of the estimated flutter derivatives is similar to the results
19 reported in the literature where the complete set of numerical simulations has been performed for
20 both heave and pitch degrees of freedom.

21
22 **KEYWORDS:** Computational fluid dynamics, bluff body aerodynamics, flutter derivatives,
23 rectangular cylinder, streamlined deck sections.

24
25 **1. INTRODUCTION**

26 Long span bridges are prone to aeroelastic phenomena such as vortex induced vibrations, flutter or
27 buffeting. In fact, safety against flutter instability is one of the fundamental requirements in long
28 span bridge design. If the wind speed exceeds the critical flutter speed of the structure, self-excited
29 oscillations of the deck would rapidly amplify causing the collapse of the bridge.

30 The most widely used method for the identification of the flutter critical wind speed is Scanlan's
31 approach, developed in the 1970s (Scanlan and Tomko, 1971), where a set of semi-empirical
32 functions, named flutter derivatives, must be identified in order to define the motion-induced
33 aerodynamic load acting on the bridge deck (Bartoli and Mannini, 2008). Traditionally, the
34 identification of flutter derivatives has been conducted by means of wind tunnel tests of sectional
35 models of bridge decks. The application in recent years of numerical methods in the identification
36 of flutter derivatives aims at avoiding expensive and cumbersome experimental campaigns which
37 are the standard approach in industrial applications currently.

38 In Computational Fluid Dynamics (CFD) modeling the flutter derivatives identification can be
39 done following two different approaches (Fransos and Bruno, 2006). The first one requires the
40 simulation of the forced harmonic oscillations in pitch and heave degrees of freedom. Then, the
41 flutter derivatives are identified from the amplitude and phase relationships between the imposed
42 displacement and the induced aeroelastic forces. The second method, based on indicial theory,

43 requires simulating an abrupt displacement of the body immersed in the flow, which causes non-
44 stationary forces. The flutter derivatives can then be computed from the ratio between the Fourier
45 transforms of the step-response non-stationary forces and the prescribed step-input displacement.
46 The methodology, based on the simulation of forced oscillations, has been, by far, more widely
47 used than the one based on the indicial approach despite the apparent efficiency of the indicial
48 function approach.

49 Focusing on applications of the harmonic forced oscillations approach, the trend in the 1990's and
50 early 2000's has been developing in-house CFD solvers based on the finite-difference, finite
51 element, finite volume or discrete vortex methods. The references in the literature are numerous
52 and some examples, without intending to be exhaustive are: Mendes and Branco (1998), Larsen
53 and Walther (1998), Morgenthal and McRobie (2002), Xiang and Ge (2002), Vairo (2003), Jeong
54 and Kwon (2003), Frandsen (2004), Zhu et al. (2007) and Zhu et al. (2009). Developing in-house
55 software has obviously been a barrier for the application of numerical methods in industrial bridge
56 design problems due to its scientific complexity and the required labor and financial resources.
57 Therefore more recently the focus has been put on applying general purpose commercial finite
58 volume solvers in bridge aerodynamics problems. An early application was authored by Bruno et
59 al. (2001) who used FLUENT for studying the aerodynamic response of a static box deck and the
60 effect of section details such as fairings and barriers. Fluid-structure interaction problems have
61 been addressed more recently. In Ge and Xiang (2008) both in-house solvers and the commercial
62 code FLUENT are applied, depending on the chosen approach for turbulence modeling. Sarwar et
63 al. (2008) obtained the flutter derivatives of a bridge deck section and high aspect ratio rectangular
64 cylinders by means of 3D Large Eddy Simulation (LES) using FLUENT. Huang et al. (2009) also
65 used FLUENT to compute the flutter derivatives of the Great Belt Bridge and the Sutong Yangtze
66 cable-stayed bridge. Starossek et al. (2009) employed the commercial software COMET to obtain
67 the flutter derivatives of 31 different bridge sections, including experimental validation for a subset
68 of 9 sections tested in a water tunnel. Bai et al. (2010) used a combination of in-house code and
69 ANSYS-CFX commercial software for computing force coefficients and flutter derivatives of
70 various 3D deck sections. Huang and Liao (2011) used FLUENT to simulate forced oscillations of
71 a flat plate and a bridge deck containing a linear combination of a set of frequencies. Also, Brusiani
72 et al. (2013) employed FLUENT to compute the flutter derivatives of the Great Belt Bridge using a
73 different turbulence model than Huang and co-workers. Of particular interest is the growing use of
74 open source general CFD solvers. In Sarkic et al. (2012), the open source code OpenFOAM is
75 applied to numerically replicate the wind tunnel test for identifying the force coefficients and flutter
76 derivatives of a box deck cross-section. A more recent application by some of the authors of the
77 former reference can be found in Sarkic and Höffer (2013) where the LES turbulence model is
78 applied to the same box deck.

79 **CFD** applications based on indicial functions are scarce in spite of its potential. In Bruno and
80 Fransos (2008) it has been remarked that in this method just a single simulation for each degree of
81 freedom is required to identify the complete set of flutter derivatives and that only the transient
82 flow needs to be simulated. Thus, this approach is less demanding in computational resources than
83 the classical forced oscillation based method. On the other hand, the problem is particularly
84 challenging from the CFD simulation perspective. Early applications are Lesieutre et al. (1994)
85 who simulated the motion of a wing in the frame of an application to aircraft manoeuvres and Brar
86 et al. (1996) who applied the Finite Element Method to obtain the flutter derivatives of an airfoil
87 and a rectangular cylinder. ~~The method~~ **A modified smoothed indicial approach** was further
88 developed in Fransos and Bruno (2006) and Bruno and Fransos (2008) who used FLUENT to

89 obtain the flutter derivatives of a flat plate of finite thickness and studied also the effect of the
90 Reynolds number on the flutter derivatives. The indicial approach has also been applied in the
91 frame of a probabilistic study of the aerodynamic and aeroelastic responses of a flat plate (Bruno et
92 al, 2009). More recently Zhu and Gu (2014) have presented a method to extract the flutter
93 derivatives of **streamlined** bridge decks, **even if the application of the modified indicial approach to**
94 **bluff bodies remains questionable.** ~~The approach is based on imposing, by means of a smooth~~
95 ~~exponential function, heave or pitch motions on the deck for the identification of the aerodynamic~~
96 ~~system and the subsequent system simulation to obtain lift and moment forces under harmonic~~
97 ~~oscillation.~~

98 From the previous review of the state of the art regarding applications of CFD in the design of long
99 span bridges, the main reasons why numerical simulations are not being generally applied in bridge
100 design in the industry to complement wind tunnel tests need to be discussed. Developing and
101 upgrading in-house software is a complex task and requires highly skilled personnel and substantial
102 funding. Consequently it can only be achieved by a small number of organizations in the world.
103 The increasing use of commercial software in recent years is making it easier to access the required
104 technology. However, the cost of licenses, particularly for running massively parallel simulations,
105 in many cases prevents the extensive use of CFD in design problems. This circumstance has made
106 particularly appealing the use of open source solvers for both industry and academia, and open
107 source software has already been applied in bridge design problems. Besides this, the increasing
108 number of published successful simulations in bridge related problems means that CFD techniques
109 are nowadays more mature and therefore more robust and reliable.

110 In spite of the dramatic improvements in computational power and access to cluster technology of
111 recent years, the computer power demands linked with modeling complex fluid-structure
112 interaction problems remains a key issue. In this respect, any method or technique which allows
113 decreasing computational demands would facilitate incorporating CFD based design in bridge
114 engineering design. A number of researchers have proposed explicit relationships between flutter
115 derivatives which have proved to be reliable for streamlined bridge decks such as Matsumoto
116 (1996), Scanlan et al. (1997), Chen and Kareem (2002) or Tubino (2005). The application of these
117 formulae allows the number of computer simulations for obtaining the flutter derivatives to be
118 reduced to just half of the number required following the standard approach based on forced
119 harmonic vibrations in heave and pitch degrees of freedom. To the authors' knowledge the
120 aforementioned approach has not been applied in CFD-based studies to date.

121 The aim of the current piece of research is to propose a cost effective, and therefore efficient,
122 computer based approach for obtaining force coefficients and flutter derivatives of bridge deck box
123 sections which could be used in industrial applications where the shape of different bridge deck
124 designs could be numerically optimized. Consequently, a 2D URANS strategy is proposed, using
125 the general purpose open source CFD solver OpenFOAM v2.1.1 in combination with the explicit
126 relationships between flutter derivatives mentioned above. The more demanding 3D Detached
127 Eddy Simulation (DES) or LES approaches, in spite of their superior accuracy, have not been
128 considered in this work since they would pose additional challenges in terms of higher computer
129 power demands and model setup.

130 A rectangular cylinder showing a **separated and reattached** ~~fully attached~~ **time-averaged** flow
131 pattern has been selected as one of the case studies for the computation of the flutter derivatives. In
132 particular, a ratio $B/H=4.9$ rectangular cylinder (B is the prism width and H is the height) was
133 chosen in order to replicate an existing sectional model at the wind tunnel of the University of

134 Nottingham. In the literature, the number of published references, both experimental and
135 computational, dealing with the response of $B/H=5$ rectangular cylinders is plentiful, to a great
136 extent thanks to the BARC initiative (Bruno et al. 2014). Taking into account the expected minimal
137 differences between the aerodynamic response of $B/H=4.9$ and $B/H=5$ rectangular cylinders, for the
138 sake of the efficiency of means in research, the authors have considered that the existing literature
139 on 5:1 rectangular cylinders is adequate for the validation of the force coefficients and the flutter
140 derivatives of the $B/H=4.9$ rectangular cylinder at 0° angle of attack. ~~However, in case that further~~
141 ~~numerical studies were conducted, for which experimental data would not be available, they could~~
142 ~~be readily validated by means of wind tunnel tests to be conducted using the existent $B/H=4.9$~~
143 ~~sectional model. However, in the case that additional numerical studies would require validation~~
144 ~~against experimental data outside the range found in the literature, further wind tunnel tests could~~
145 ~~readily be conducted using the existing $B/H=4.9$ sectional model.~~

146 The second application case has been the G1 generic box section described in Scanlan and Tomko
147 (1971) and Larsen and Walther (1998). The modern practice in long span bridge design has
148 incorporated box deck cross-sections as the most common choice for these challenging structures.
149 There are several reasons for this: a good aerodynamic and aeroelastic response characteristic of
150 streamlined cross-sections, high torsional stiffness, construction economy and, in many cases,
151 superior aesthetic value compared to truss girders. Recent examples of applications comprising box
152 decks are the Forth Replacement Crossing in the United Kingdom, the Normandy Bridge and
153 Millau Viaduct, in France, the Sutong Bridge in China or the Russky Bridge in Russia, amongst
154 many others.

155 In the first part of this paper, the fundamental formulation and the numerical approach adopted,
156 along with the computational models, for simulating the aerodynamic response of the bridge decks
157 are explained. Then, the results of the study of the sensitivity of the solution to the spatial and
158 temporal discretisations for the G1 generic section are summarized. Next the aerodynamic
159 characteristics of the static $B/H=4.9$ rectangular cylinder are analyzed based on the values of the
160 Strouhal number, force coefficients and the distribution of the averaged pressure coefficient and its
161 standard deviation. Then the flutter derivatives of the rectangular cylinder, where the relationships
162 between flutter derivatives have been applied, are reported and compared with wind tunnel data. It
163 follows the analysis of the characteristics of the static G1 section based on force coefficients and
164 the distribution of the averaged pressure coefficient. The results section ends with the report of the
165 flutter derivatives of the G1 section and the corresponding comparison with experimental and other
166 numerical data in the literature. Finally, conclusions are drawn from the work reported herein.

167 2. NUMERICAL FORMULATION

168 The flow around the bluff bodies of interest is modeled by means of the unsteady Reynolds-
169 averaged Navier-Stokes equations considering incompressible flow. A 2D URANS approach has
170 been preferred which, according to Brusiani et al. (2013), is equivalent to imposing the perfect
171 correlation of the flow structures in the span-wise direction.

172 The time averaging of the equations for conservation of mass and momentum gives the Reynolds
173 averaged equations of motion in conservative form. According to Wilcox (2006):

174

$$\frac{\partial U_i}{\partial x_i} = 0 \quad (1.a)$$

$$\rho \frac{\partial U_i}{\partial t} + \rho U_j \frac{\partial U_i}{\partial x_j} = -\frac{\partial P}{\partial x_i} + \frac{\partial}{\partial x_j} (2\mu S_{ij} - \rho \overline{u'_i u'_j}) \quad (1.b)$$

175

176

177

178

179

where U_i is the mean velocity vector, x_i is the position vector, t is the time, ρ is the fluid density, assumed constant, u'_i is the fluctuating velocity and the overbar represents the time average, P is the mean pressure, μ is the fluid viscosity and S_{ij} is the mean strain-rate tensor. From the above equation, the specific Reynolds stress tensor is defined as:

$$\tau_{ij} = -\overline{u'_i u'_j} \quad (2)$$

180

181

182

which is an additional unknown to be modeled based on the Boussinesq assumption for one and two equation turbulence models (Wilcox, 2006).

$$\tau_{ij} = 2\nu_T S_{ij} - \frac{2}{3}k\delta_{ij} \quad (3)$$

183

184

185

where ν_T is the kinematic eddy viscosity, S_{ij} is the mean strain-rate tensor and k is the turbulent kinetic energy per unit mass.

186

187

In this work the closure problem is solved applying Menter's $k-\omega$ SST model for incompressible flows, reported in Menter and Esch (2001).

188

189

190

191

For the simulations where forced oscillations of the bluff body have been imposed, the Arbitrary Lagrangian Eulerian (ALE) formulation has been applied for allowing movements of the mesh inside the computational domain. The conservation of mass and momentum equations are written as follows (Bai et al., 2010, Sarkic et al., 2012):

$$\frac{\partial(U_i - U_{gi})}{\partial x_i} = 0 \quad (4.a)$$

$$\rho \frac{\partial U_i}{\partial t} + \rho U_j \frac{\partial(U_i - U_{gi})}{\partial x_j} = -\frac{\partial P}{\partial x_i} + \frac{\partial}{\partial x_j} (2\mu S_{ij} - \rho \overline{u'_i u'_j}) \quad (4.b)$$

192

193

where U_{gi} is the grid velocity in the i -th direction.

194

195

3. FORCE COEFFICIENTS AND FLUTTER DERIVATIVES COMPUTATION BY MEANS OF FORCED OSCILLATION SIMULATIONS

196

The definition of the force coefficients considered in this study is given in (5):

$$C_d = \frac{D}{\frac{1}{2}\rho U^2 B} \quad C_l = \frac{L}{\frac{1}{2}\rho U^2 B} \quad C_m = \frac{M}{\frac{1}{2}\rho U^2 B^2} \quad (5)$$

197

198

199

200

In the former expressions D is the drag force per span length, positive in the windward direction, L is the lift force per span length, positive upwards, and M is the pitching moment per span length, positive clockwise, ρ is the fluid density, U is the flow speed and B is the bluff body width.

Flutter derivatives are semi-empirical parameters which relate motion-induced forces and with the displacements of the structure and their time derivative. These parameters have traditionally been identified using wind tunnel tests, but more recently, numerical based simulations have been applied.

According to Simiu and Scanlan (1996), the aeroelastic forces on a bridge deck, considering two degrees of freedom (heave and pitch), can be written as follows:

$$L_{ae} = \frac{1}{2}\rho U^2 B \left[KH_1^* \frac{\dot{h}}{U} + KH_2^* \frac{B\dot{\alpha}}{U} + K^2 H_3^* \alpha + K^2 H_4^* \frac{h}{B} \right] \quad (6.a)$$

$$M_{ae} = \frac{1}{2}\rho U^2 B^2 \left[KA_1^* \frac{\dot{h}}{U} + KA_2^* \frac{B\dot{\alpha}}{U} + K^2 A_3^* \alpha + K^2 A_4^* \frac{h}{B} \right] \quad (6.b)$$

207

where L_{ae} is the aeroelastic force per unit of span length, M_{ae} is the aeroelastic moment per unit of span length, ρ is the fluid density, U is the flow speed, $K = (B\omega)/U$ is the reduced frequency, B is the deck width, ω the circular frequency of oscillation, h is the heave displacement, α is the torsional rotation, \dot{h} and $\dot{\alpha}$ are the time derivatives and H_i^* and A_i^* ($i = 1, \dots, 4$) are the flutter derivatives.

Assuming prescribed harmonic forced oscillations $h = h_0 e^{i\omega t}$ and $\alpha = \alpha_0 e^{i\omega t}$, where h_0 and α_0 are the amplitudes of the oscillations, and also that motion-induced forces are linear functions of the movement; after some manipulation, the following expressions are obtained for the identification of the flutter derivatives:

$$H_1^* = -\left(\frac{U}{Bf}\right)^2 \frac{C_l \sin \varphi_{L-h}}{(2\pi)^2 h_0/B} \quad (7.a) \quad A_1^* = -\left(\frac{U}{Bf}\right)^2 \frac{C_m \sin \varphi_{M-h}}{(2\pi)^2 h_0/B} \quad (7.e)$$

$$H_2^* = -\left(\frac{U}{Bf}\right)^2 \frac{C_l \sin \varphi_{L-\alpha}}{(2\pi)^2 \alpha_0} \quad (7.b) \quad A_2^* = -\left(\frac{U}{Bf}\right)^2 \frac{C_m \sin \varphi_{M-\alpha}}{(2\pi)^2 \alpha_0} \quad (7.f)$$

$$H_3^* = \left(\frac{U}{Bf}\right)^2 \frac{C_l \cos \varphi_{L-\alpha}}{(2\pi)^2 \alpha_0} \quad (7.c) \quad A_3^* = \left(\frac{U}{Bf}\right)^2 \frac{C_m \cos \varphi_{M-\alpha}}{(2\pi)^2 \alpha_0} \quad (7.g)$$

$$H_4^* = \left(\frac{U}{Bf}\right)^2 \frac{C_l \cos \varphi_{L-h}}{(2\pi)^2 h_0/B} \quad (7.d) \quad A_4^* = \left(\frac{U}{Bf}\right)^2 \frac{C_m \cos \varphi_{M-h}}{(2\pi)^2 h_0/B} \quad (7.h)$$

217

where φ_{L-h} , $\varphi_{L-\alpha}$, φ_{M-h} and $\varphi_{M-\alpha}$ are the phase lags of the fluctuating aeroelastic lift and moment with respect to the heave and pitch harmonic oscillations and C_l and C_m are the amplitudes of the non-dimensional aeroelastic lift and moment.

It must be borne in mind that in Larsen and Walther (1998), whose results are used later for validation, the flutter derivatives are computed dividing equations (7.a) to (7h.) by 2.

223 4. RELATIONSHIPS BETWEEN FLUTTER DERIVATIVES

As mentioned in the introduction, a number of publications can be found in the literature reporting several relationships amongst flutter derivatives. Tubino (2005) has derived the following relationships between heave-related and pitch-related flutter derivatives assuming the linear formulation hypothesis for the self-excited forces:

227

$$H_1^*(K) = KH_3^*(K) - \frac{C_d}{K} \quad (8.a)$$

$$A_1^*(K) = KA_3^*(K) \quad (8.c)$$

$$H_4^*(K) = -KH_2^*(K) \quad (8.b)$$

$$A_4^*(K) = -KA_2^*(K) \quad (8.d)$$

The above equations are similar to the ones reported by Matsumoto (1996) apart from the (H_1^*, H_3^*) relationship, that does not consider the term containing the drag coefficient. For streamlined sections with low drag coefficient its contribution is nearly negligible.

Experimental validation of the former relationships reported in Tubino (2005), has shown that the relationships between (H_1^*, H_3^*) and (A_1^*, A_3^*) were satisfied for all the cases considered while the relationships between (H_2^*, H_4^*) and (A_2^*, A_4^*) were closely verified for streamlined deck cross-sections, since minor discrepancies are identified between experimental realizations and the approximated values. In Matsumoto (1996), the reported relationships between flutter derivatives are confirmed for rectangular cylinders less affected by vortex generation, proposing as a reference lower bound a 5:1 ratio.

5. GEOMETRY AND COMPUTER MODELING

Two different geometries have been considered as case studies in the present work: a $B/H=4.9$ rectangular cylinder (H is the section depth or height), and the generic G1 deck section, described in Larsen and Walther (1998), representative of streamlined box decks.

5.1. $B/H=4.9$ rectangular cylinder

Figure 1 shows the layout of the flow domain and boundary conditions employed in the rectangular cylinder simulations. The flow domain considered for the rectangular cylinder case is $40.8B$ by $30B$ similar to the size employed in successful simulations by other researchers such as Fransos and Bruno (2010).

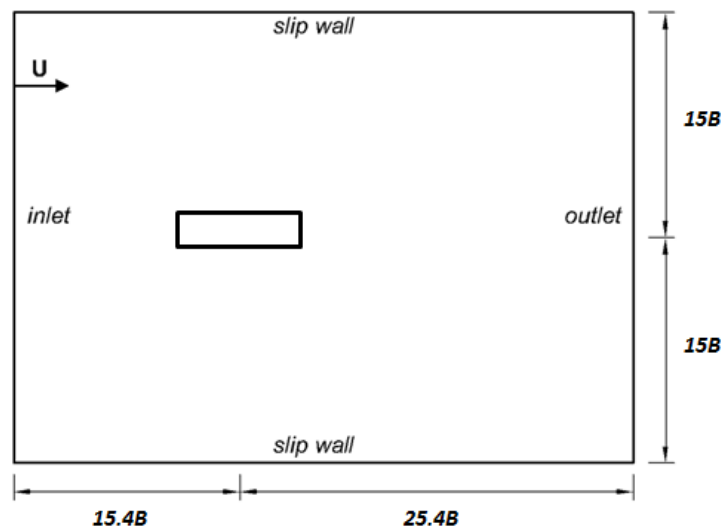


Figure 1. Flow domain definition and boundary conditions for the $B/H=4.9$ rectangular cylinder (not to scale).

A constant velocity inlet has been set at the upwind boundary (the left side in the figure) of the computational domain. The incoming flow has a turbulence intensity of 1 % along with a $0.1B$ turbulent length scale as per Ribeiro (2011). As boundary conditions, a constant velocity inlet has

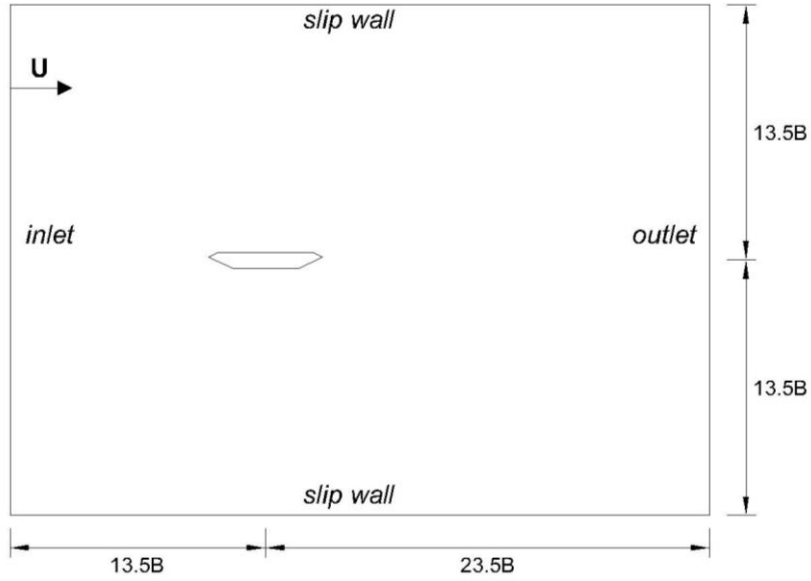
253 ~~been set at the left side of the rectangular fluid domain. Turbulence intensity of 1% has been~~
254 ~~chosen, along with a $0.1B$ turbulent length scale for the incoming flow as in Ribeiro (2011). A~~
255 ~~pressure outlet at atmospheric pressure has been imposed at the right side (see figure 1). The upper~~
256 ~~and lower boundaries have been defined as slip walls. The corners of the prism have been modeled~~
257 ~~as sharp and its walls are defined as non-slip. When the rectangular cylinder is forced to oscillate~~
258 ~~the resultant velocity field around the rectangular cylinder wall is corrected, so that the velocity of~~
259 ~~the flow at the moving boundary is equal to the mesh velocity and therefore no flux across the wall~~
260 ~~takes place. The same boundary conditions have been applied in the G1 section case.~~

261 The numerical schemes adopted in the simulations reported herein are summarized next. The
262 interpolation of values from the cell centers to face centers is done using a linear scheme. The
263 gradient terms are discretised using the Gauss scheme with a linear interpolation scheme. For the
264 divergence terms, the Gauss scheme is also selected, adopting linear upwind and limited linear
265 interpolation schemes. For the Laplacian terms the choice has been the Gauss scheme with a linear
266 interpolation scheme and a limited surface normal gradient scheme. The Euler first order bounded
267 implicit scheme was set for the first time derivative terms.

268 A block structured mesh with a topology similar to the one in Braun and Awruch (2003), has been
269 generated. The total number of cells is 148320, and the number of cells around the walls of the
270 rectangular cylinder is 460. For the first layer of cells, the height to width ratio is $\delta_1/B = 5.11 \times$
271 10^{-4} , for which the mean value of the non-dimensional height ($y^+ = (\delta_1 u_*)/\nu$, where δ_1 is the
272 height of the first prismatic grid layer around the deck and u_* is the friction velocity) is about 1.8
273 and the maximum value is close to 8 at $Re = 1.01 \times 10^5$. These bounds are ~~the~~ similar to those
274 reported in Sarkic et al. (2012), and in this model, the number of cells with $y^+ > 4$ is about 5% of
275 the total number of cells around the rectangular cylinder and they are located mainly in the
276 windward corners. In both static and forced harmonic oscillations a maximum Courant number of 1
277 has been imposed, which produces for the static prism at the Reynolds number of reference a mean
278 non-dimensional time step $\overline{\Delta s} = \overline{\Delta t}U/B = 6.7 \times 10^{-4}$. The abundant literature reporting
279 numerical studies on rectangular cylinders means verification studies concerning mesh size and
280 time step refinements for the rectangular cylinder case can be avoided, since the authors have used
281 common mesh topologies and have adopted mesh characteristics and a time step more demanding
282 than other successful simulations.

283 5.2. G1 generic deck cross-section

284 The detailed geometry of the G1 generic cross-section is depicted in figure 8. The flow domain size
285 in this case is $37B$ by $27B$ (B is the deck width), similar to the size employed in the rectangular
286 cylinder case. **The boundary conditions are the same as in the rectangular cylinder case.**



287

288 Figure 2. Flow domain definition and boundary conditions for the G1 section (not to scale).

289 To verify the spatial discretisation, for the streamlined G1 deck section three different grids, with
 290 different mesh densities, have been considered for the static deck case with a 0° angle of attack.
 291 The meshes are identified as Coarse, Medium and Fine grids. In all the cases, a 2D block structured
 292 regular mesh has been used. A high density mesh has been defined around the deck cross-section,
 293 the so-called boundary layer mesh, taking special care in order to obtain maximum values for the
 294 first grid non-dimensional height y^+ below 4, which is a more demanding bound than the one set
 295 by Sarkic et al. (2012) for a similar problem. In this manner, no wall functions are required and the
 296 turbulence model equations are integrated along the viscous sublayer. The thickness of this layer is
 297 $B/25$. The Coarse mesh comprises 25 rows of elements in this zone and the height of the first
 298 element around the cross-section is defined as $\delta_1/B = 2.08 \times 10^{-4}$, while the expansion ratio
 299 between the end cell and the start cell is 25. For the Medium (Figure 3) and Fine meshes the
 300 boundary layer definition was identical: 50 rows considering an expansion ratio of 10, which gives
 301 a first cell non-dimensional height $\delta_1/B = 2.03 \times 10^{-4}$, very close to the Coarse mesh case in
 302 order to be able to drive conclusions from the verification analyses since the y^+ values are
 303 comparable for the three cases. For a Reynolds number $Re = 1.07 \times 10^5$, these mesh arrangements
 304 offer a mean value of the y^+ around the deck close to 1, with a very limited number of cells with
 305 $y^+ > 2$ located at the windward corners of the deck. The maximum value of y^+ for the three cases
 306 is about 3.7.

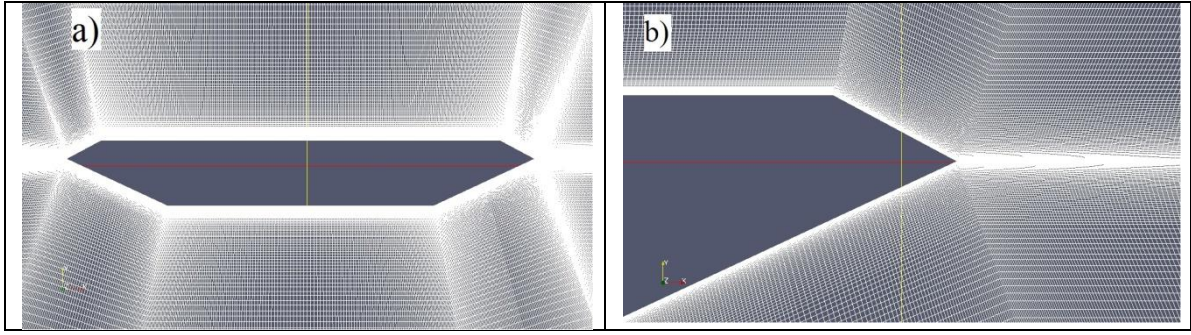
307 In table 1 the total number of cells, the number of cells around the deck section and the integral
 308 aerodynamic parameters are reported along with the standard deviation (prime symbol) values of
 309 the force coefficients for each mesh.

Table 1. Properties and results of the grid-refinement study for the G1 section.

| Grid | Total cells | Cells around deck | S_t | C_d | C_l | C_m | C'_d | C'_l | C'_m |
|--------|-------------|-------------------|-------|-------|--------|-------|--------|--------|--------|
| Coarse | 149600 | 640 | 0.20 | 0.056 | -0.026 | 0.035 | 0.0003 | 0.010 | 0.0022 |
| Medium | 268150 | 770 | 0.19 | 0.057 | -0.033 | 0.034 | 0.0006 | 0.022 | 0.0047 |
| Fine | 363300 | 770 | 0.19 | 0.057 | -0.034 | 0.034 | 0.0006 | 0.022 | 0.0047 |

310

311



312 Figure 3. G1 section block structured grid: a) general view of the flow domain b) close-up of the
 313 deck and e b) detail around the lee-ward corner of the deck.

314 ~~From the results in table 1 it can be inferred that no significant differences are found in the results~~
 315 ~~depending on the grid discretisation.~~ The main discrepancies found have been the lower values in
 316 the standard deviation of the force coefficients and the slight underestimation of the lift coefficient
 317 when the coarse mesh has been used. Consequently the Coarse mesh has been disregarded and
 318 Medium mesh is adopted hereafter since the results are similar to the ones obtained using the Fine
 319 mesh at a lower computational cost.

320 Regarding the analysis of the sensitivity of the solution depending on the chosen time step, two
 321 different maximum Courant numbers equal to 1 and 0.5 have been considered in order to check the
 322 influence of the temporal discretisation (Mannini et al., 2010). In table 2, where the non-
 323 dimensional time step is defined as $\overline{\Delta s} = \overline{\Delta t}U/B$, the numerical results obtained are reported,
 324 finding that they offer very close figures; therefore the higher maximum Courant number is
 325 retained for the remaining simulations.

Table 2. Results of the time-refinement study for the G1 section.

| Max. Co. numb. | $\overline{\Delta s}$ | S_t | C_d | C_l | C_m | C'_d | C'_l | C'_m |
|----------------|-----------------------|-------|-------|--------|-------|--------|--------|--------|
| 1 | 3.5e-4 | 0.19 | 0.057 | -0.033 | 0.034 | 0.0006 | 0.022 | 0.0047 |
| 0.5 | 1.8e-4 | 0.20 | 0.058 | -0.037 | 0.034 | 0.0006 | 0.019 | 0.0040 |

326

327 5.3. Grid movement strategy

328 The computer implementation of the ALE formulation requires a mesh-update method that assigns
 329 mesh-node velocities or displacements at each calculation time step (Donea et al., 2004).

330 In the simulations conducted in this research the boundary motion is defined by the prescribed
 331 forced oscillations of the bluff body, which follows a sinusoidal law with given frequency and
 332 amplitude. On the other hand, the exterior boundaries of the fluid domain are fixed along the
 333 simulations. The whole mesh is allowed to deform between the moving and fixed boundaries.

334 Amongst the available mesh movement algorithms a Laplacian smoothing technique for each
 335 component of the node-mesh position has been chosen (Oliver, 2009). According to Jasak and
 336 Rusche (2009), the Laplace equation can be expressed as:

$$\nabla \cdot k \nabla \mathbf{u} = 0 \quad (9)$$

337 where \mathbf{u} is the node-mesh displacement vector and k is the diffusion coefficient.

1
2
3
4
5
6
7
8
9
10
11
12
13
14
15
16
17
18
19
20
21
22
23
24
25
26
27
28
29
30
31
32
33
34
35
36
37
38
39
40
41
42
43
44
45
46
47
48
49
50
51
52
53
54
55
56
57
58
59
60
61
62
63
64
65

338 In this work the mesh control is achieved by computing the motion of the grid points solving the
 339 Laplace equation with variable diffusivity using a method based on the quadratic inverse distance
 340 from the oscillating boundary. This prevents the distortion of the smallest elements around the
 341 rectangular cylinder (Löhner, 2008).

342 5.4. *Forced oscillations characteristics and application of relationships between flutter*
 343 *derivatives*

344 With the aim of limiting the computational cost of obtaining the set of 8 flutter derivatives, the
 345 relationships between flutter derivatives (8.a–8.d) reported in Tubino (2005) are applied. As a
 346 consequence, only half of the simulations are required, which represents a substantial reduction in
 347 the computational demands of the problem. The pitch degree of freedom has been chosen as the
 348 one for carrying out the numerical simulations; therefore the H_2^* , H_3^* , A_2^* and A_3^* flutter derivatives
 349 are computed by means of the CFD simulations, while the H_1^* , H_4^* , A_1^* and A_4^* flutter derivatives are
 350 estimated using equations (8.a) to (8.d). The amplitude of the forced oscillations in the present
 351 work is $\alpha_0 = 1^\circ$ for the two considered application examples. The sign convention adopted herein
 352 has been the same as in Sarkar et al. (2009): heave and aeroelastic lift force positive downward,
 353 while the aeroelastic moment and rotation have been considered positive for a nose-up rotation.

354

355 **6. RESULTS AND DISCUSSION**

356 6.1 *B/H=4.9 rectangular cylinder*

357 6.1.1 Flow simulation around the static *B/H=4.9* rectangular cylinder

358 In table 3 the Strouhal number, the mean drag coefficient and the standard deviation of the lift and
 359 drag coefficients at $Re = 1.01 \times 10^5$ are presented along with experimental data from Schewe
 360 (2009) and the numerical data computed using two different 2D URANS approaches. The URANS
 361 references which have been considered for comparison are: Ribeiro (2011) who reports, amongst
 362 others, the results of a Reynolds Stress Model (RSM) simulation and Mannini et al. (2011) where
 363 the Linearised Explicit Algebraic (LEA) version of the Explicit Algebraic Reynolds Stress Model
 364 (EARSMS) coupled with the standard $k-\omega$ turbulence model is employed. It must be borne in mind
 365 that in the references used for validation the ratio of the rectangular cylinder is $B/H=5$. In table 3,
 366 the reference dimension for drag coefficient and the standard deviations is B , therefore the data in
 367 Mannini et al. (2011), Ribeiro (2011) and Schewe (2009) which are based on H , have been
 368 modified for a better comparison. For the simulation of the $B/H=4.9$ static rectangular cylinder the
 369 simulated length has been about 100 non-dimensional time units and the reported results in table 3
 370 have been averaged along a non-dimensional time $s = tU/B = 74$.

Table 3. *B/H=4.9* rectangular cylinder: Strouhal number and force coefficients.

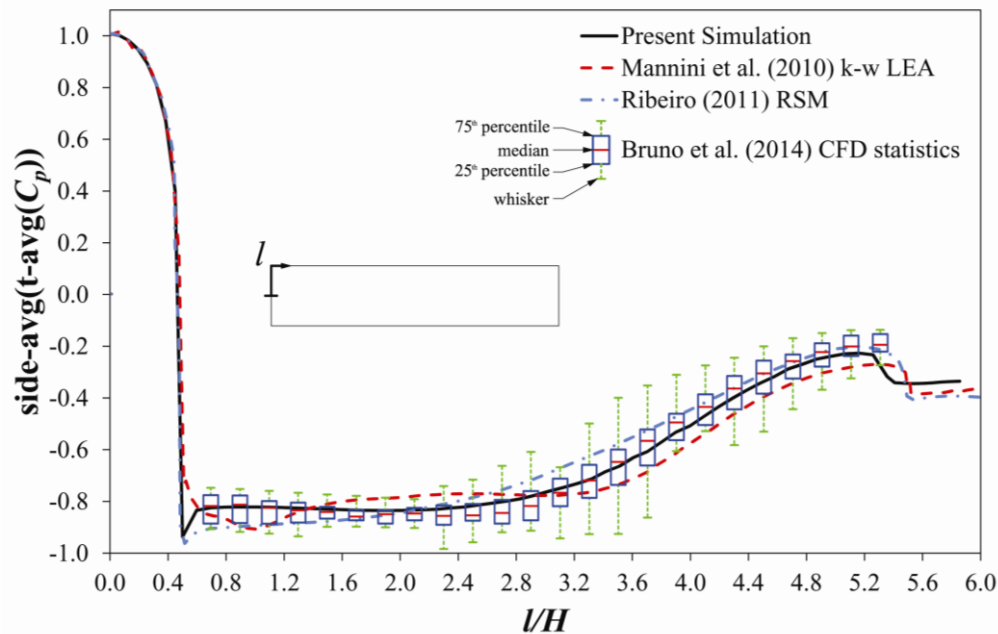
| | S_t | C_d | C'_d | C'_l |
|--|-------|-------|--------|----------------|
| Present simulation | 0.123 | 0.227 | 0.0049 | 0.193 |
| Mannini et al. (2011) – LEA $k-\omega$ | 0.094 | 0.212 | 0.0038 | 0.215 |
| Ribeiro (2011) - RSM | 0.073 | 0.234 | | 0.18 |
| Schewe, (2009) – EXP. | 0.111 | 0.206 | | ≈ 0.08 |

371

372 Table 3 shows a good agreement with the experimental and numerical data, particularly taking into
 373 account that, since the aspect ratio of the rectangular cylinder considered in the simulation is lower
 374 than 5, it must show slightly higher values for both Strouhal number and drag force coefficients

375 according with the trend in drag coefficient and Strouhal number for rectangular cylinders with
 376 aspect ratios between 4 and 6, reported in Shimada and Ishihara (2012). It is notable how Menter's
 377 $k-\omega$ SST turbulence model considered in this simulation offers results comparable with the
 378 sophisticated LEA approach in Mannini et al. (2011). The proximity of the Strouhal number in this
 379 simulation to the experimental value obtained in Schewe (2009) should also be highlighted and
 380 therefore a better prediction of this parameter than in Ribeiro (2011) has been obtained.

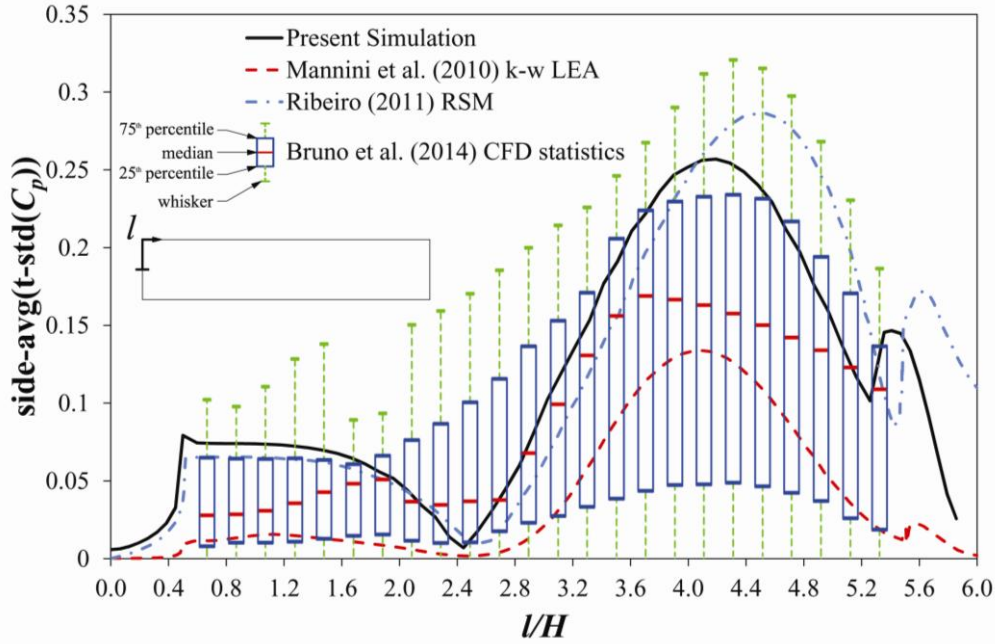
381 As a further validation of the reported simulations, in figure 4 the side-averaged (between the upper
 382 and lower half perimeters) and time-averaged distribution of the pressure coefficient C_p of the
 383 static ratio $B/H=4.9$ rectangular cylinder are reported along with the results in Mannini et al. (2010)
 384 for the $k-\omega$ LEA turbulence model, Ribeiro (2011) for the RSM and the statistics for the CFD
 385 realizations reported in Bruno et al. (2014). The side-averaged and time-averaged pressure
 386 coefficient of the ratio 4.9 rectangular cylinder is very close to the median values on the long side
 387 of the rectangular cylinder (l/H between 0.7 and 5.3, being l the length along the half of the
 388 perimeter of the rectangular cylinder, as it is described in figure 4) which indicates that the
 389 accuracy of the simulation is comparable with the CFD realizations in the frame of the BARC
 390 initiative. Furthermore, the numerical results correctly reproduce the experimental data for the 5:1
 391 rectangular cylinder, bearing in mind the scattering in the wind tunnel tests available in the
 392 literature.



393
 394 Figure 4. Side-averaged and time-averaged C_p distributions around $B/H=4.9$ and $B/H=5$
 395 rectangular cylinders.

396 In figure 5, the side-averaged distribution of the standard deviation in-time of the pressure
 397 coefficient is reported along with the statistical data for the CFD realizations in Bruno et al. (2014)
 398 and the simulations in Mannini et al. (2010) and Ribeiro (2011). In Bruno et al. (2014) the scatter
 399 in the distribution of the standard deviation of the pressure coefficient has been shown for both
 400 experimental and numerical realizations. The standard deviation distribution of the C_p reported for
 401 the $B/H=4.9$ rectangular cylinder is well inside the boundaries of the BARC realizations and it is
 402 particularly close to the RSM simulation in Ribeiro (2011). It has reported in Bruno et al. (2014)
 403 that RANS simulations present a minimum in the standard deviation of the pressure coefficient at

404 about $2H$ from the windward corner. This minimum is also present in the simulation reported in
 405 this work.



406

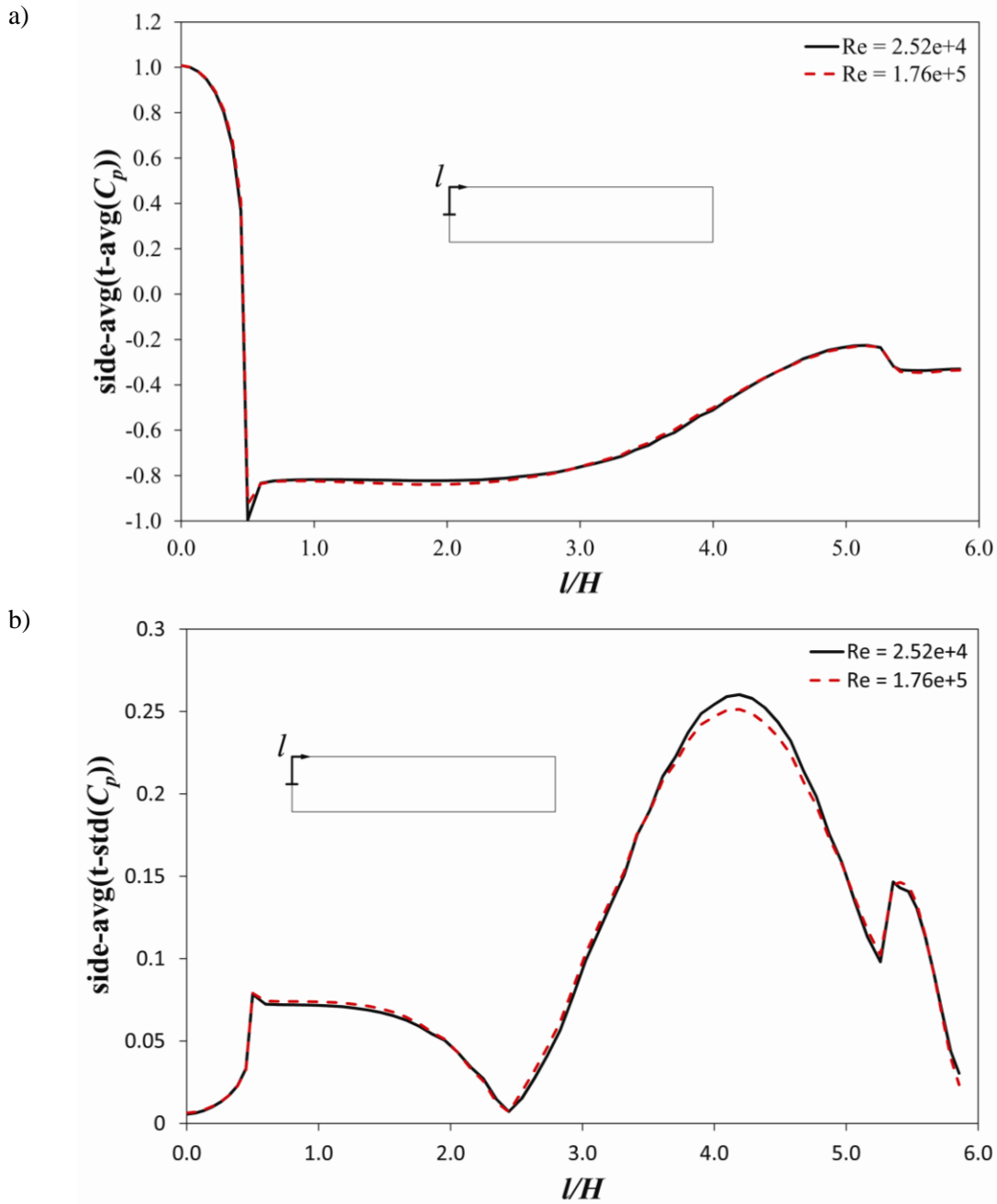
407 Figure 5. Side-averaged distributions around $B/H=4.9$ and $B/H=5$ rectangular cylinders of the
 408 standard deviation in time of C_p .

409 Based on the comparison of the drag coefficient, the standard deviation of the lift coefficient, the
 410 Strouhal number and the distribution to the time-averaged and time-standard deviation of the
 411 pressure coefficient, the agreement of the present simulation with the experimental and numerical
 412 data in the literature can be considered adequate.

413 6.1.2 Flutter derivatives of the $B/H=4.9$ rectangular cylinder

414 The flutter derivatives for the aspect ratio 4.9 rectangular cylinder have been computed over a
 415 range of reduced velocities $U_R = U/(f \cdot B) = (0.88, 26.40)$. In order to cover the whole range of
 416 reduced velocities, three frequencies of oscillation have been considered (0.5 Hz., 1 Hz. and 3 Hz.)
 417 in conjunction with flow speeds between 1 m/s and 7 m/s, which means that the range of covered
 418 Reynolds number is between 2.52×10^4 and 1.76×10^5 . In some cases ($U_R = 2.6, 5.3, 10.6$ and 15.84),
 419 the same reduced velocity has been computed with different combinations of flow velocity and
 420 frequency of oscillation in order to verify the independence of the results with the combination of
 421 both parameters.

422 Since the same mesh has been retained for the all the simulations, the non-dimensional height y^+
 423 reaches a maximum value close to 11 for the maximum Reynolds number ($Re = 1.76 \times 10^5$; $U = 7$
 424 m/s), while the mean value of y^+ is about 2.7. For the minimum Reynolds number ($Re =$
 425 2.52×10^4 ; $U = 1$ m/s), the maximum y^+ reaches a value close to 3.5 and the mean value of y^+ is
 426 0.6. With the aim of ascertaining the effect of the differences in the y^+ numbers on the simulations
 427 at the lower and upper bounds of the Reynolds number, as well as the dependency of the
 428 aerodynamic characteristics with the Reynolds number, the side-averaged and time-averaged along
 429 with the side-averaged time-standard deviation distributions of the pressure coefficient are
 430 presented for $U = 1$ and $U = 7$ m/s (Figure 6).

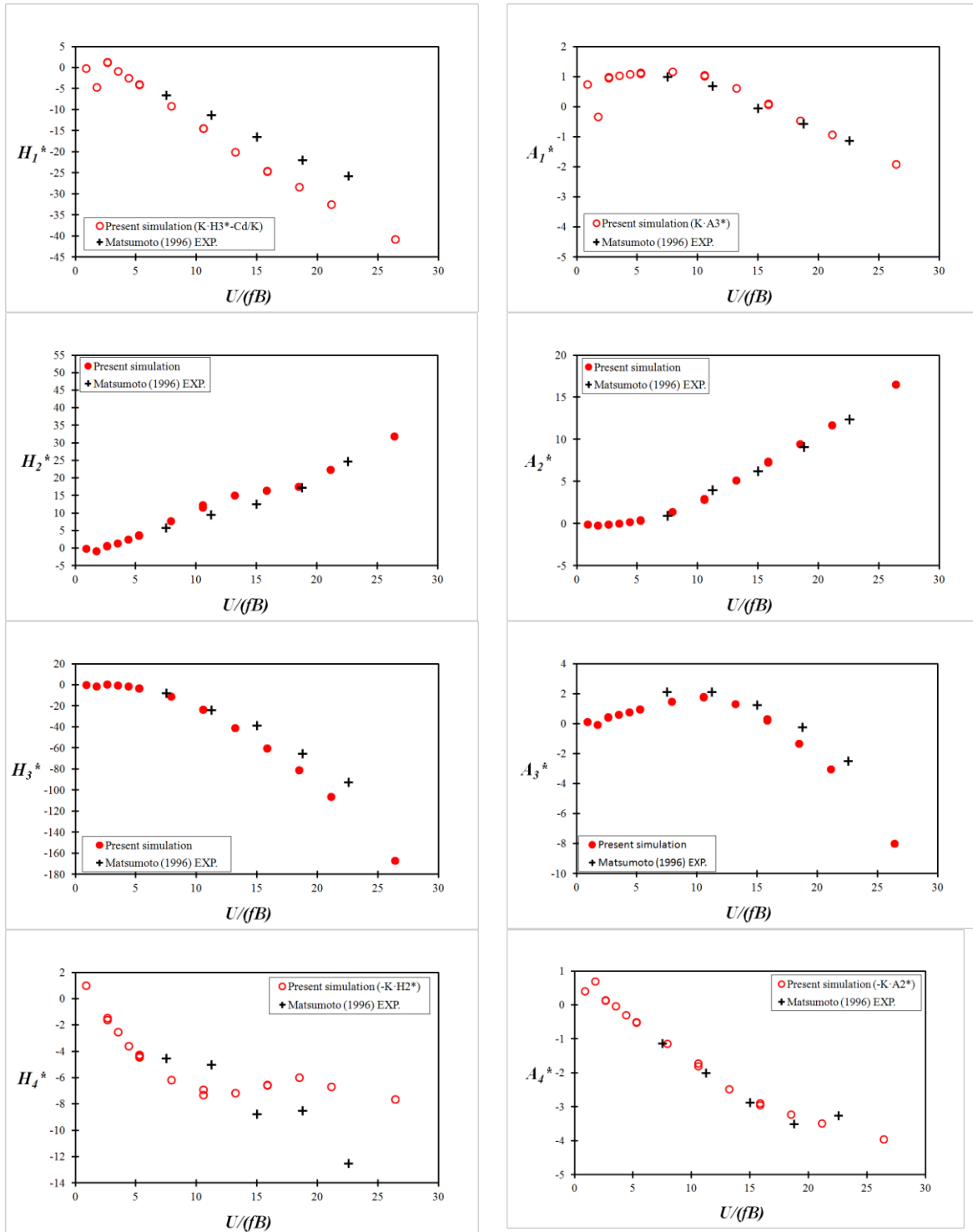


431 Figure 6. Side-averaged distributions around $B/H=4.9$ rectangular cylinder of the a) time-averaged
 432 and b) time-standard deviation of C_p for $U = 1$ and $U = 7$ m/s.

433 Figure 6 shows similar results for the side-averaged distributions of the time-averaged and the
 434 standard deviation of the pressure coefficient. Only minimal small differences in the peak value of
 435 the distribution of the standard deviation of the pressure coefficient around the rectangular prism
 436 can be identified. Consequently, the relatively high values of the maximum y^+ at $U = 7$ m/s do not
 437 jeopardize the accuracy of the simulation. At the same time, the aerodynamic characteristics of the
 438 static sharp edged rectangular cylinder at 0° angle of attack seems to be quite insensitive to the
 439 Reynolds number, as it has been reported in Holmes (2007), citing Scruton (1981). Besides this, in
 440 the set of reduced velocities considered for the computation of the flutter derivatives, the maximum
 441 flow speed of 7 m/s is adopted for a single reduced velocity $U_R = 18.48$. In the same manner, the
 442 flow speed of 6 m/s is employed only for repeated values of $U_R = 5.3$ and $U_R = 15.84$. Therefore,

443 in the set of flutter derivatives which are presented next, the majority of the simulations have been
 444 conducted at $Re \leq 1.26 \times 10^5$.

445 In figure 7 the flutter derivatives computed from these simulations are reported along with the
 446 experimental data in Matsumoto (1996). The length of the simulations reported in the following has
 447 been between 40 and 260 non-dimensional time units, depending on the flow speed and the
 448 frequency of oscillation.



449 Figure 7. Flutter derivatives of the $B/H=4.9$ rectangular cylinder: computed flutter derivatives and
 450 comparison with experimental data in Matsumoto (1996).

451 ~~The flutter derivatives presented herein offer a good agreement with the experimental data along~~
 452 ~~the complete range of reduced velocities studied.~~ The estimated flutter derivatives agree well with
 453 the experimental data and only the H_4^* flutter derivative shows some discrepancies with the wind
 454 tunnel values. These differences in H_4^* are comparable with the ones **found in CFD simulations**
 455 **where forced oscillations in the heave degree of freedom have been conducted,** ~~that can be found in~~
 456 ~~direct evaluations from heave oscillation simulations~~ such as in Sarwar et al. (2008) for a $B/H=20$
 457 rectangular cylinder or Huang (2009). There are no significant differences for the repeated
 458 simulations at the same reduced velocities, which points out the relative independence of the results
 459 with the various combinations of flow speed and frequency of oscillation.

460 6.2 G1 generic deck cross-section

461 6.2.1 Flow simulation around the static G1 section

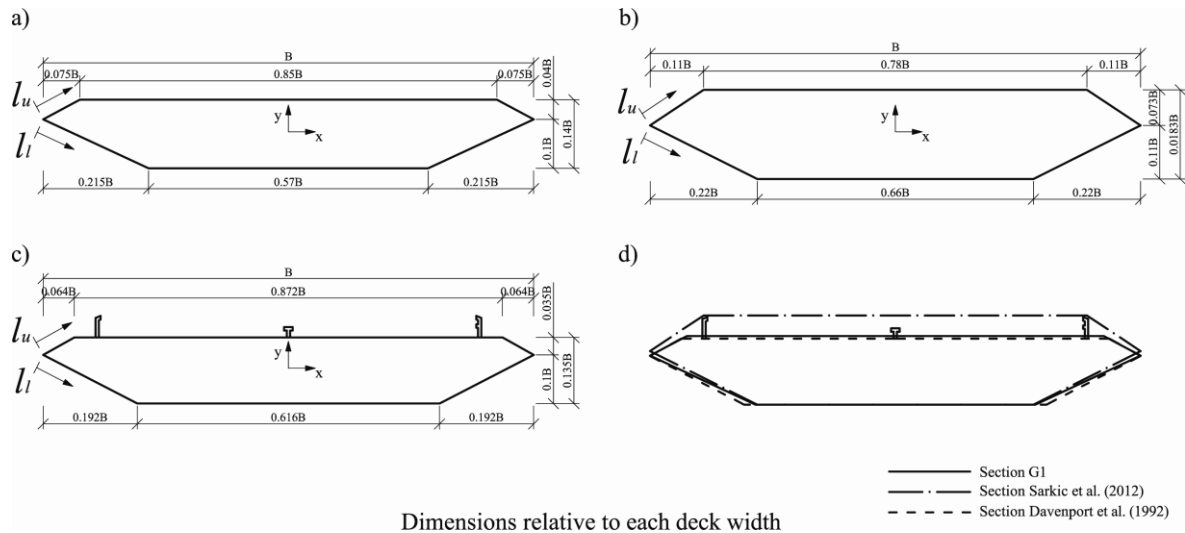
462 The drag coefficient, the root mean square of the lift coefficient time history and the Strouhal
 463 number of the G1 section for 0° angle of incidence computed in this study are compared in table 4
 464 with the numerical results reported in Larsen and Walther (1998) who applied the Discrete Vortex
 465 Method in their simulations. In this case the numerical simulation of the static G1 section has been
 466 extended along 65 non-dimensional time units. **The time statistics have been obtained from the**
 467 **final 45 non-dimensional time units.**

Table 4. Static G1 section: drag coefficient, RMS of the lift coefficient and Strouhal number.

| | C_d | C_l^{RMS} | S_t |
|---------------------------|-------|-------------|-------|
| Present simulation | 0.06 | 0.04 | 0.19 |
| Larsen and Walther (1998) | 0.08 | 0.07 | 0.17 |

468

469 The agreement amongst the results for the 0° angle of attack is reasonable, however as a further
 470 validation of the numerical approach chosen by the authors, the time-averaged pressure coefficient
 471 distribution along the deck is going to be presented and compared with the experimental data
 472 reported in Sarkic et al. (2012), where the time-averaged pressure coefficient distribution along a
 473 bare box deck is provided. For further comparison, the experimental data in Bruno and Khris
 474 (2003) (taken from Larose, 1992) of the smooth flow tests of a taut strip model of the Great Belt
 475 Bridge fitted with barriers, has also been included. The geometry of the deck and the position of the
 476 pressure probes in the aforementioned reference are taken from Davenport et al. (1992). The
 477 distribution of the ~~time~~ standard deviation of the pressure coefficient is not reported since the
 478 unsteadiness of the flow was rather weak, providing values of the pressure coefficient standard
 479 deviation well below the available experimental data, particularly on the windward half of the cross
 480 section. A similar behavior is described in Sarkic et al. (2012). In figure 8, the geometry of the
 481 bridge decks considered for validation is described, while in figure 9 the time-averaged pressure
 482 coefficient distribution is shown.



Dimensions relative to each deck width

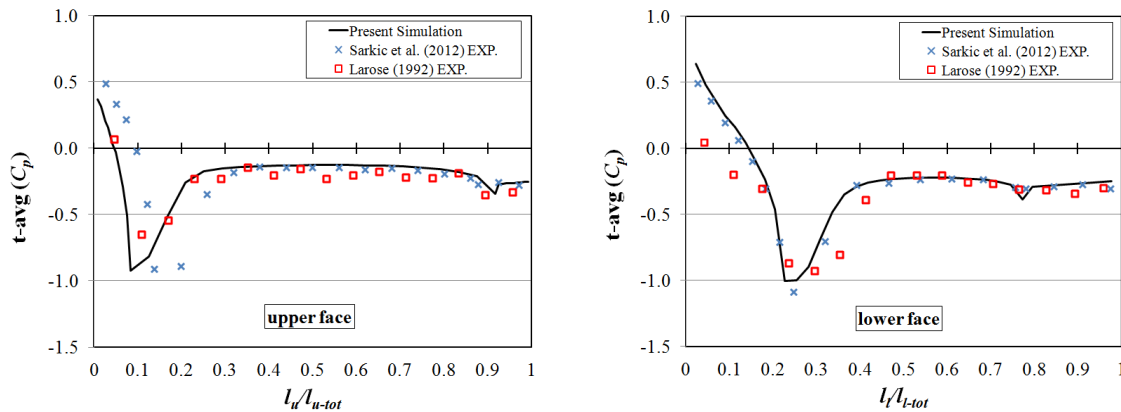
— Section G1
 - - - Section Sarkic et al. (2012)
 - - - Section Davenport et al. (1992)

483

484

485

Figure 8. Geometry: a) G1 section b) section in Sarkic et al. (2012) c) section in Davenport et al. (1992) d) comparison between sections.



486

487

Figure 9. Time-averaged pressure coefficient distribution: numerical results and comparison with experimental data in Sarkic et al. (2012) and Larose (1992).

488

489

490

491

492

493

494

495

The agreement in the pressure coefficient distribution between the numerical simulation and the wind tunnel data in Sarkic et al. (2012) is **good** **remarkable**. On the upper face, the peak values at the windward corner are correctly simulated and the lateral shift is due to the differences in the geometry in the upper surface (see figure 8). Also the mean pressure distribution along the horizontal and the leeward plates have been accurately obtained. The agreement is even better on the lower surface, since the geometry of the two sections is nearly identical. In the authors' opinion the similitude in the Reynolds number ($Re \approx 1 \times 10^5$) of the numerical simulation and the wind tunnel test has contributed to this close agreement.

496

497

498

499

500

When the numerical results are compared with the wind tunnel data from Larose (1992), some discrepancies can be identified, which can arguably be related to the difference in the Reynolds number of the wind tunnel tests ($Re = 7 \times 10^4$) as well as the presence of the barriers in the tested model. Besides this, discrepancy in the moderate suction on the windward surface in the lower side of the deck has already been commented in Bruno and Khris (2003).

501

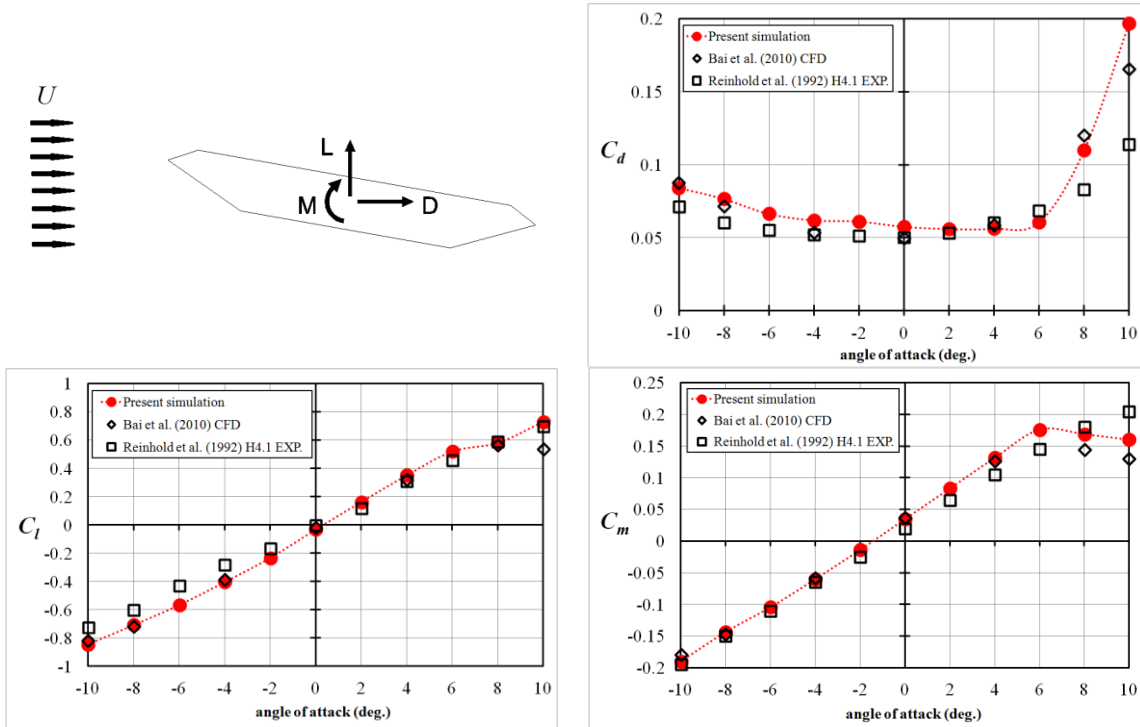
502

503

In order to provide a more complete view of the aerodynamic characteristics of the static G1 cross section, the force coefficients in the range of angles of attack (-10° , 10°) are computed with an interval of 2° . The results are compared with the experimental data reported in Reinhold et al.

504 (1992) for the H4.1 section of the Great Belt Bridge design studies and the 2D numerical results
 505 published in Bai et al. (2010), for the G1 section.

506 Figure 10 shows the force coefficients of the G1 section. A very good agreement has been obtained
 507 between the computational results and the experimental data for the similar geometry of the H4.1
 508 box deck section. In fact, the change in the slope of the moment coefficient for angles of incidence
 509 higher than 6° has been correctly captured as well as the step increment in the drag coefficient
 510 for angles of attack higher than 6° . The accuracy of the slopes in the vicinity of 0° for both lift
 511 and moment coefficients should also be noted.



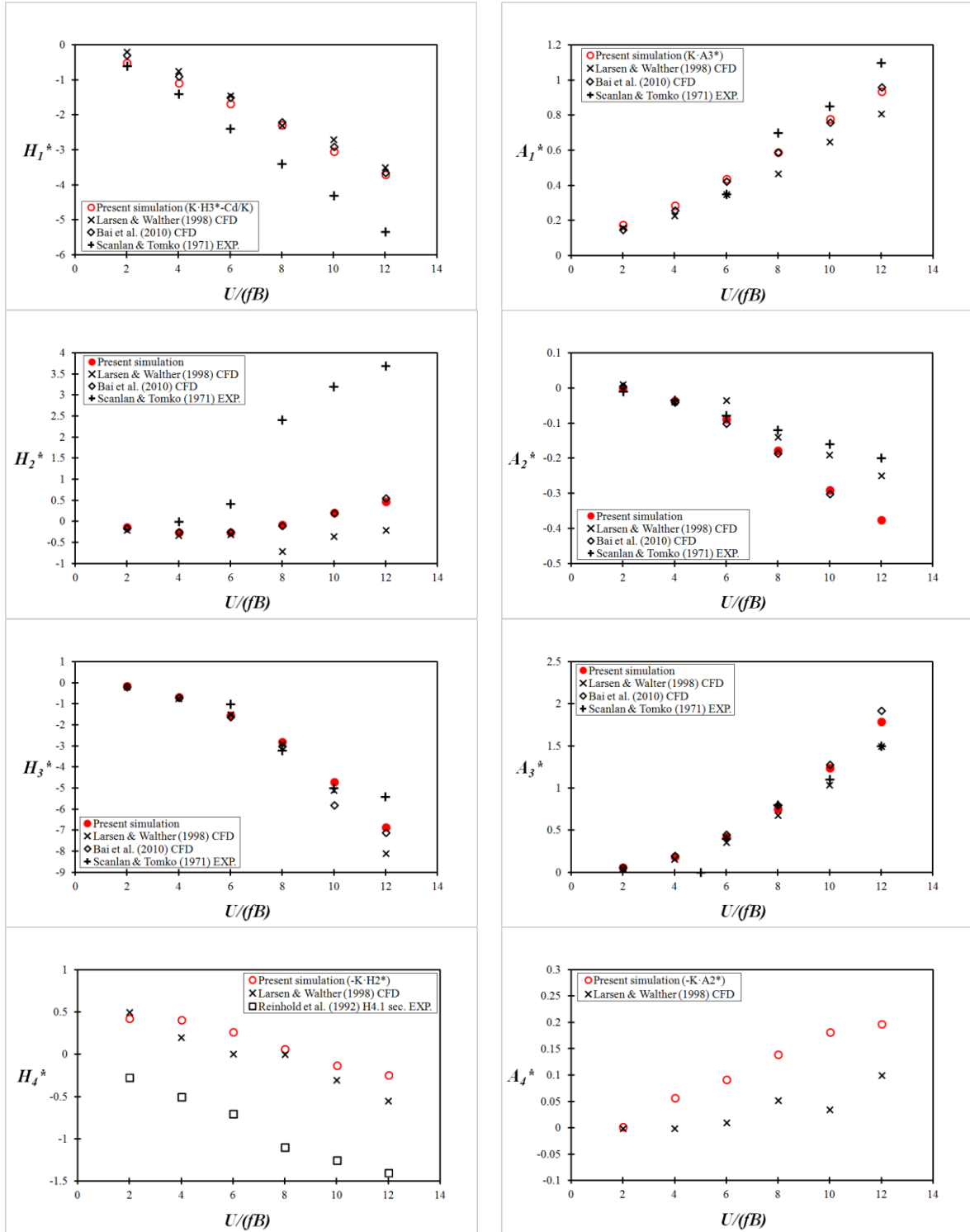
512 Figure 10. G1 section force coefficients: numerical results and comparison with experimental
 513 (Reinhold et al., 1992) and other numerical data (Bai et al., 2010).

514 6.2.2 Flutter derivatives of the G1 section

515 In order to identify by means of a computational approach the flutter derivatives of the G1 generic
 516 section, forced oscillation simulations were carried out at reduced velocities $U/(fB)$ equal to 2, 4,
 517 6, 8 10 and 12, as in Larsen and Walther (1998). Also, the formulae applied for identifying the
 518 flutter derivatives are the ones reported in Larsen and Walter (1998) and Bai et al (2010), therefore
 519 the expressions in equations (7.a) to (7h) are divided by 2. The same procedure as in the
 520 rectangular cylinder case has been applied for decreasing the computational cost. As a
 521 consequence, instead of 12 computer simulations, only 6 are required, one for each reduced
 522 velocity considered. In this case the flow velocity is the same in all the simulations and the
 523 frequency of oscillation is modified in the range (0.833, 5) Hz in order to obtain the reduced
 524 velocities of interest. The solution for the fixed G1 section has been set as the initial condition for
 525 the forced oscillation simulations. Since this allows shortening the initial transient, the
 526 computations have been extended for about 50 non-dimensional time units. For the highest value of
 527 the reduced velocity, $U_R=12$, four complete oscillation periods have been simulated, which is
 528 greater than the 2.5 periods span adopted in Larsen and Walther (1998).

529
530
531
532
533
534
535

In figure 11 the numerical results obtained for H_i^* and A_i^* ($i = 1, \dots, 3$) are compared with the experimental ones reported in Scanlan and Tomko (1971). The numerical results obtained by Larsen and Walther (1998), and Bai et al. (2010) for the same deck section are also included in the charts. Since no experimental results are available for the H_4^* and A_4^* flutter derivatives of the G1 cross-section, the results for the H_4^* flutter derivative of the H4.1 section in Reinhold et al (1992) are provided. No experimental data for the A_4^* flutter derivative of the H4.1 section are available in the literature to the authors' knowledge.



10
11
12
13
14
15
16
17
18
19
20
21
22
23
24
25
26
27
28
29
30
31
32
33
34
35
36
37
38
39
40
41
42
43
44
45
46
47
48
49
50
51
52
53
54
55
56
57
58
59
60
61
62
63
64
65

536 Figure 11. Flutter derivatives of the G1 generic section: numerical results and comparison with
 537 experimental (Scanlan and Tomko, 1971; Reinhold et al., 1992) and numerical (Larsen and
 538 Walther, 1998; Bai et al., 2010) data.

539 A very good agreement has been found for the flutter derivatives related to the pitch forced
 540 oscillation: H_3^* , A_2^* and A_3^* , which have been obtained from the numerical simulations. For the H_2^*
 541 flutter derivative, similar discrepancies as in Bai et al. (2010) have been obtained. In fact, for this
 542 flutter derivative, in the case of box decks, differences between experimental data and CFD based
 543 evaluations can be found in other references in the literature, such as Jeong and Kwon (2003), Zhu
 544 et al. (2007), Ge and Xiang (2008) or Brusiani et al. (2013). For the approximated heave-related
 545 flutter derivatives H_1^* and A_1^* the obtained results agree with wind tunnel test data and their
 546 accuracy is comparable with the other CFD-based simulations. For the flutter derivatives H_4^*
 547 and A_4^* it is more difficult to properly assess the reliability of the approximated values since
 548 experimental data are not available. It has been found that for the H_4^* flutter derivative the present
 549 simulation provides values very similar to those reported by Larsen and Walther (1998). In the
 550 same manner, the slope is almost the same as for the H4.1 experimental flutter derivative and the
 551 upwards shift of the numerical results can also be found, for instance, in Brusiani et al. (2013)
 552 where the flutter derivatives of the H4.1 section were specifically computed. For the A_4^* flutter
 553 derivative the approximated values do not show important differences in value with respect to the
 554 ones in Larsen and Walther (1998).

555 In order to assess the degree of accuracy in the simulations reported in this work, in table 5 the
 556 relative errors in the value of the flutter derivatives H_1^* , H_2^* , H_3^* , A_1^* , A_2^* and A_3^* , for which
 557 experimental data are available, are reported. It must be borne in mind that the data for the lower
 558 reduced velocities cannot be identified from the charts in Scanlan and Tomko (1971) for some of
 559 the flutter derivatives.

560 The relative errors of the numerical values taking as reference the experimental values are
 561 evaluated according to the following formula:

$$e = \frac{|exp. value - num. value|}{|exp. value|} \quad (9)$$

562

563 Table 5. Relative errors in the evaluation of the flutter derivatives of the G1 section

| Flutter derivative | U_R | Present simulation | Larsen and Walther (1998) | Bai et al. (2010) |
|--------------------|-------|--------------------|---------------------------|-------------------|
| H_1^* | 2 | 0.14 | 0.67 | 0.50 |
| | 4 | 0.23 | 0.46 | 0.36 |
| | 6 | 0.30 | 0.40 | 0.38 |
| | 8 | 0.33 | 0.32 | 0.35 |
| | 10 | 0.29 | 0.37 | 0.33 |
| | 12 | 0.31 | 0.34 | 0.32 |
| H_2^* | 6 | 1.60 | 1.71 | 1.57 |
| | 8 | 1.03 | 1.29 | 1.04 |
| | 10 | 0.93 | 1.11 | 0.94 |
| | 12 | 0.87 | 1.05 | 0.85 |
| H_3^* | 6 | 0.54 | 0.50 | 0.60 |

| | | | | |
|---------|----|------|------|------|
| | 8 | 0.12 | 0.09 | 0.06 |
| | 10 | 0.06 | 0.02 | 0.16 |
| | 12 | 0.27 | 0.50 | 0.31 |
| A_1^* | 6 | 0.25 | 0.00 | 0.21 |
| | 8 | 0.16 | 0.33 | 0.16 |
| | 10 | 0.08 | 0.24 | 0.11 |
| | 12 | 0.15 | 0.26 | 0.13 |
| A_2^* | 2 | 0.95 | 2.00 | 1.50 |
| | 4 | 0.03 | 0.14 | 0.14 |
| | 6 | 0.09 | 0.56 | 0.25 |
| | 8 | 0.47 | 0.17 | 0.54 |
| | 10 | 0.81 | 0.19 | 0.88 |
| | 12 | 0.88 | 0.25 | |
| A_3^* | 6 | 0.04 | 0.10 | 0.13 |
| | 8 | 0.06 | 0.15 | 0.00 |
| | 10 | 0.13 | 0.05 | 0.16 |
| | 12 | 0.19 | 0.00 | 0.28 |

564

565 From table 5, it can be concluded that the accuracy of the three simulations is equivalent, being the
566 median of the relative errors 0.26 in the present simulation, and 0.33 and 0.32 in Larsen and
567 Walther (1998) and Bai et al. (2010). In this respect, it is notable how the approximated values
568 obtained using the proposed approach for the H_1^* and A_1^* flutter derivatives are comparable with the
569 values reported in Larsen and Walther (1998) and Bai et al. (2010) where the harmonic oscillations
570 in the heave degree of freedom were explicitly computed.

571 7. CONCLUDING REMARKS

572 In this article, the force coefficients and the flutter derivatives of an aspect ratio 4.9 rectangular
573 cylinder and a streamlined deck type G1 cross-section have been computed based on a 2D URANS
574 approach, applying Menter's $k-\omega$ SST turbulence model. A block structured mesh has been used
575 and the open source CFD solver OpenFOAM has been applied.

576 The static response of the rectangular cylinder at a 0° angle of attack has agreed well with the
577 experimental data in Schewe (2009), the RSM simulation in Ribeiro (2011) and sophisticated 2D
578 numerical simulations where the Boussinesq assumption is substituted by an EARSM approach
579 (Mannini et al., 2011).

580 For the G1 section, the influence of the spatial and temporal discretisations in the numerical results
581 has been studied. Since both experimental and numerical results of the force coefficients and flutter
582 derivatives are available in the literature for this particular cross-section, the current computational
583 results have been validated against the experimental ones and also the accuracy of the simulations
584 reported herein can be compared with CFD results published by other researchers.

585 The distribution of the time-averaged pressure coefficient around the G1 section agrees well with
586 experimental data available in the literature for similar geometries. The force coefficients of the
587 deck cross-section for angles of attack in the range -10° and $+10^\circ$ have been obtained. It has been

588 found that they are in good agreement with the experimental and numerical data in Reinhold et al.
589 (1992) and Bai et al. (2010).

590 A notable contribution of this work has been the application of the existing formulae relating the
591 flutter derivatives (Tubino, 2005) in a CFD based approach. This has allowed the computer
592 demands of this burdensome problem to be reduced. The pitch-related flutter derivatives have been
593 extracted from the pitch forced oscillation simulations while the heave-related ones have been
594 estimated using the expressions in the literature. For the two cases studied a very good agreement
595 with the experimental flutter derivatives has been found, and at least comparable accuracy with
596 other numerical simulations where both pitch and heave forced oscillations had been numerically
597 computed.

598 This work can be considered a step forward towards the routine use of CFD based techniques in the
599 aerodynamic and aeroelastic design of long span bridges since it has been demonstrated the
600 adequacy of the computational results using an efficient 2D approach. Furthermore it ~~but~~ is also a
601 step forward in the application of numerical optimization techniques in the shape design of bridges,
602 for which efficient, reliable and computational non-cumbersome CFD techniques are a must. In this
603 respect, a fully computational approach for the evaluation of force coefficients and flutter
604 derivatives, as the one reported herein, is required for the application of numerical optimization
605 techniques.

606 8. ACKNOWLEDGMENTS

607 This work has been mainly funded by the Spanish Ministry of Education, Culture and Sport under
608 the Human Resources National Mobility Program of the R-D+i National Program 2008-2011,
609 extended by agreement of the Cabinet Council on October 7th 2011. It has also been partially
610 financed by the Galician Government (including FEDER funding) with reference GRC2013-056
611 and by the Spanish Minister of Economy and Competitiveness (MINECO) with reference
612 DPI2013-41893-R. The authors fully acknowledge the support received.

613 The authors are grateful for access to the University of Nottingham High Performance Computing
614 Facility and the Breogán Cluster at the University of La Coruña.

615 REFERENCES

- 616 Bai, Y., Sun, D., Lin, J. (2010) Three dimensional numerical simulations of long-span bridge
617 aerodynamics using block-iterative coupling and DES. *Computers and Fluids*; 39, 1549-1561.
- 618 Bartoli, G., Mannini, C. (2008) A simplified approach to bridge deck flutter. *Journal of Wind
619 Engineering and Industrial Aerodynamics*; 96, 229-256.
- 620 Brar, P.S., Raul, R., Scanlan, R.H. (1996) Numerical calculation of flutter derivatives via indicial
621 functions. *Journal of Fluids and Structures*; 10, 337-351.
- 622 Braun, A.L., Awruch, A.M. (2003) Numerical simulation of the wind action on a long-span bridge
623 deck. *Journal of the Brazilian Society of Mechanical Sciences and Engineering*; 25(4), 352-
624 363.
- 625 Bruno, L., Canuto, C., Fransos, D. (2009) Stochastic aerodynamics and aeroelasticity of a flat plate
626 via generalized Polynomial Chaos. *Journal of Fluids and Structures*; 25, 1158-1176.
- 627 Bruno, L., Fransos, D. (2008) Evaluation of Reynolds number effects on flutter derivatives of a flat
628 plate by means of a computational approach. *Journal of Fluids and Structures*; 24, 1058-1076.
- 629 Bruno, L., Fransos, D., Coste, N., Bosco, A. (2010) 3D flow around a rectangular cylinder: a
630 computational study. *Journal of Wind Engineering and Industrial Aerodynamics*; 98, 263-276.

- 631 Bruno, L., Khris, S. (2003) The validity of 2D numerical simulations of vortical structures around a
632 bridge deck. *Mathematical and Computer Modelling*; 37, 795-828.
- 633 Bruno, L., Khris, S., Marcillat, J. (2001) Numerical simulation of the effect of section details and
634 partial streamlining on the aerodynamics of bridge decks. *Wind and Structures*; 4(4), 315-332.
- 635 Bruno, L., Salvetti, M.V., Ricciardelli, F. (2014) Benchmark on the aerodynamics of a rectangular
636 5:1 cylinder: an overview after the first four years of activity. *Journal of Wind Engineering and*
637 *Industrial Aerodynamics*; 126, 87-106.
- 638 Brusiani, F., de Miranda, S., Patruno, L., Ubertini, F., Vaona, P. (2013) On the evaluation of bridge
639 deck flutter derivatives using RANS turbulence models. *Journal of Wind Engineering and*
640 *Industrial Aerodynamics*; 119, 39-47.
- 641 Chen, X., Kareem, A. (2002) Advances in modeling of aerodynamic forces on bridge decks.
642 *Journal of Engineering Mechanics*; 128, 1193-1205.
- 643 Davenport, A.G., King, J.P.C., Larose, G.L. (1992) Taut strip model tests. In: Larsen, A. (Ed.),
644 *Proceedings of the 1st International Symposium on Aerodynamics of Large Bridges*,
645 Copenhagen, Denmark.
- 646 Donea, J., Huerta, A., Ponthot, J.Ph., Rodríguez-Ferrán, A. (2004) Arbitrary Lagrangian-Eulerian
647 methods. In *Encyclopedia of Computational Mechanics*. Vol 1: Fundamentals. Stein, E., de
648 Borst, R, Hughes, J.R. (Eds.). John Wiley & Sons, Ltd.
- 649 Frandsen, J.B. (2004) Numerical bridge deck studies using finite elements. Part I: flutter. *Journal of*
650 *Fluids and Structures*; 19, 171-191.
- 651 Fransos, D., Bruno, L. (2006) Determination of the aeroelastic transfer functions for streamlined
652 bodies by means of a Navier-Stokes solver. *Mathematical and Computer Modelling*; 43, 506-
653 529.
- 654 Fransos, D., Bruno, L. (2010) Edge degree-of-sharpness and free-stream turbulence scale effects on
655 the aerodynamics of a bridge deck. *Journal of Wind Engineering and Industrial Aerodynamics*;
656 98, 661-671.
- 657 Ge, Y.J., Xiang, H.F. (2008) Computational models and methods for aerodynamic flutter of long-
658 span bridges. *Journal of Wind Engineering and Industrial Aerodynamics*; 96, 1912-1924.
- 659 Holmes, J.D. (2007) *Wind loading of structures*. 2nd Edition. Taylor and Francis.
- 660 Huang, L., Liao, H., Wang, B., Li, Y. (2009) Numerical simulation for aerodynamic derivatives of
661 bridge deck. *Simulation Modelling Practice and Theory*; 17, 719-729.
- 662 Jasak, H, Rusche, H. (2009) Dynamic mesh handling in OpenFOAM. In: *Fourth OpenFOAM*
663 *workshop*. Montreal, Canada.
- 664 Jeong, U.Y., Kwon, S. (2003) Sequential numerical procedures for predicting flutter velocity of
665 bridge sections. *Journal of Wind Engineering and Industrial Aerodynamics*; 91, 291-305.
- 666 Larose, G.L. (1992) The response of a suspension bridge deck to turbulent wind: the taut-strip
667 model approach. M. Eng. Sc., The University of Western Ontario.
- 668 Larsen, A., Walther, J.H. (1998) Discrete vortex simulation of flow around five generic bridge deck
669 sections. *Journal of Wind Engineering and Industrial Aerodynamics*; 77-78, 591-602.
- 670 Lesieur, D., Reithel, P., Dillenius, M. (1994) A practical approach for calculating
671 aerodynamic indicial functions with Navier-Stokes solver. AIAA 94-0059.
- 672 Löhner, R. (2008) *Applied computational fluid dynamics techniques: an introduction based on*
673 *finite element methods (2^o Edition)*. John Wiley & Sons Ltd.
- 674 Mannini, C., Soda, A., Schewe, G. (2010) Unsteady RANS modeling of flow past a rectangular
675 cylinder: investigation of Reynolds number effects. *Computers and Fluids*; 30, 1609-1624.
- 676 Mannini, C., Soda, A., Schewe, G. (2011) Numerical investigation on the three-dimensional
677 unsteady flow past a 5:1 rectangular cylinder. *Journal of Wind Engineering and Industrial*
678 *Aerodynamics*; 99, 469-482.

- 679 Mannini, C., Soda, A., Voß, R., Schewe, G. (2010) Unsteady RANS simulation of flow around a
680 bridge section. *Journal of Wind Engineering and Industrial Aerodynamics*; 98, 742-753.
- 681 Matsumoto, M. (1996) Aerodynamic damping of prisms. *Journal of Wind Engineering and*
682 *Industrial Aerodynamics*; 59, 159-175.
- 683 Mendes, P.A., Branco, F.A. (1998) Numerical wind studies for the Vasco da Gama Bridge,
684 Portugal. *Structural Engineering International*; 8(2), 124-128.
- 685 Menter, F., Esch, T. (2001) Elements of industrial heat transfer prediction. 16th Brazilian Congress
686 of Mechanical Engineering.
- 687 Morgenthal, G., McRobie, A. (2002) A comparative study of numerical methods for fluid-structure
688 interaction analysis in long-span bridge design. *Wind and Structures*; 5(2-4), 101-114.
- 689 Oliver, A. (2009) Mesh motion alternatives in OpenFOAM. PhD course in CFD with OpenSource
690 software project report. http://www.tfd.chalmers.se/~hani/kurser/OS_CFD_2009/. Accessed
691 July, 18th 2014.
- 692 Reinhold, T.A., Brinch, M., Damsgaard, A. (1992) Wind tunnel tests for the Great Belt Link. In:
693 Larsen, A. (Ed.), *Proceedings of the 1st International Symposium on Aerodynamics of Large*
694 *Bridges*, Copenhagen, Denmark.
- 695 Ribeiro, A.F.P. (2011) Unsteady RANS modeling of flow past a rectangular 5:1 cylinder:
696 investigation of edge sharpness effects. In: *Proc. of the 13th International Conference on Wind*
697 *Engineering*, Amsterdam, The Netherlands.
- 698 Sarkar, P.P., Caracoglia, L., Haan Jr., F.L., Sato, H., Murakoshi, J. (2009) Comparative and
699 sensitivity study of flutter derivatives of selected bridge deck sections, Part 1: analysis of inter-
700 laboratory experimental data. *Engineering Structures*; 31, 158-169.
- 701 Sarkic, A., Fisch, R., Hoffer, R., Bletzinger, K. (2012) Bridge flutter derivatives based on
702 computed, validated pressure fields. *Journal of Wind Engineering and Industrial*
703 *Aerodynamics*; 104-106, 141-151.
- 704 Sarkic, A., Hoffer, R. (2013) Improved numerical simulation of bridge deck aeroelasticity by
705 model validation. In: *Proceedings of the Sixth European-African Conference on Wind*
706 *Engineering*. Cambridge, UK.
- 707 Sarwar, M.W., Ishihara, T., Shimada, K., Yamasaki, Y., Ikeda, T. (2008) Prediction of
708 aerodynamic characteristics of a box girder bridge section using the LES turbulence model.
709 *Journal of Wind Engineering and Industrial Aerodynamics*; 96, 1895-1911.
- 710 Scanlan, R.H., Jones, N.P., Singh, L. (1997) Inter-relations among flutter derivatives. *Journal of*
711 *Wind Engineering and Industrial Aerodynamics*; 69-71, 829-837.
- 712 Scanlan, R.H., Tomko, J.J. (1971) Airfoil and bridge deck flutter derivatives. *Journal of the*
713 *Engineering Mechanics Division*. EM6, 1717-1737.
- 714 Schewe, G. (2009) Reynolds-number-effects in flow around a rectangular cylinder with aspect ratio
715 1:5. In: Borri, C., Augusti, G., Bartoli, G., Gacchini, L. (Eds.) *Proceedings of the Fifth*
716 *European and African Conference on Wind Engineering*. Firenze University Press, Florence,
717 Italy.
- 718 Scruton, C. (1981) *An introduction to wind effects on structures*. Oxford University Press.
- 719 Shimada, K., Ishihara, T. (2012) Predictability of unsteady two-dimensional k- ϵ model on the
720 aerodynamic instabilities of some rectangular prisms. *Journal of Fluids and Structures*; 28, 20-
721 39.
- 722 Simiu, E., Scanlan, R.H. (1996) *Wind effects on structures*. 3rd Edition; John Wiley & Sons, Inc.
- 723 Starossek, U., Aslan, H., Thiesemann, L. (2009) Experimental and numerical identification of
724 flutter derivatives for nine bridge deck sections. *Wind and Structures*; 12, 519-540.

725 Tubino, F. (2005) Relationships among aerodynamic admittance functions, flutter derivatives and
1 726 static coefficients for long-span bridges. *Journal of Wind Engineering and Industrial*
2 727 *Aerodynamics*; 93, 929-950.
3
4 728 Vairo, G. (2003) A numerical model for wind loads simulation on long-span bridges. *Simulation*
5 729 *Modelling Practice and Theory*; 11, 315-351.
6 730 Wilcox, D.C. (2006) *Turbulence modeling for CFD*. 3rd Edition; DCW Industries, Inc.
7 731 Xiang, H., Ge, Y. (2002) Refinements on aerodynamic stability analysis of super long-span
8 732 bridges. *Journal of Wind Engineering and Industrial Aerodynamics*; 90, 1493-1515.
9 733 Zhu, Z., Gu, M. (2014) Identification of flutter derivatives of bridge decks using CFD-based
10 734 discrete-time aerodynamic models. *Wind and Structures*; 18(3), 215-233.
11 735 Zhu, Z., Chen, Z., Gu, M (2009) CFD based simulations of flutter characteristics of ideal thin
12 736 plates with and without central slot. *Wind and Structures*; 12(1), 1-19.
13 737 Zhu, Z., Gu, M., Chen, Z. (2007) Wind tunnel and CFD study on identification of flutter
14 738 derivatives of a long-span self-anchored suspension bridge. *Computer-Aided Civil and*
15 739 *Infrastructure Engineering*; 22, 514-554.
16
17
18
19
20
21
22
23
24
25
26
27
28
29
30
31
32
33
34
35
36
37
38
39
40
41
42
43
44
45
46
47
48
49
50
51
52
53
54
55
56
57
58
59
60
61
62
63
64
65

Response to Reviewer #1's comments:

Reviewer #1: The authors have addressed all the comments expressed during the past review.

The paper has been significantly improved in its revised version.

The overall manuscript is complete and clear enough to deserve publication in the Journal of Wind Engineering and Industrial Aerodynamics without need of further reviews. Nevertheless, minor comments and suggestions are provided to the Authors by the reviewer. They are listed in the following.

1- Introduction, page 2, line 79 "CFD applications based on indicial functions are scarce in spite of their potential" instead of "Applications based on indicial functions are scarce in spite of its potential".

The sentence has been modified accordingly with the reviewer's comment.

2- Introduction, page 2, line 87 "A modified smoothed indicial approach was further developed in ..." instead of "The method was further developed in"

The sentence has been modified accordingly with the reviewer's comment.

3- Introduction, page 3, line 91-95 "More recently Zhu and Gu (2014) have extended the method to extract the flutter derivatives of bridge decks, even if the application of the modified indicial approach to bluff bodies remains questionable." instead of "More recently Zhu and Gu (2014) have presented a method to extract the flutter derivatives of bridge decks. The approach is based on imposing, by means of a smooth exponential function, heave or pitch motions on the deck for the identification of the aerodynamic system and the subsequent system simulation to obtain lift and moment forces under harmonic oscillation".

The sentence has been modified accordingly with the reviewer's comment:

"More recently Zhu and Gu (2014) have presented a method to extract the flutter derivatives of **streamlined** bridge decks, **even if the application of the modified indicial approach to bluff bodies remains questionable**"

4- Introduction, page 3, line 128 "A rectangular cylinder showing a separated and reattached time-averaged flow pattern has been selected" instead of "A rectangular cylinder showing a fully attached time averaged flow pattern has been selected".

The sentence has been modified accordingly with the reviewer's comment.

5- Figure 3a should be removed, because it does not provide significant further information than the one in Figures 1 and 2.

The figure has been removed accordingly with the reviewer's suggestion.

Response to Reviewer #2's comments:

Reviewer #2: Comments to specific lines in the paper:

Line 123: Include version of OpenFoam as the software is evolving and can change.

The version of the software (v2.1.1) has been included.

Line 235: "H is the section depth or height". Isn't it sufficient to write height?

The term depth has been deleted accordingly with the reviewer's comment.

Line 277: Perhaps also include the boundary conditions here as you do for the rectangular case. Or write that they are identical to the rectangular case.

In the text it is indicated in line 286 (in the track version of the actual manuscript) that the boundary conditions are the same as in the rectangular cylinder case. It has been eliminated in line 252 in the former version of the manuscript "The same boundary conditions have been applied in the G1 section case".

Line 281: Add to figure caption that it is the geometry of the G1 section.

The figure caption has been modified accordingly with the reviewer's comment.

Line 307: I think it is a little bit misleading to write that no significant differences are found when you find quite large differences in the standard deviations for the coarse mesh. As you also mention in the following sentence.

The sentence in lines 307-308 has been eliminated.

Line 374: Perhaps write that it is span-averaged (if it is) instead of side-averaged. Just to be clearer in the formulation.

We are following here the terminology in Bruno et al. (2014), which is the reference used for validation. Side-averaged means that the distribution of the pressure coefficient is averaged between the upper and lower half perimeters. We are not considering the average in the span-wise direction since our simulations are 2D.

In the manuscript we have included the formal definition of "side-averaged".

Line 388 and line 464 It's not necessary to write time-standard deviation or standard deviation in time as it is obvious that it is of the time history.

The references to time have been eliminated in those two lines.

Line 414: "for the all the simulations" (rephrase)

The sentence has been corrected.

In lines 414-417 you write the y^+ values for the maximum and minimum Re numbers. Here it would be good to also report the Re number and not only the velocities for more easy comparison to the y^+ values you report earlier in the paper.

Accordingly with the reviewer's suggestion the Reynolds numbers have been included in the text.

Line 424: You write minimal differences. Perhaps its better to write good agreement and then elaborate with the maximum deviation in the reported std value.

The sentences in lines 433-436 (in the track version of the actual manuscript) have been modified following the reviewer's suggestion.

In line 440-441 you start with writing that the flutter derivatives offer a good agreement along the completer range of the reduced velocities. Even though there are some discrepancies which you also write about in the following sentences. Therefore I thin the sentence in line 440-441 is misleading and should be omitted or rephrased.

The sentence has been eliminated, accordingly with the suggestion of the reviewer.

444: "direct evaluations". Please elaborate that.

The term "direct evaluations" has been eliminated and the sentence rephrased as:

"...are comparable with the ones found in CFD simulations where forced oscillations in the heave degree of freedom have been conducted, such as in..."

454: You write that the simulations has been extended along 65 non-dimensional time units. I would prefer some other word than extended where you write clearly that this is the sampling duration for the time statistics and not including the initial time of the simulation (if that's the case).

In the manuscript it has been added that the time statistics correspond to the final 45 non-dimensional time units.

In line 476 you write that the agreement is remarkable. Is that the case? I can see it is a good agreement. However, isn't it in general you get good agreement between RANS simulations and the simulated time-averaged quantities? Therefore I would prefer you use another word than remarkable if that is the case.

It has been changed "remarkable" by "good".

lines 555-557: This is good how you enhance the good agreement with your results with the "reduced" simulations.

Thank you for the comment.

In general:

The structure of the paper is highly improved and your aim and contribution to the field of research is much clearer than before.

However, I still experience some of the sentences as confusing to read. (An example is in lines 138-140, lines 245-247).

The aforementioned sentences have been rephrased as:

“However, in the case that additional numerical studies would require validation against experimental data outside the range found in the literature, further wind tunnel tests could readily be conducted using the existing $B/H=4.9$ sectional model.”

“A constant velocity inlet has been set at the upwind boundary (the left side in the figure) of the computational domain. The incoming flow has a turbulence intensity of 1 % along with a $0.1B$ turbulent length scale as per Ribeiro (2011).”

Figure 1
[Click here to download high resolution image](#)

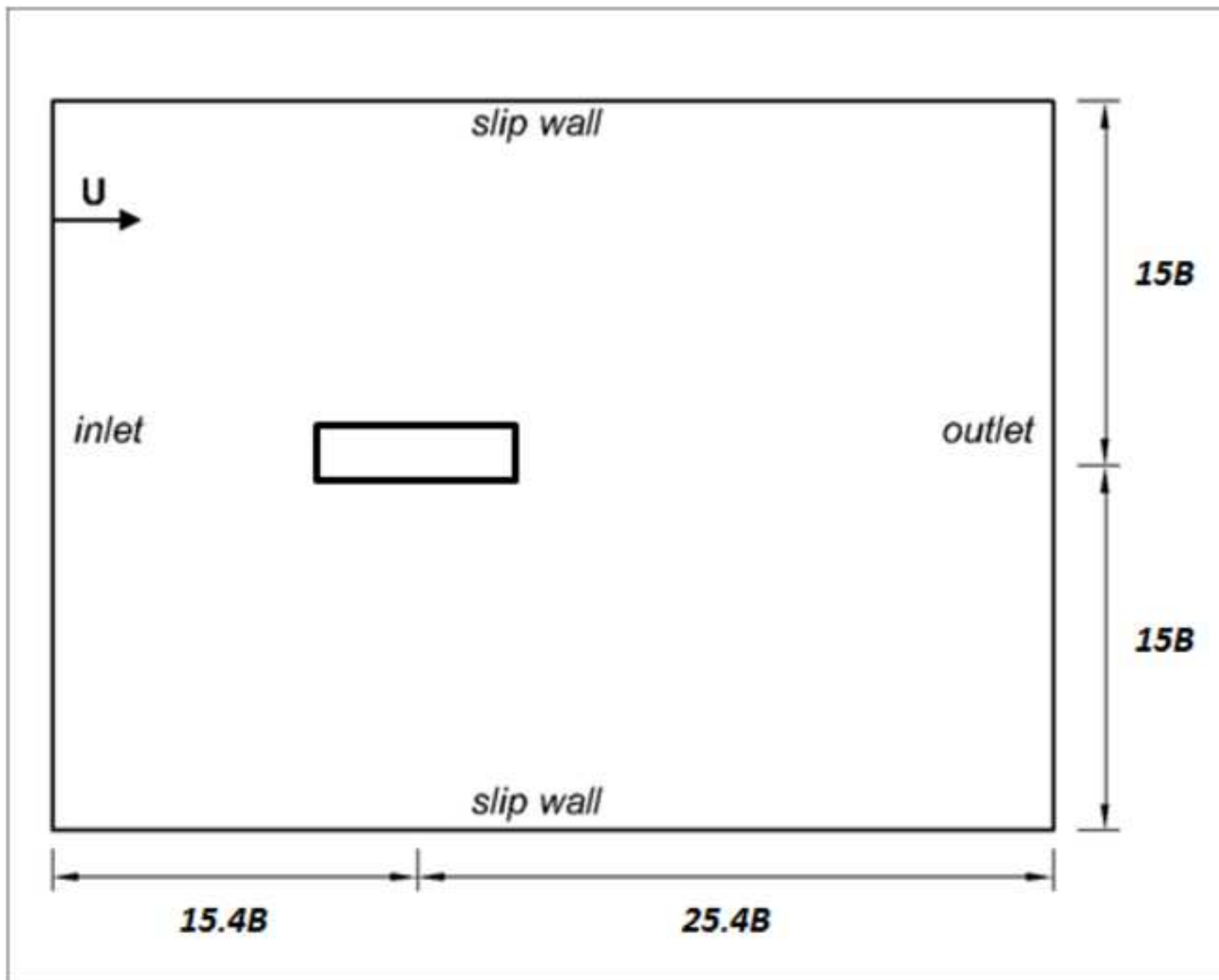


Figure 2
[Click here to download high resolution image](#)

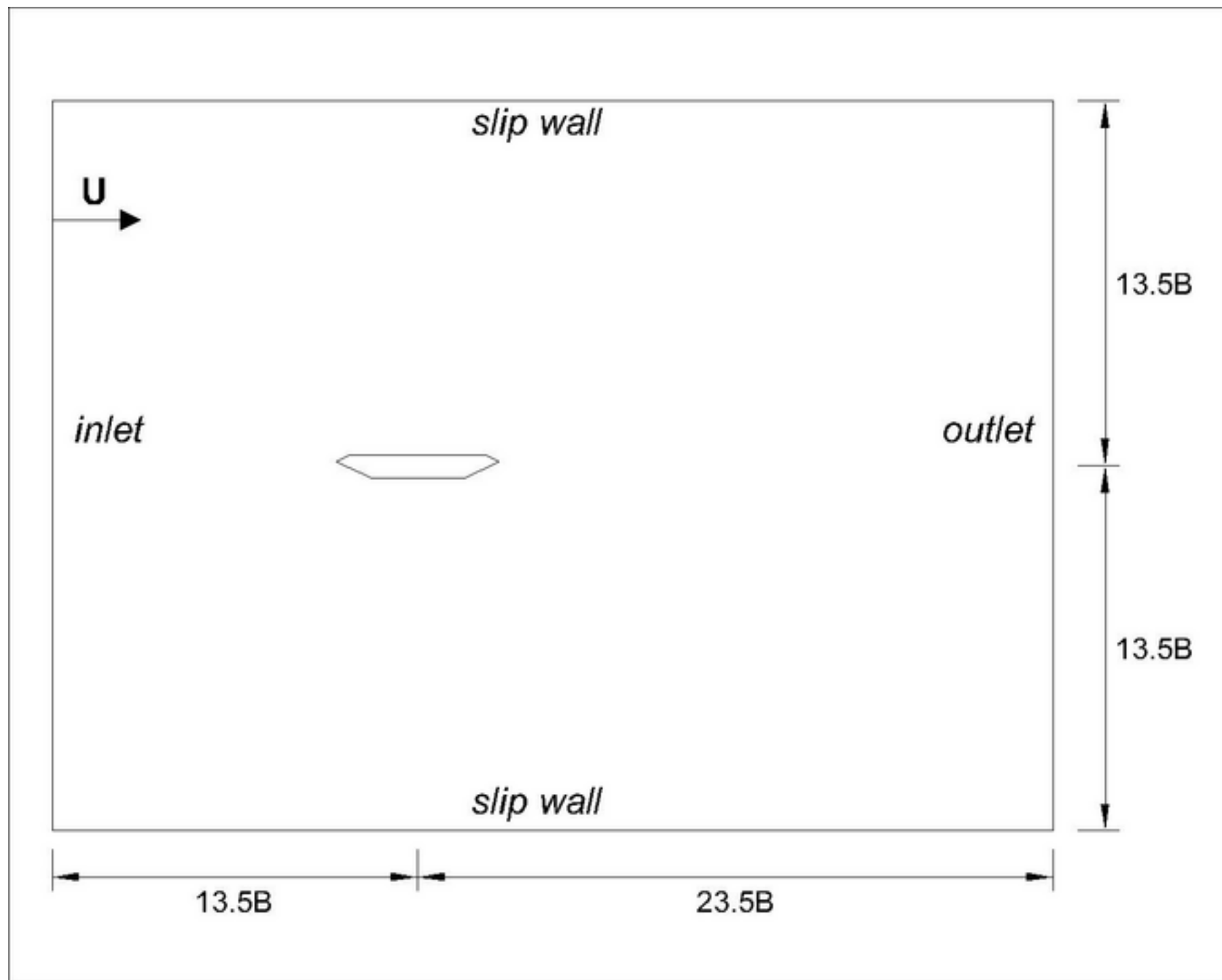


Figure 3a
[Click here to download high resolution image](#)

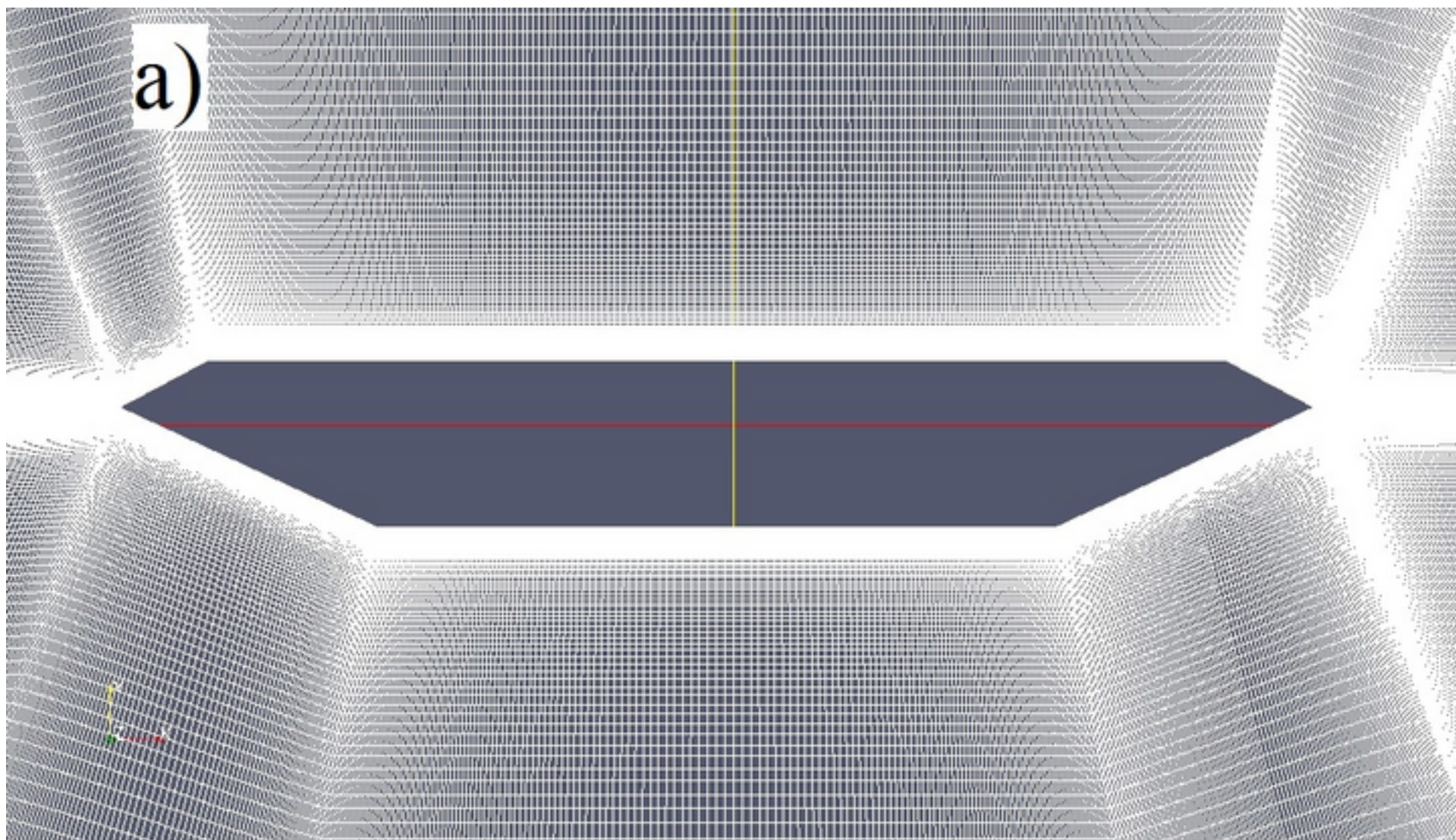


Figure 3b
[Click here to download high resolution image](#)

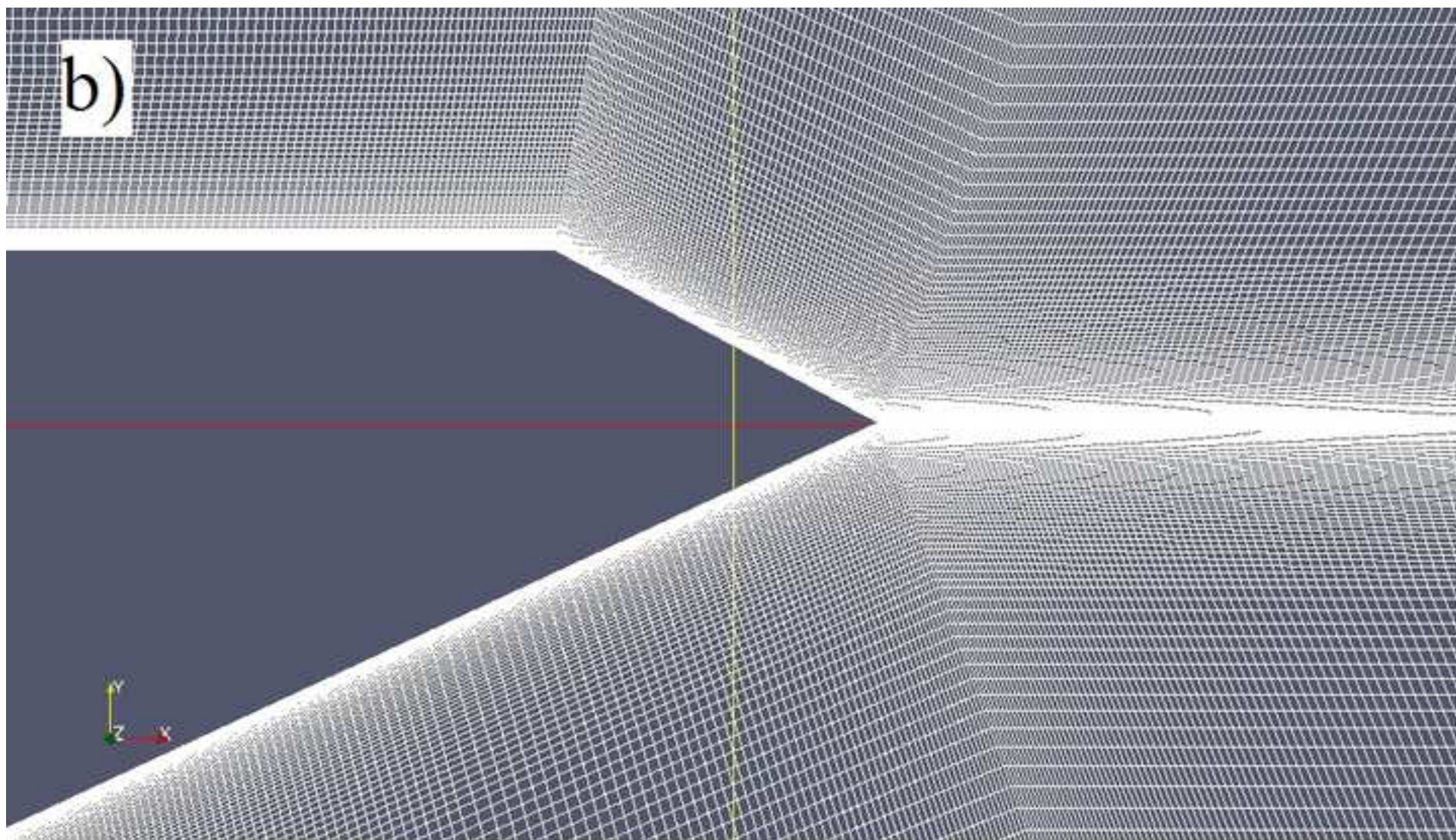


Figure 4
[Click here to download high resolution image](#)

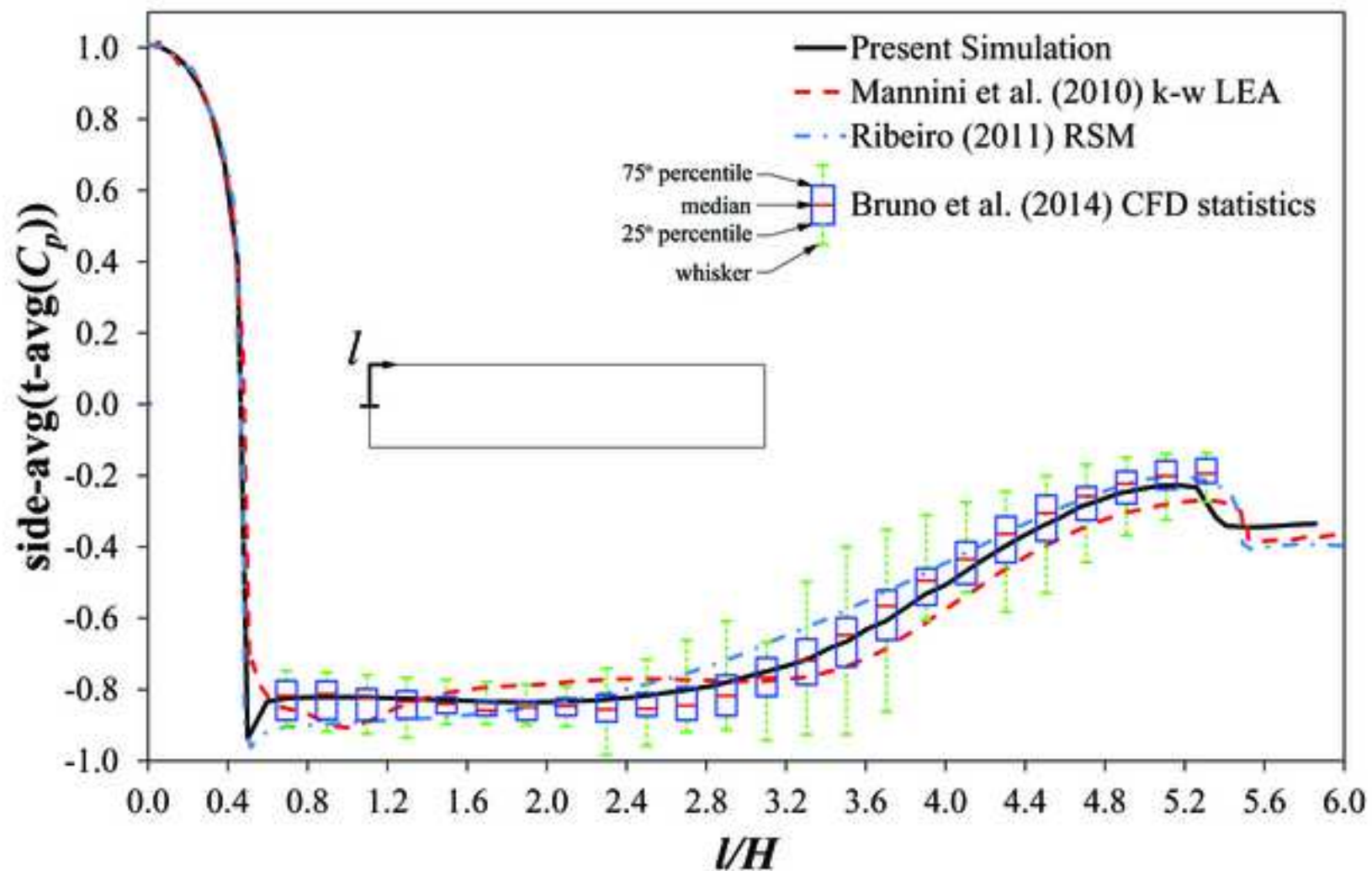


Figure 5
[Click here to download high resolution image](#)

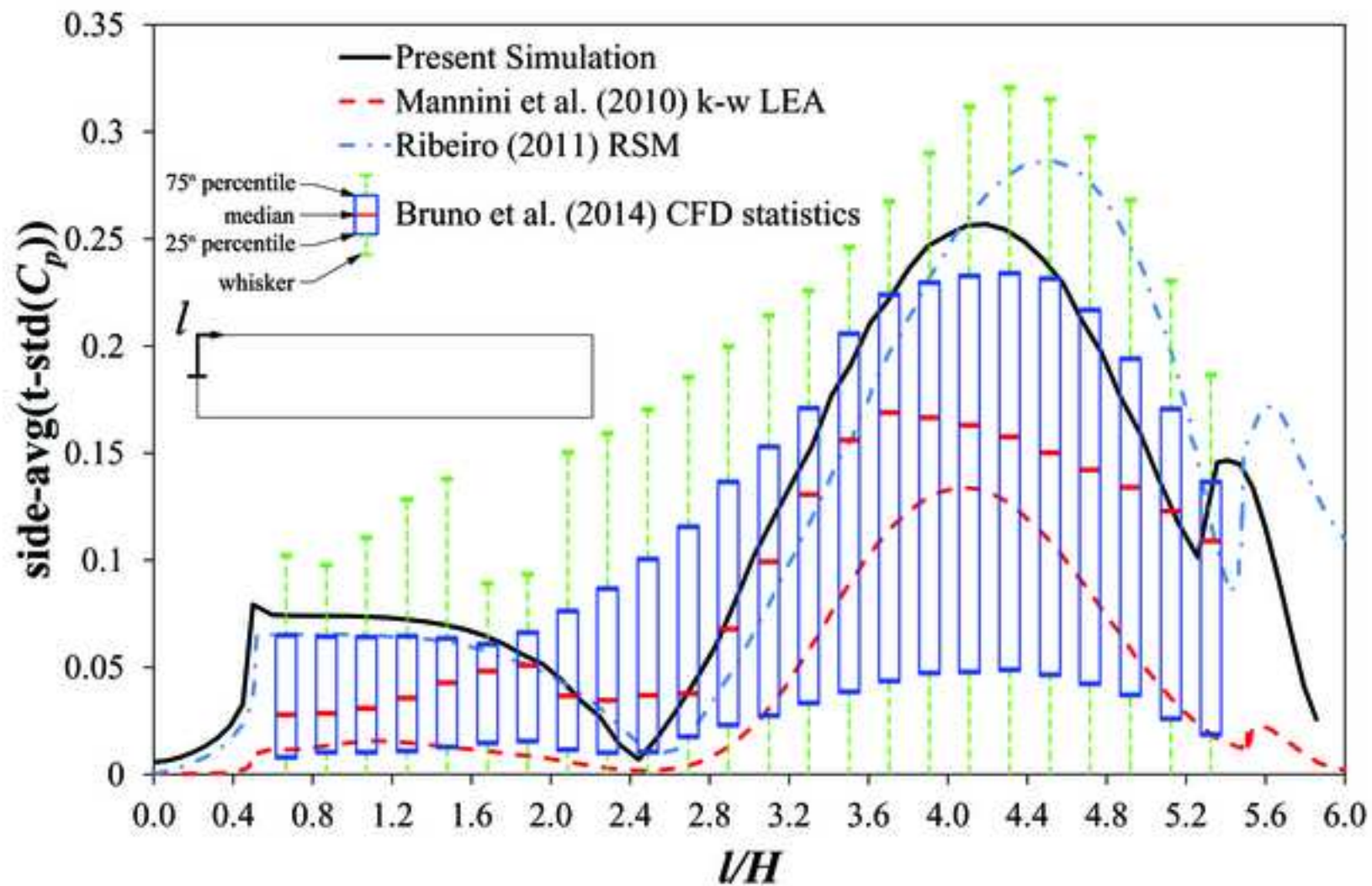


Figure 6a
[Click here to download high resolution image](#)

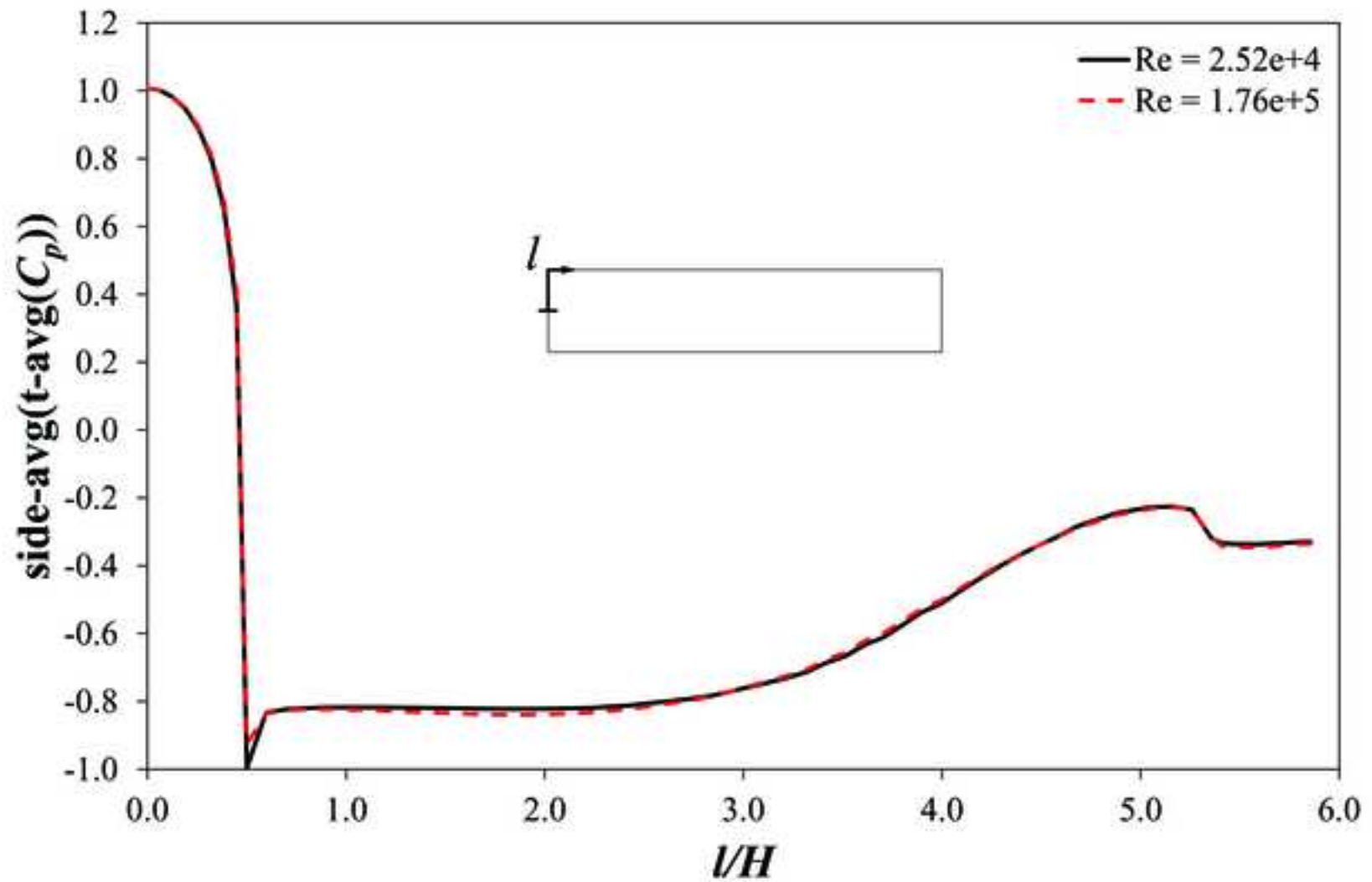


Figure 6b
[Click here to download high resolution image](#)

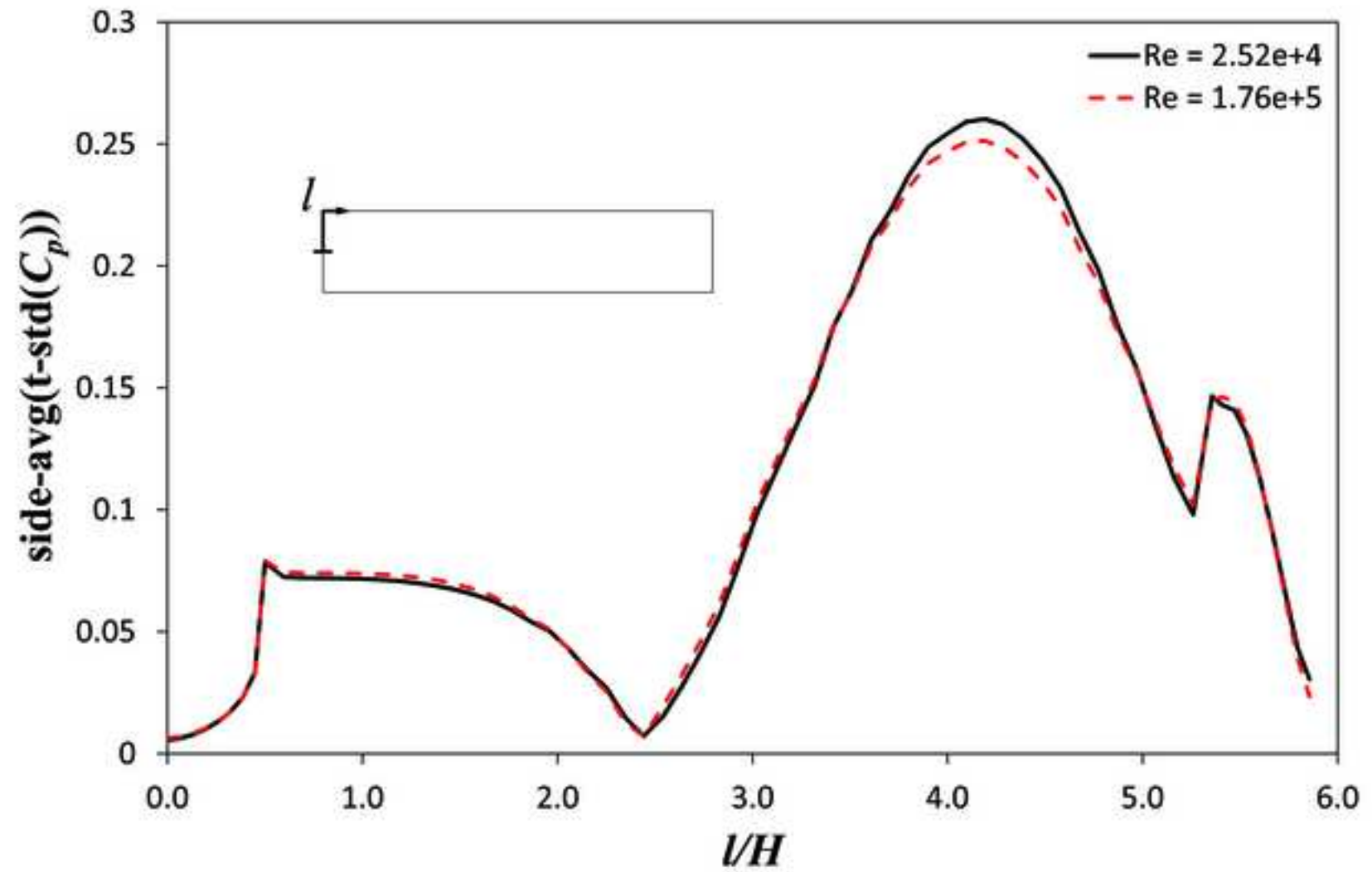


Figure 7 A1

[Click here to download high resolution image](#)

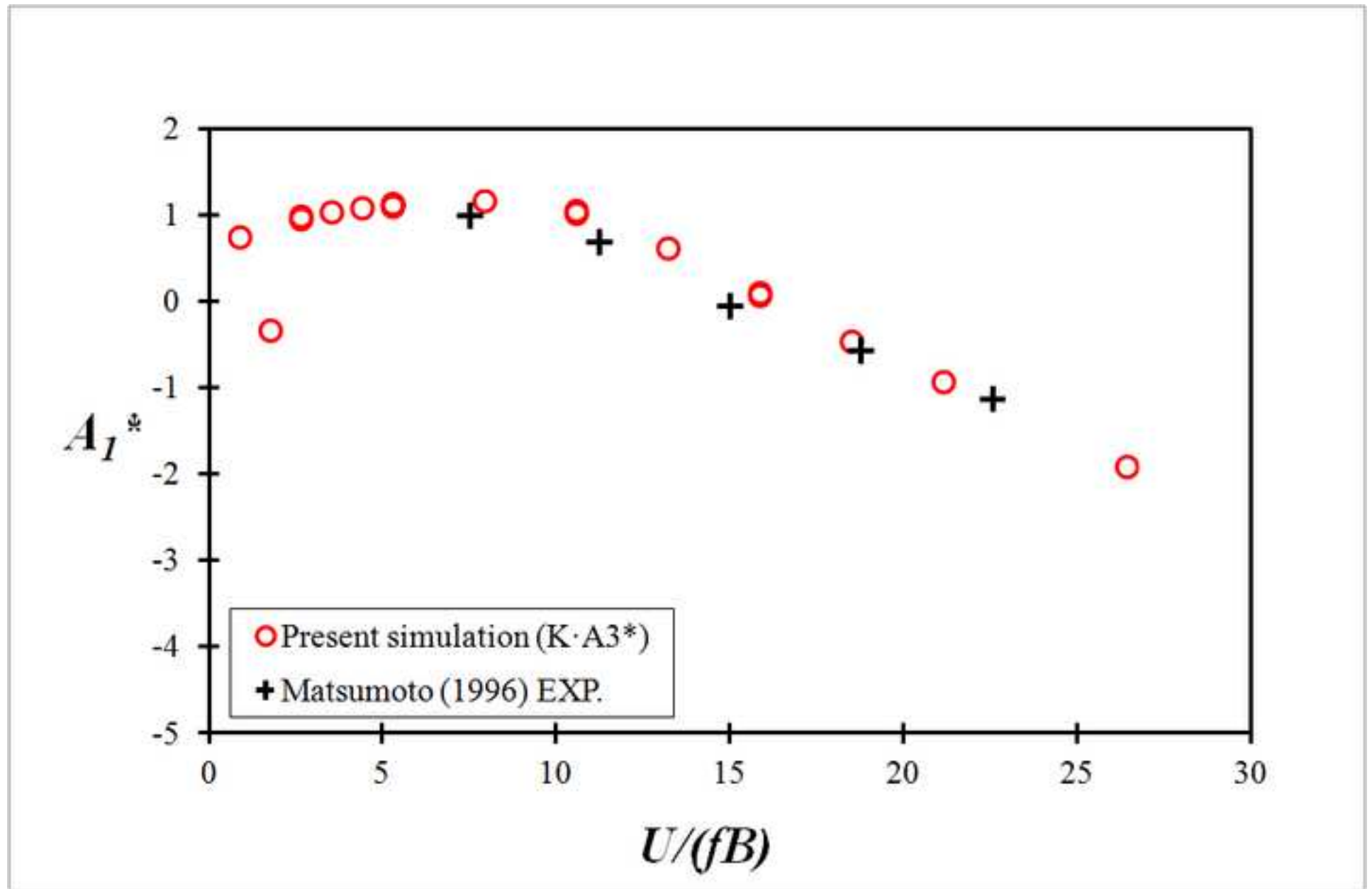


Figure 7 A2
[Click here to download high resolution image](#)

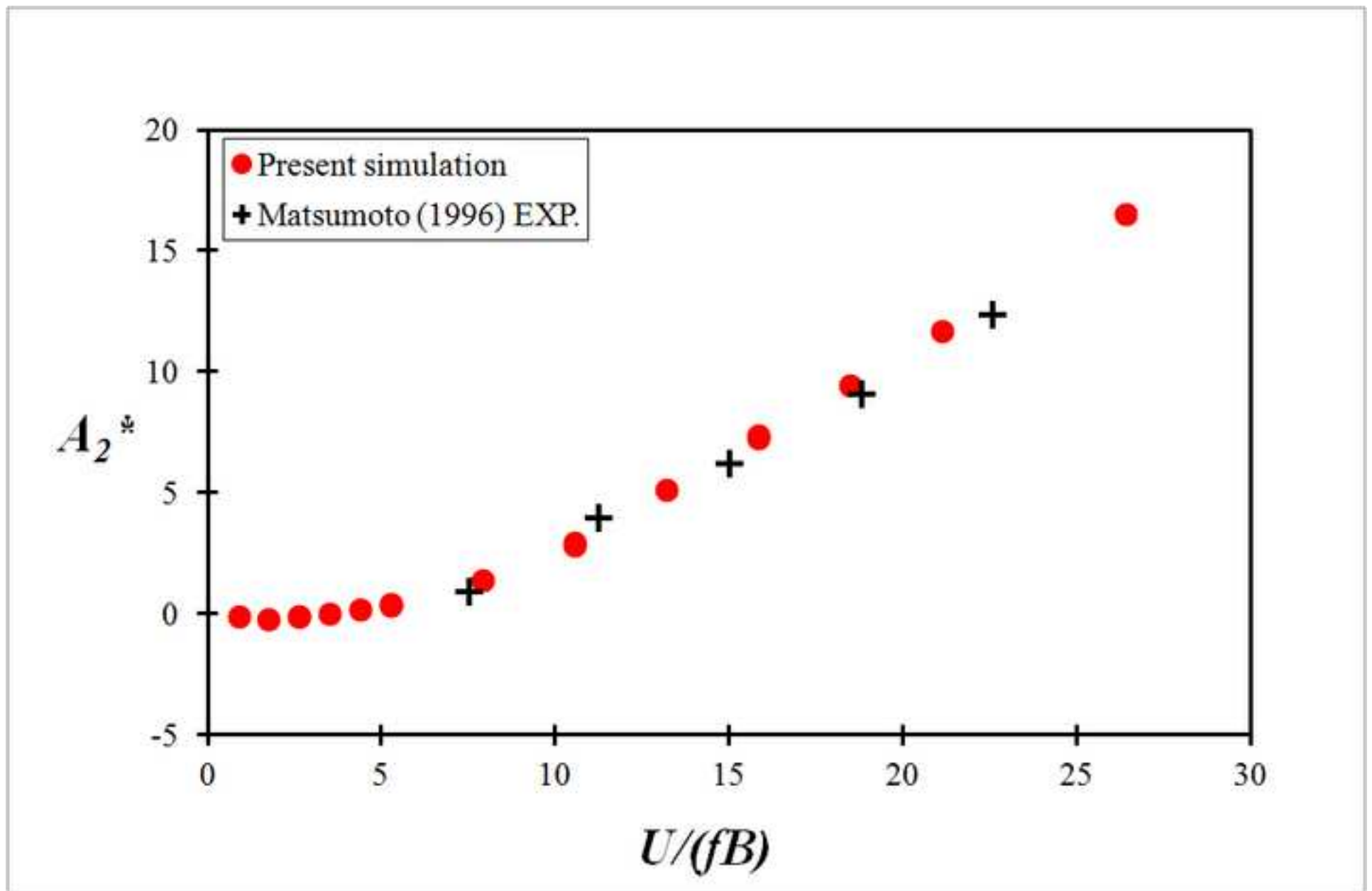


Figure 7 A3
[Click here to download high resolution image](#)

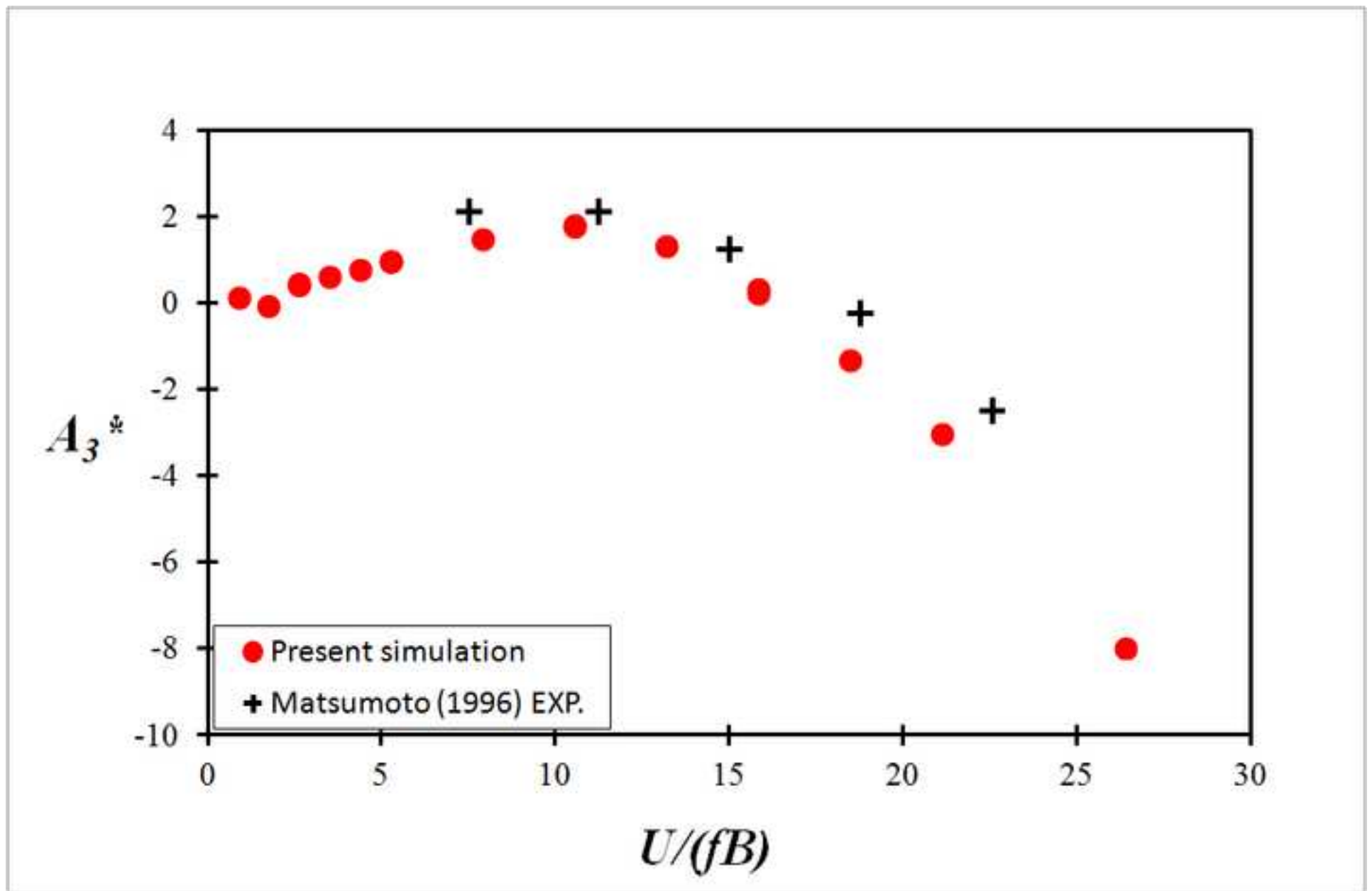


Figure 7 A4

[Click here to download high resolution image](#)

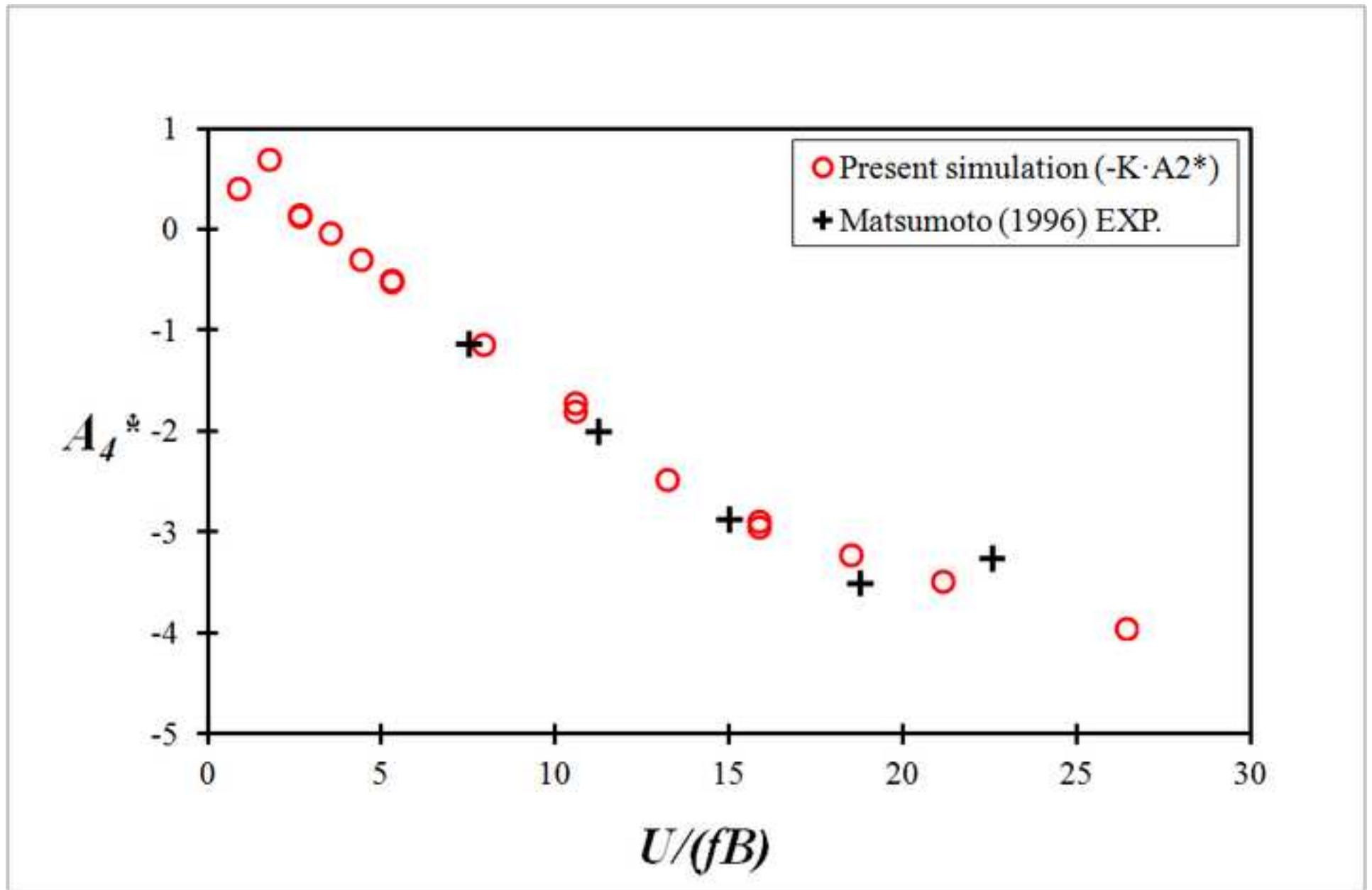


Figure 7 H1

[Click here to download high resolution image](#)

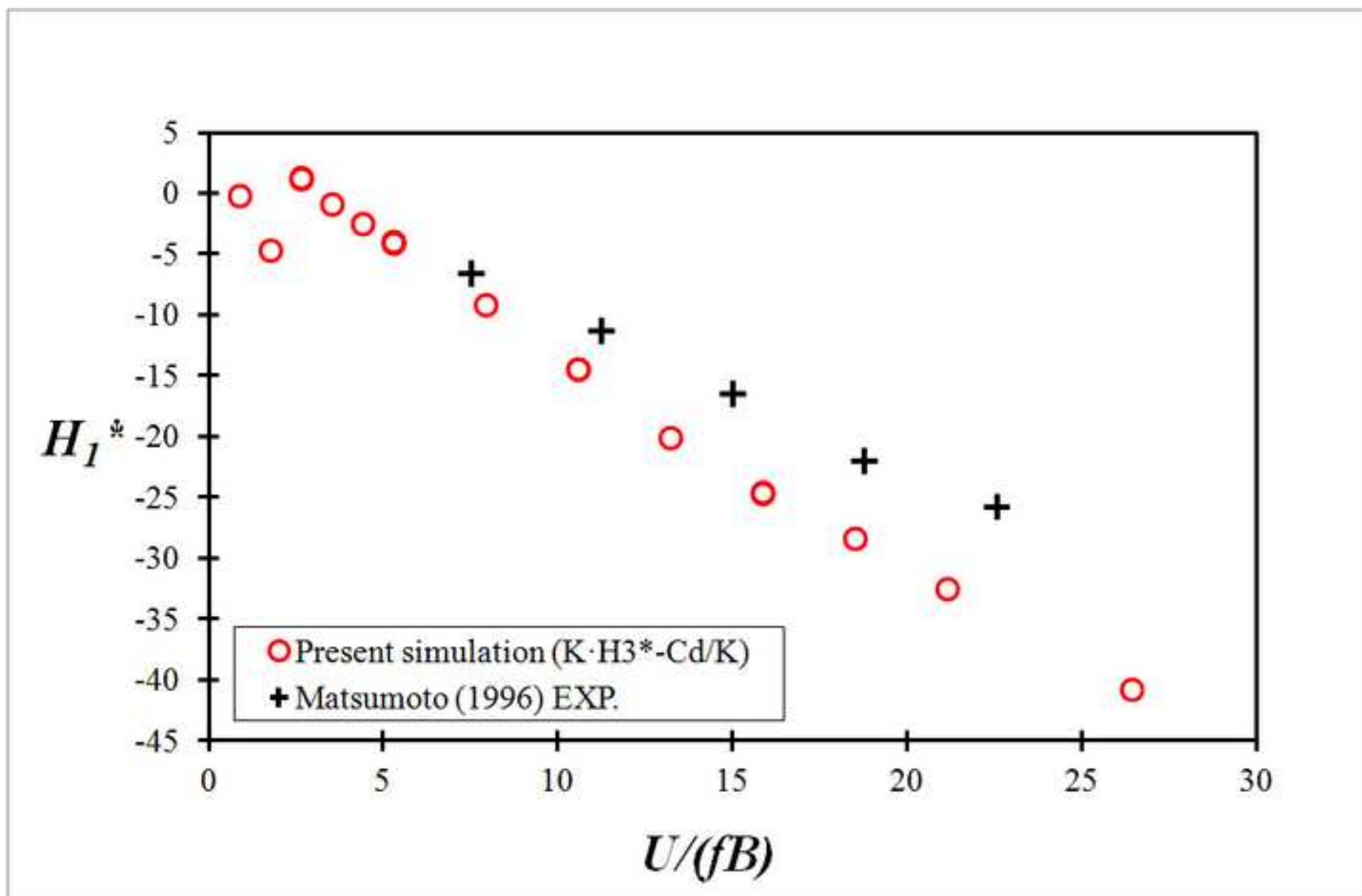


Figure 7 H2

[Click here to download high resolution image](#)

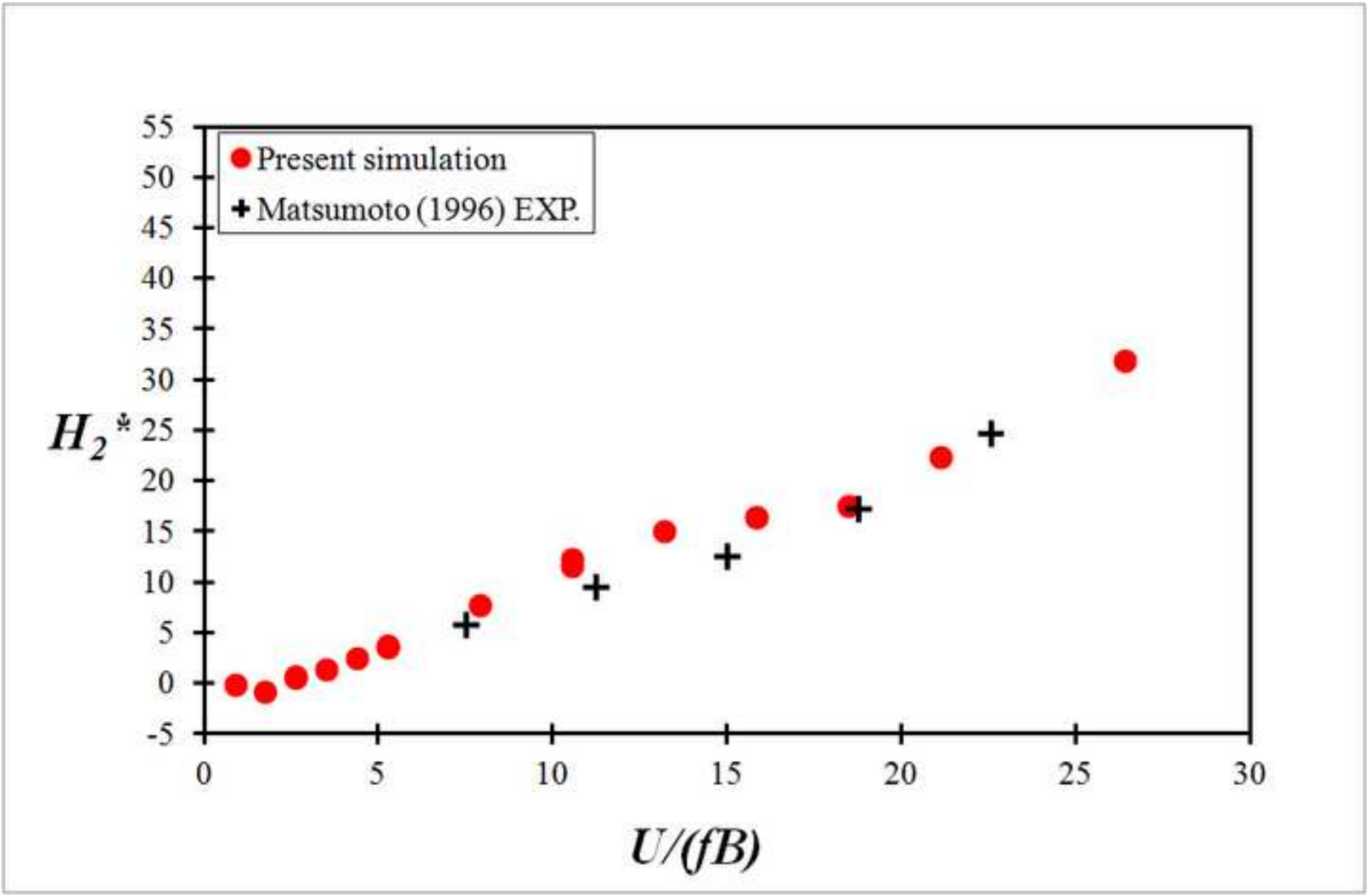


Figure 7 H3
[Click here to download high resolution image](#)

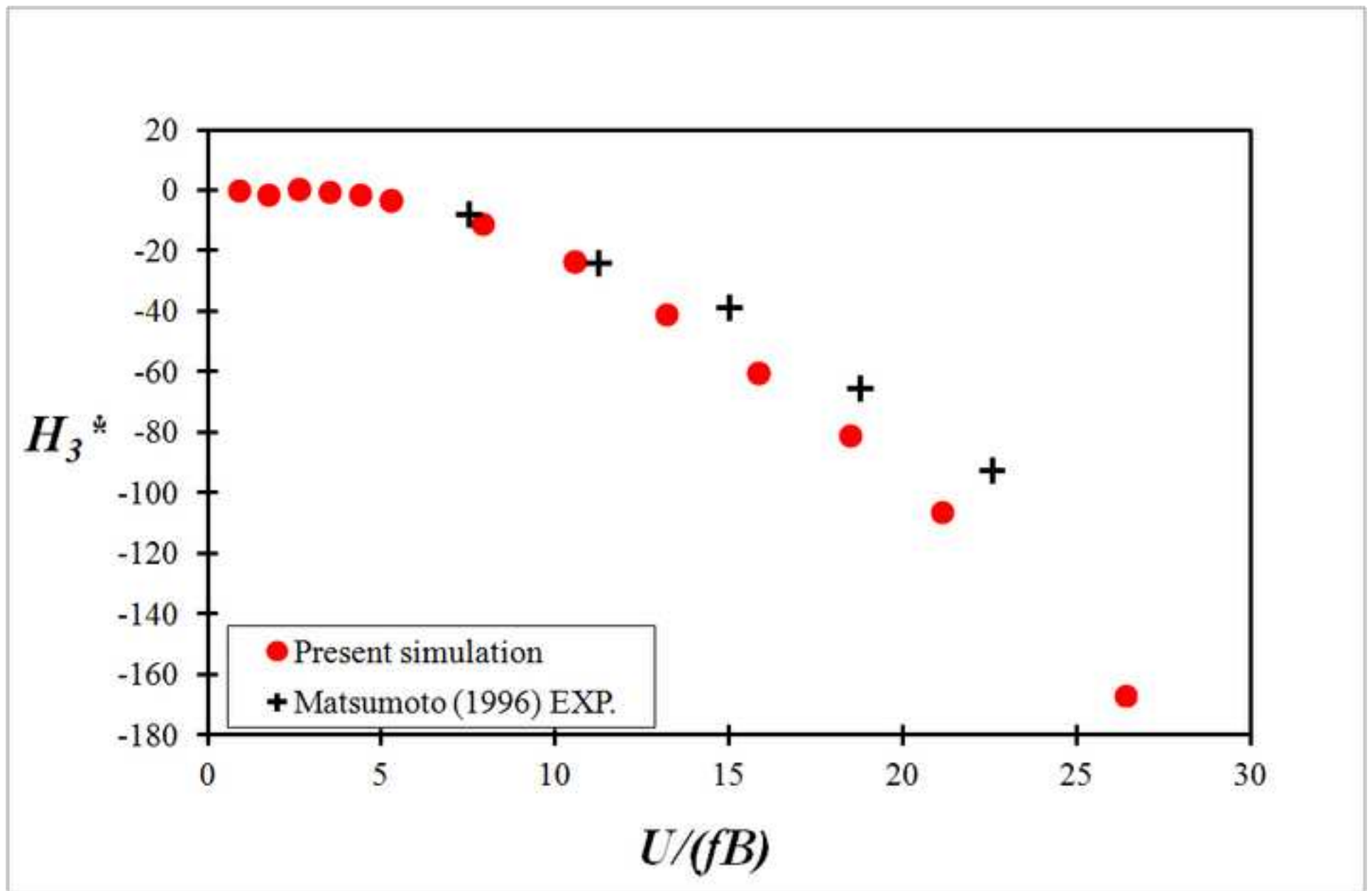


Figure 7 H4
[Click here to download high resolution image](#)

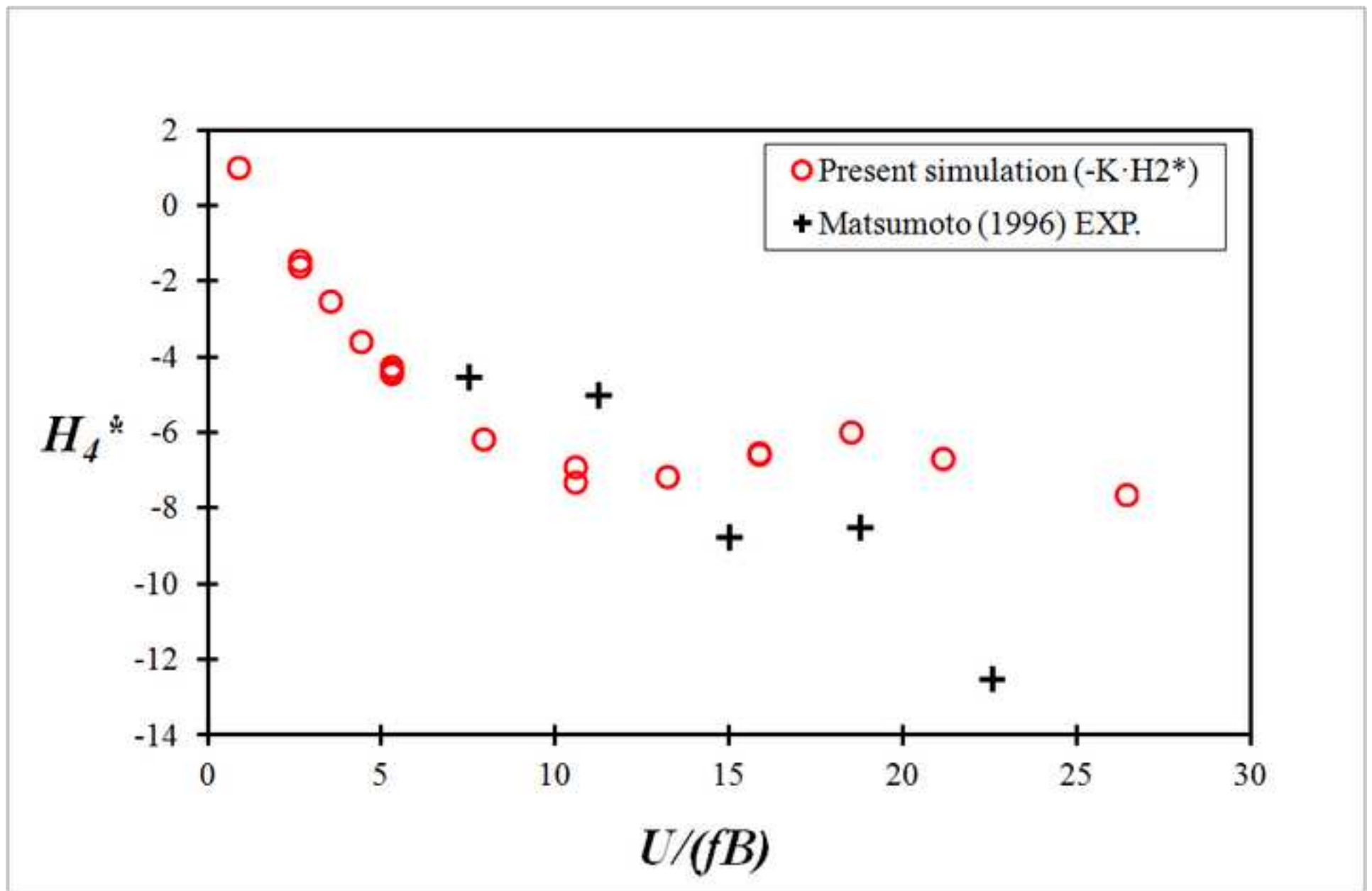


Figure 8
[Click here to download high resolution image](#)

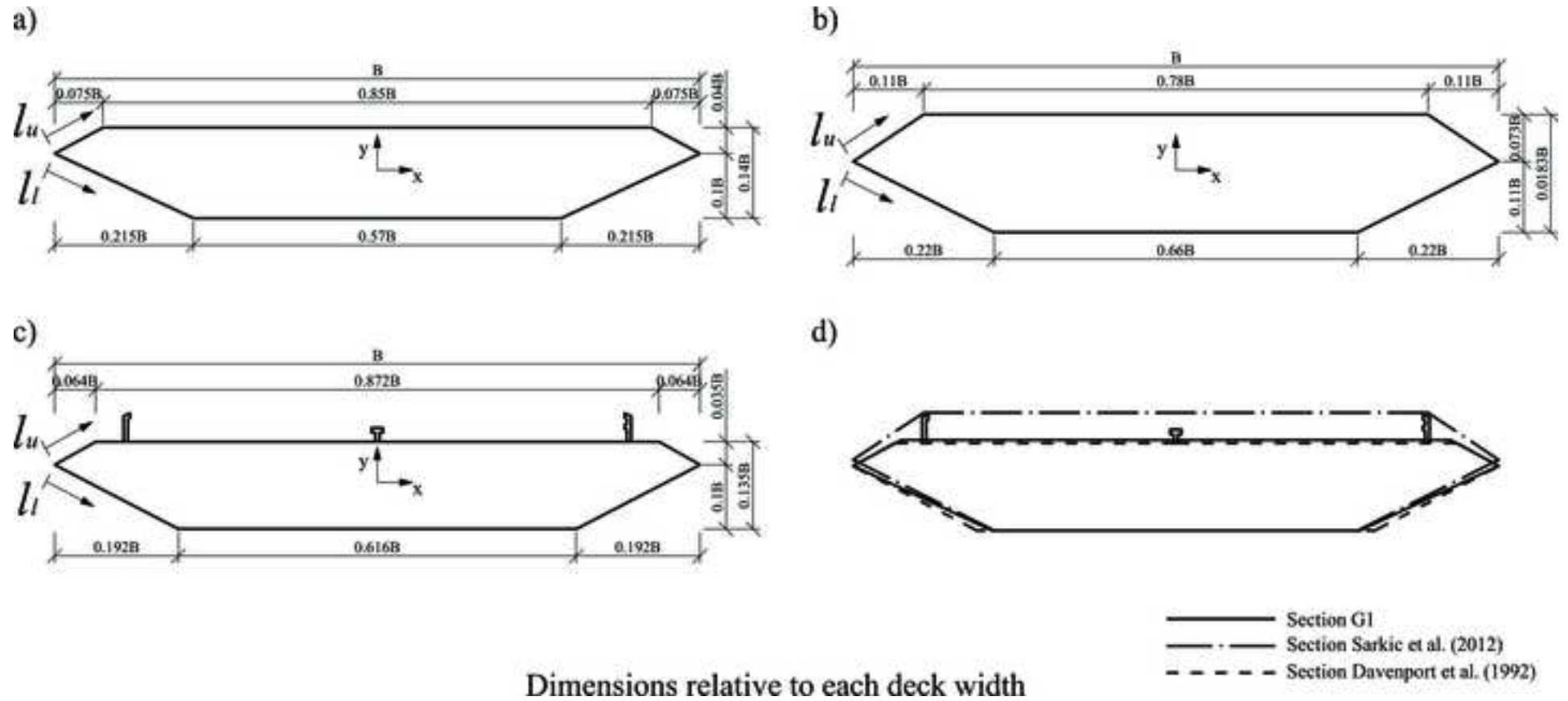


Figure 9a
[Click here to download high resolution image](#)

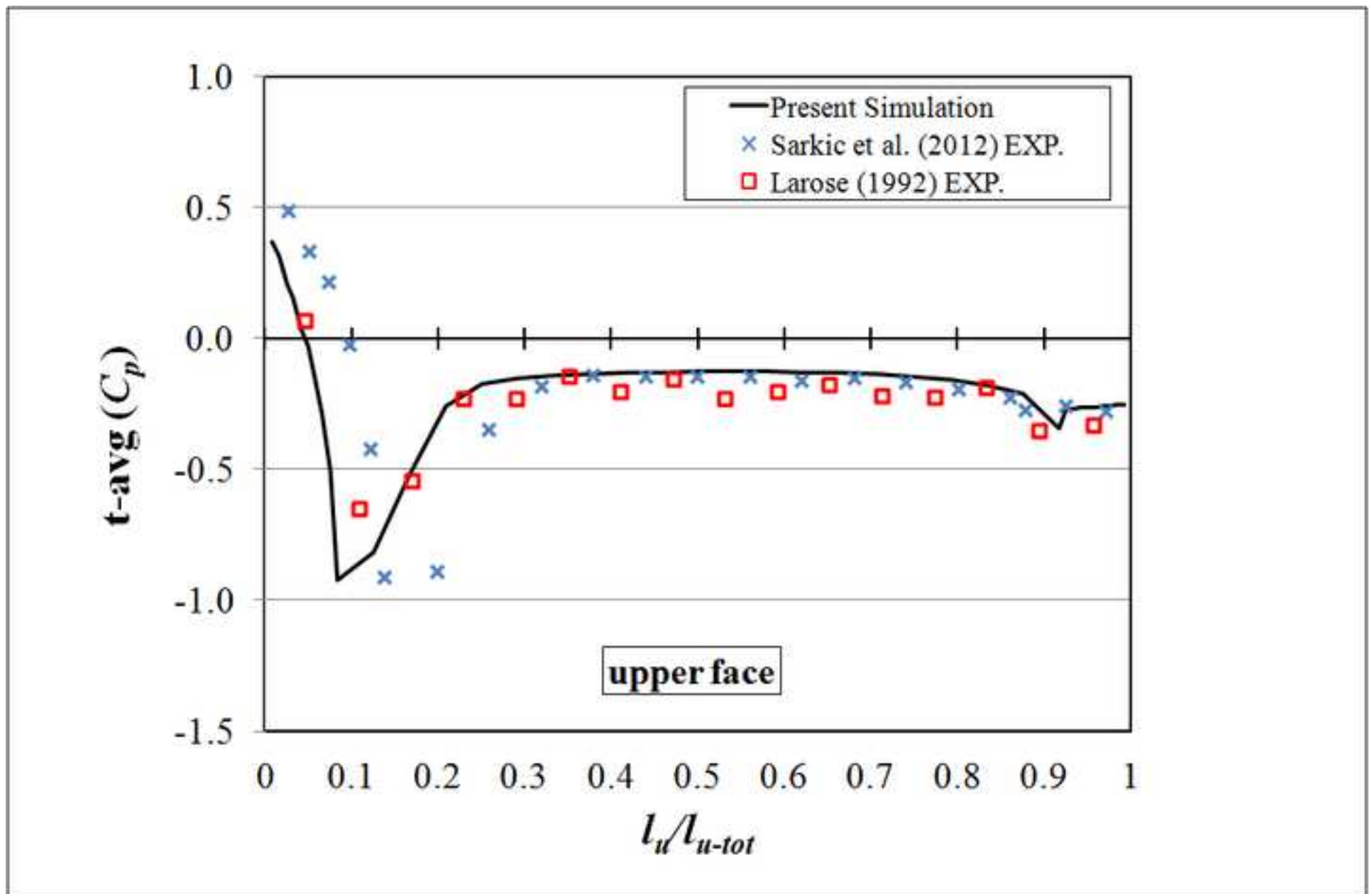


Figure 9b
[Click here to download high resolution image](#)

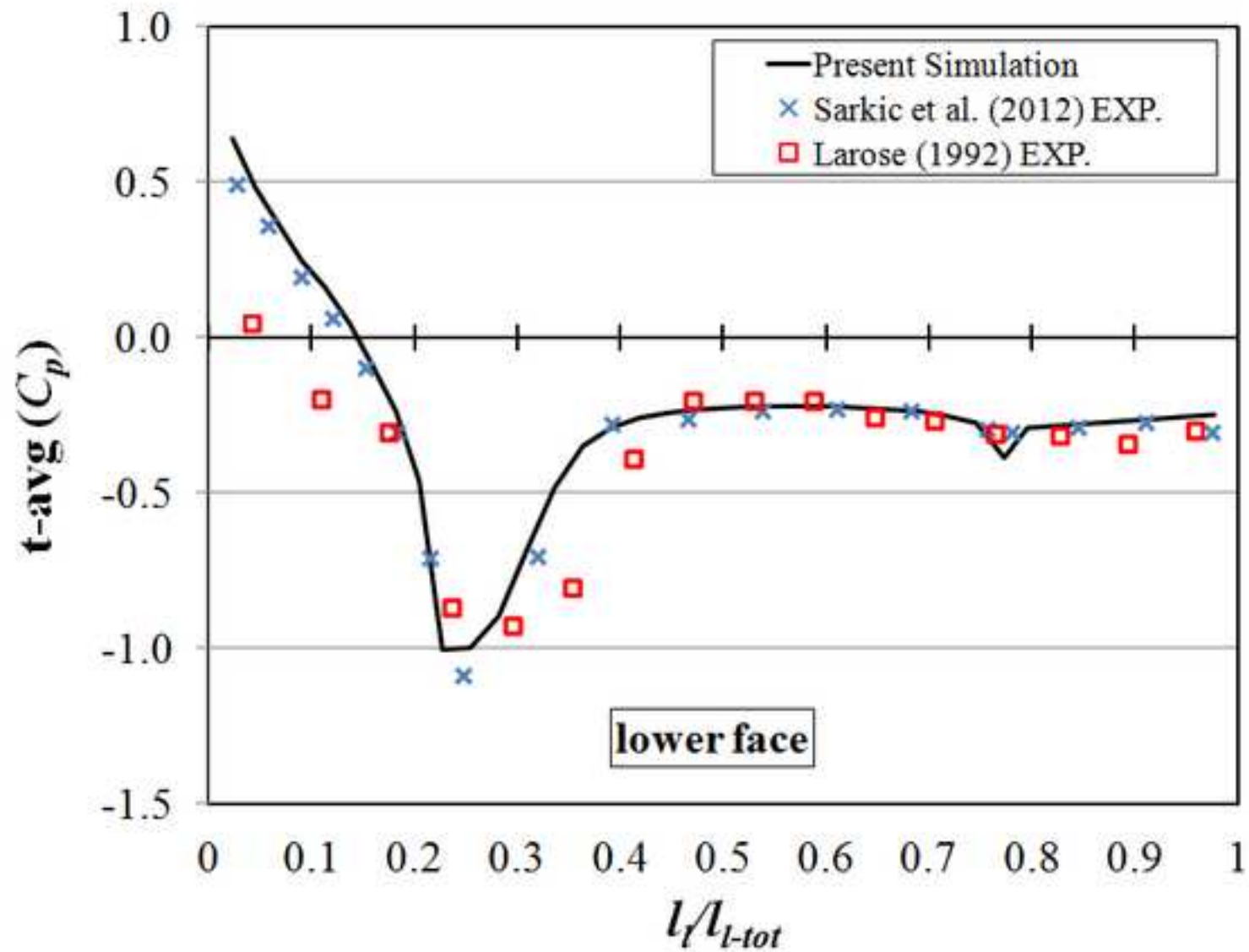


Figure 10
[Click here to download high resolution image](#)

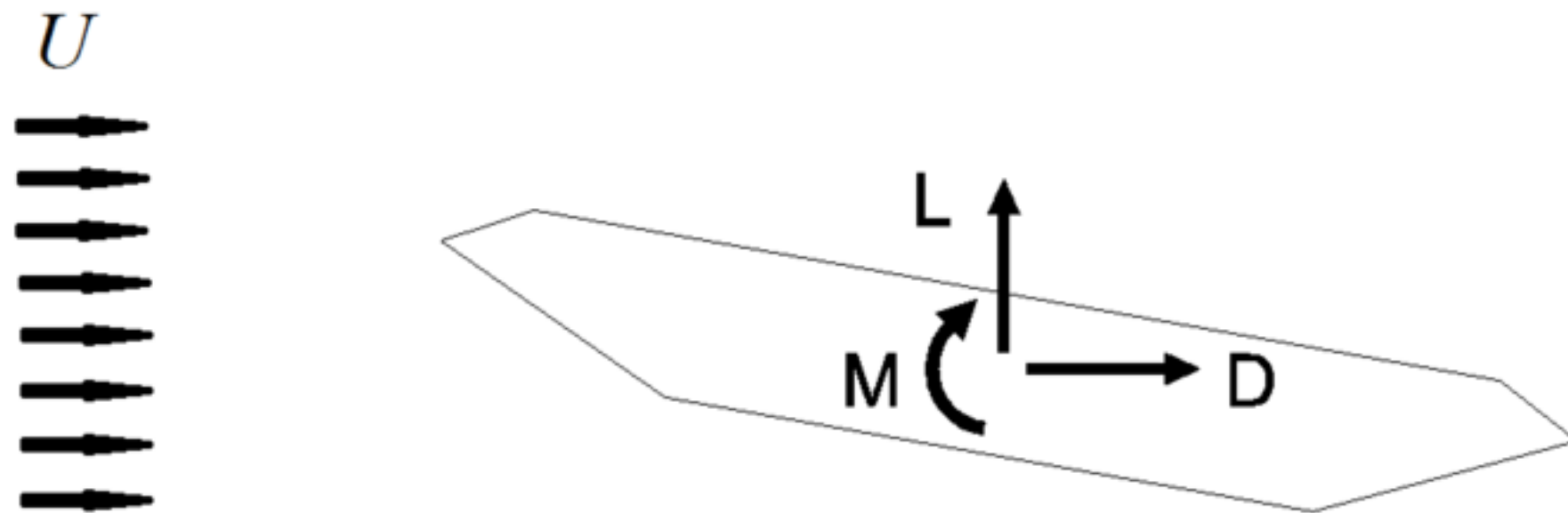


Figure 10 b
[Click here to download high resolution image](#)

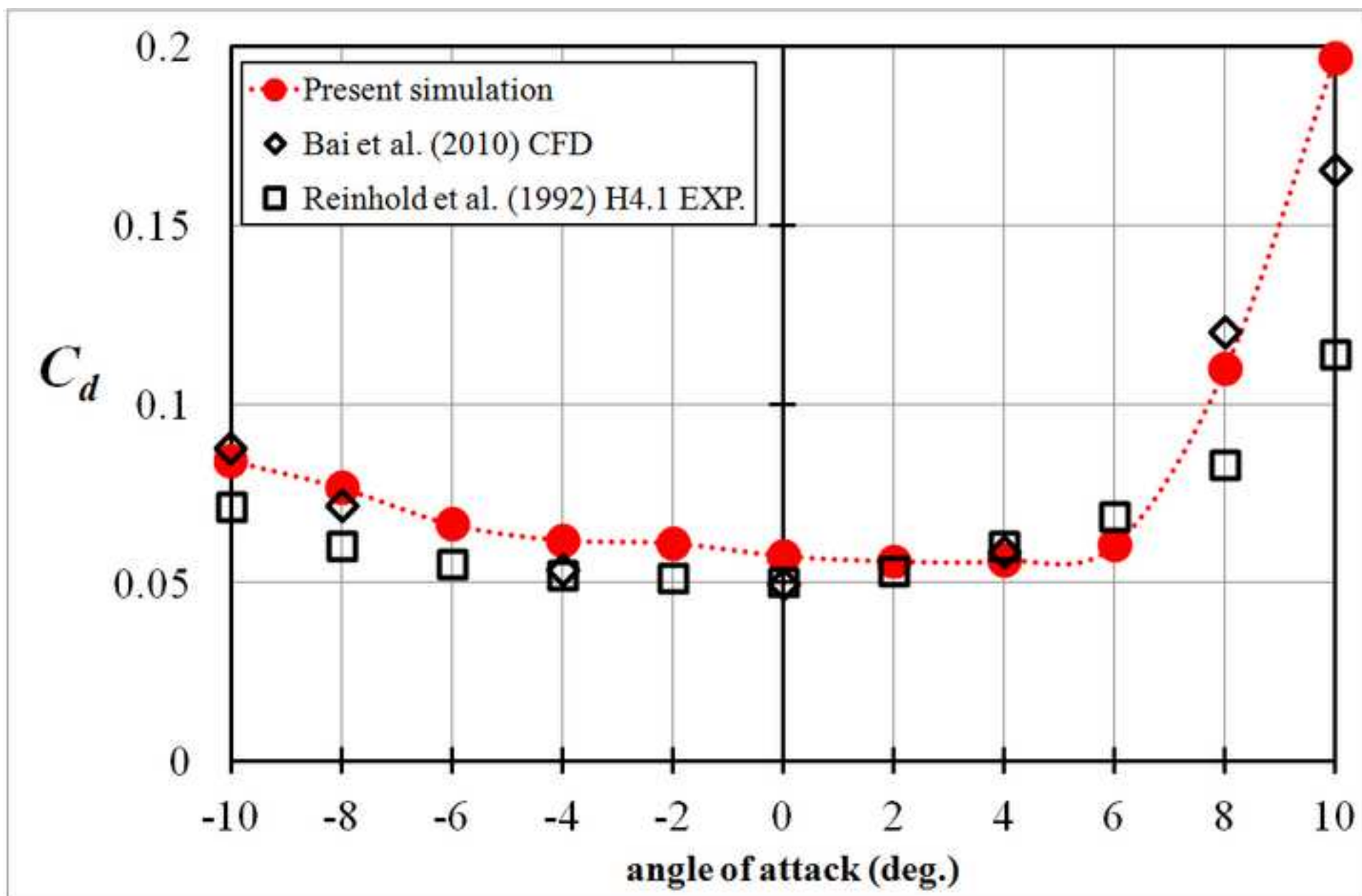


Figure 10 c
[Click here to download high resolution image](#)

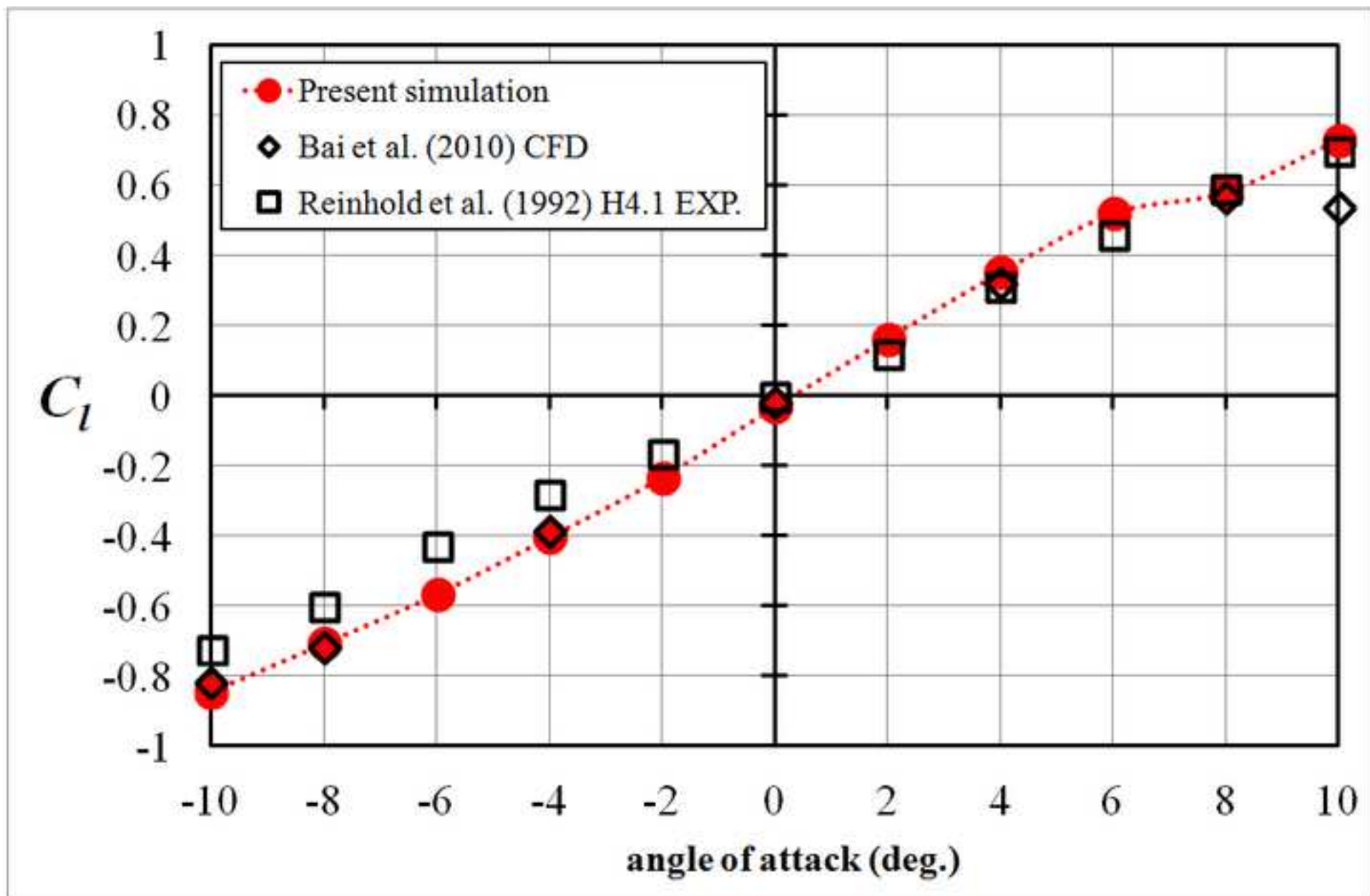


Figure 10 d
[Click here to download high resolution image](#)

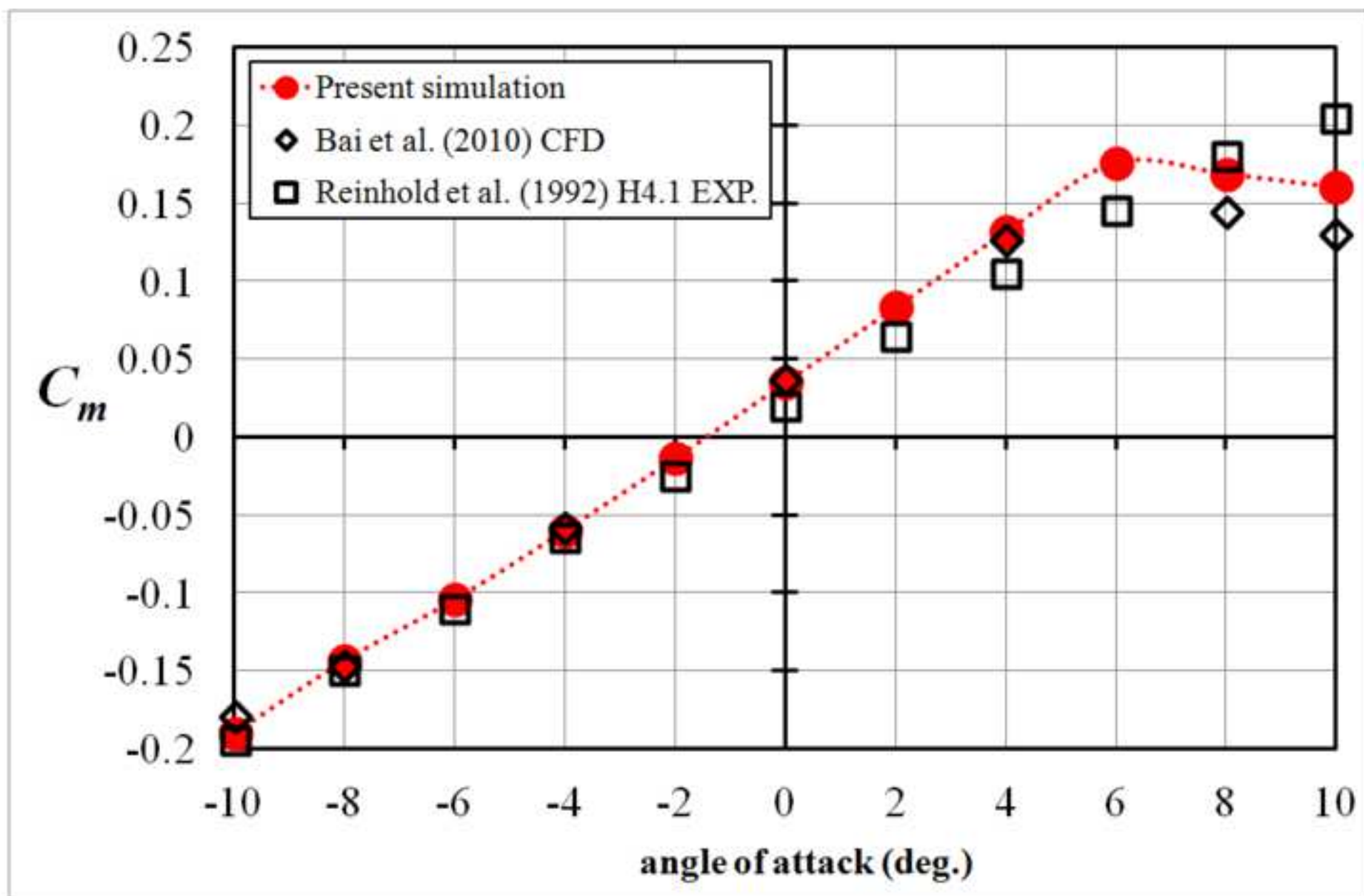


Figure 11 A1

[Click here to download high resolution image](#)

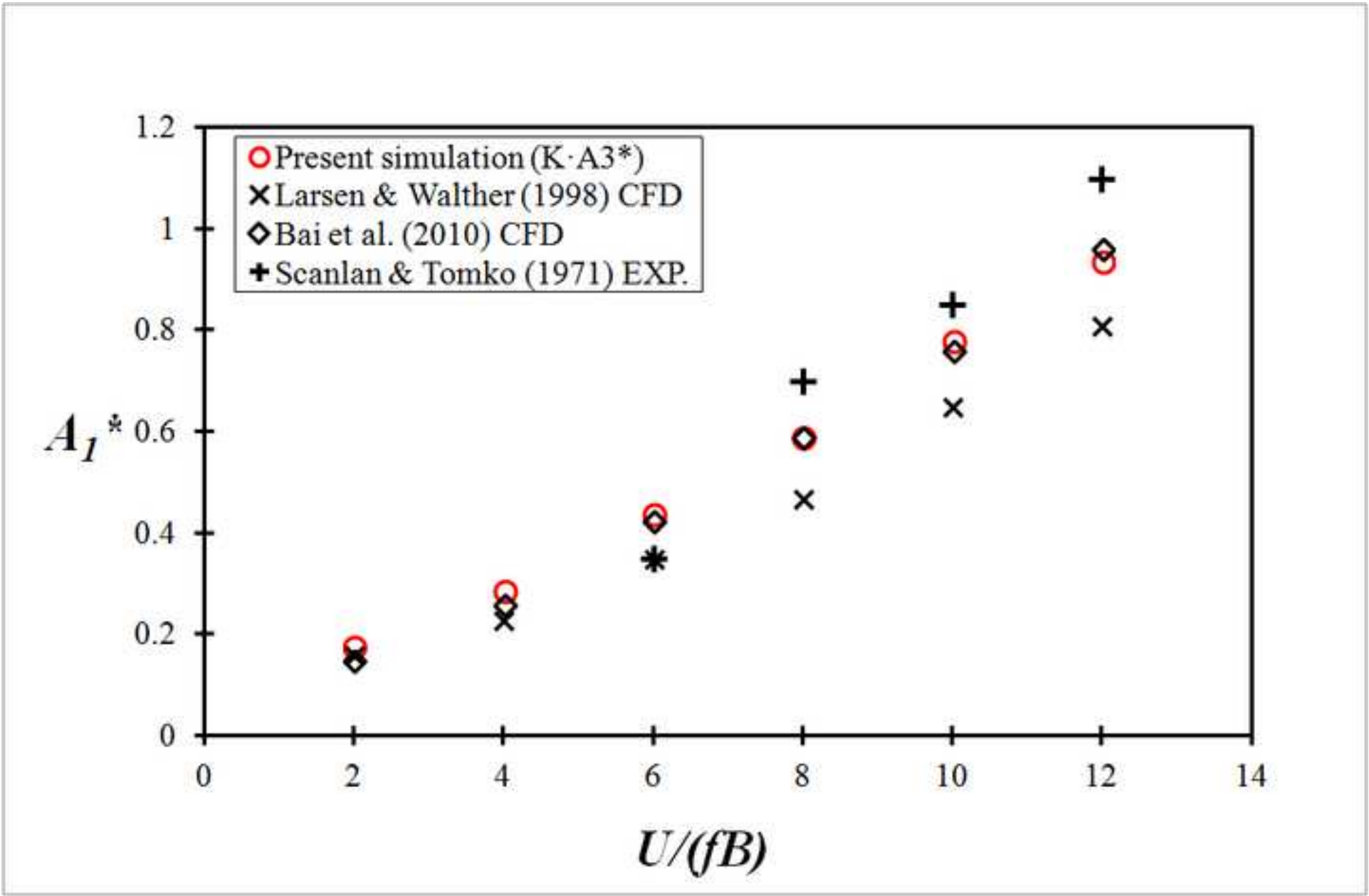


Figure 11 A2

[Click here to download high resolution image](#)

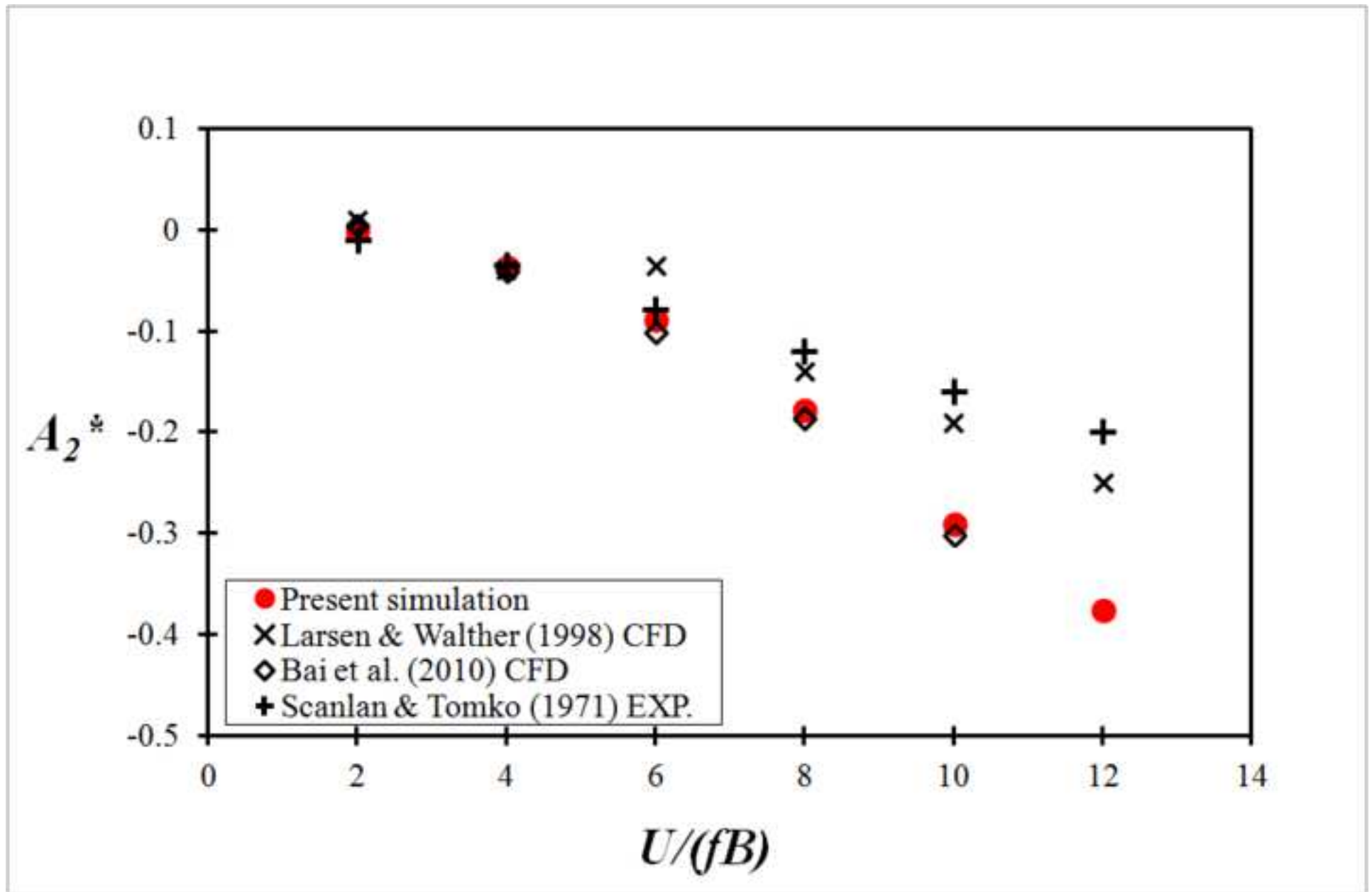


Figure 11 A3

[Click here to download high resolution image](#)

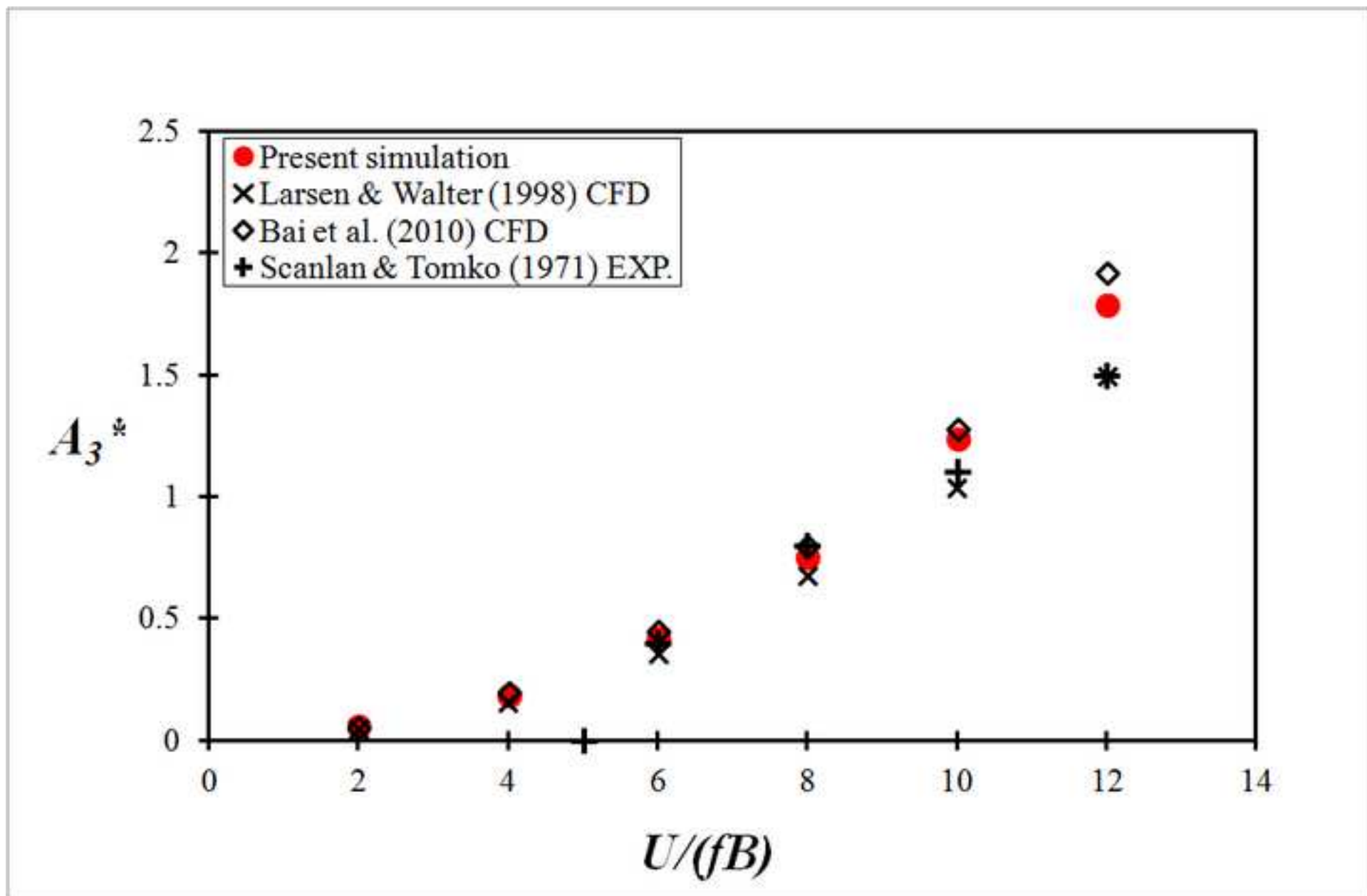


Figure 11 A4

[Click here to download high resolution image](#)

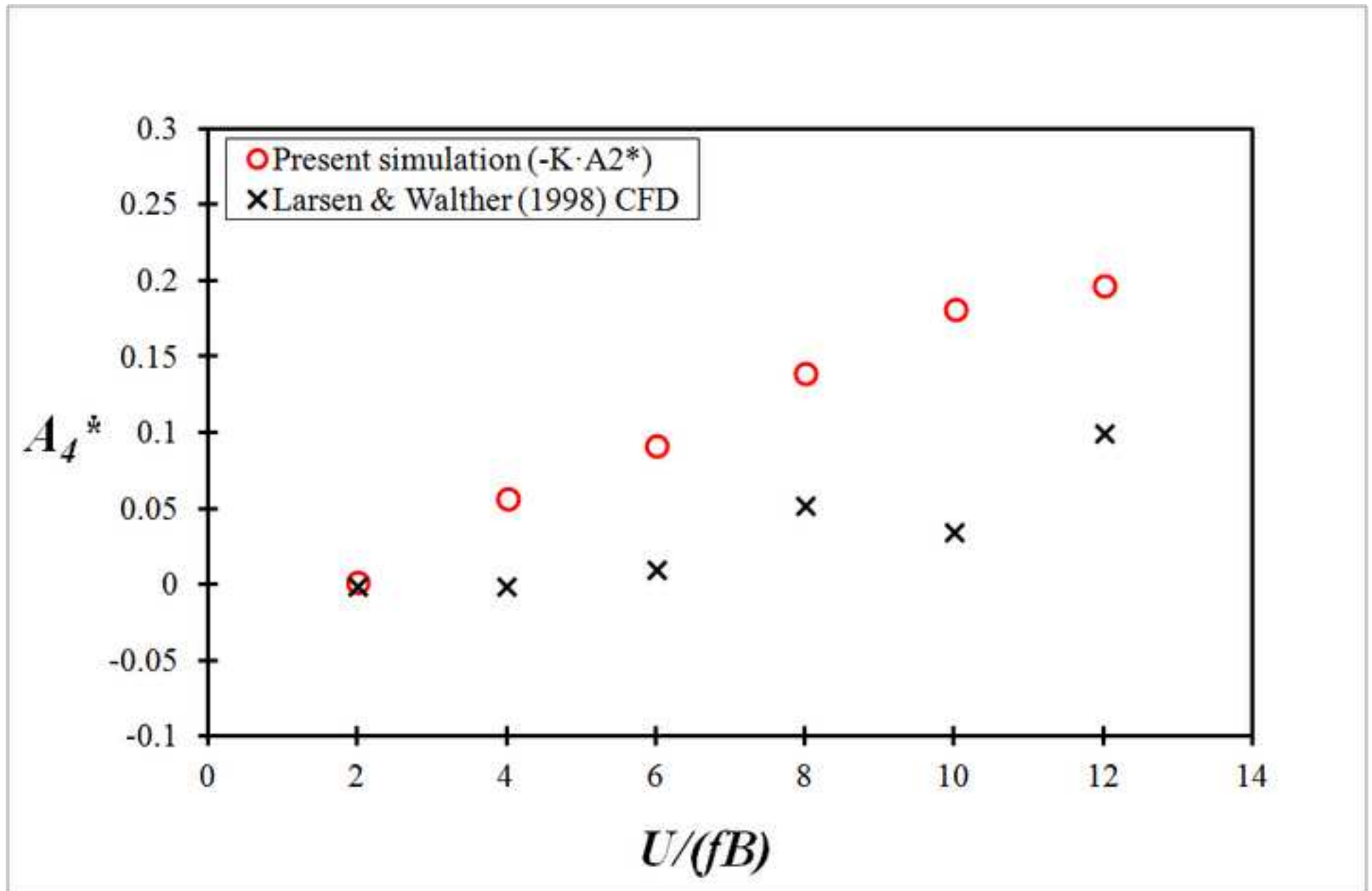


Figure 11 H1

[Click here to download high resolution image](#)

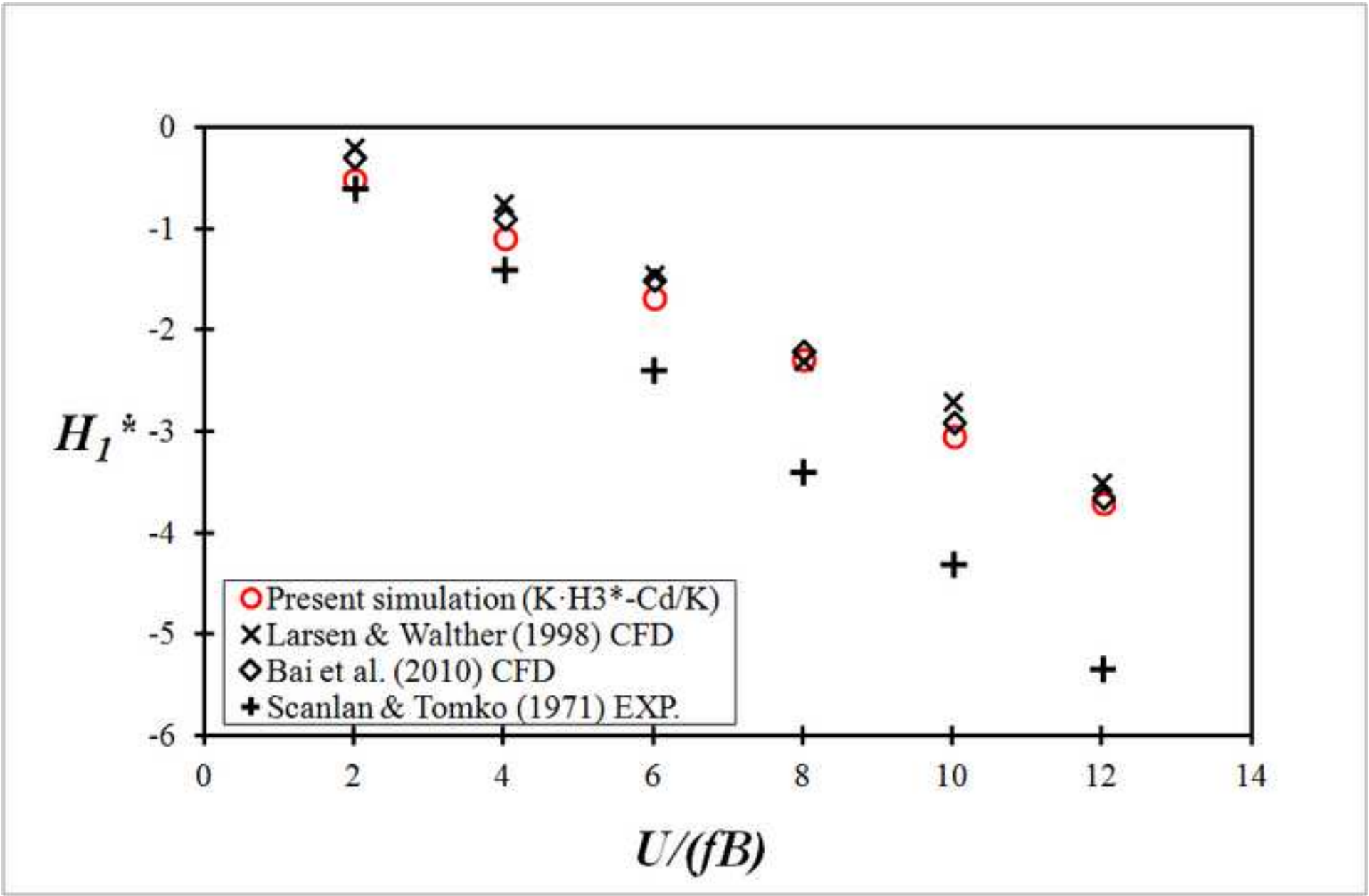


Figure 11 H2

[Click here to download high resolution image](#)

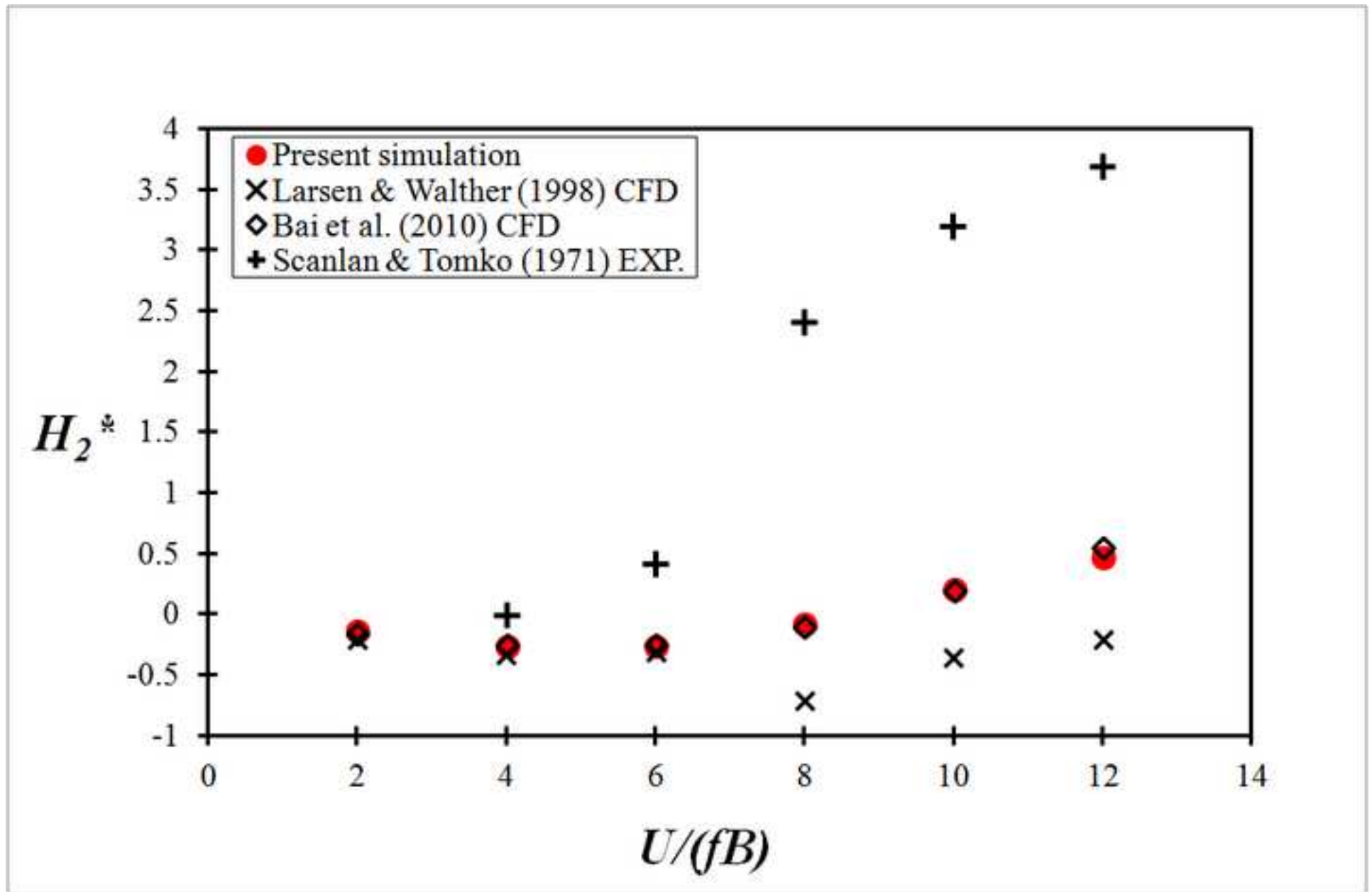


Figure 11 H3

[Click here to download high resolution image](#)

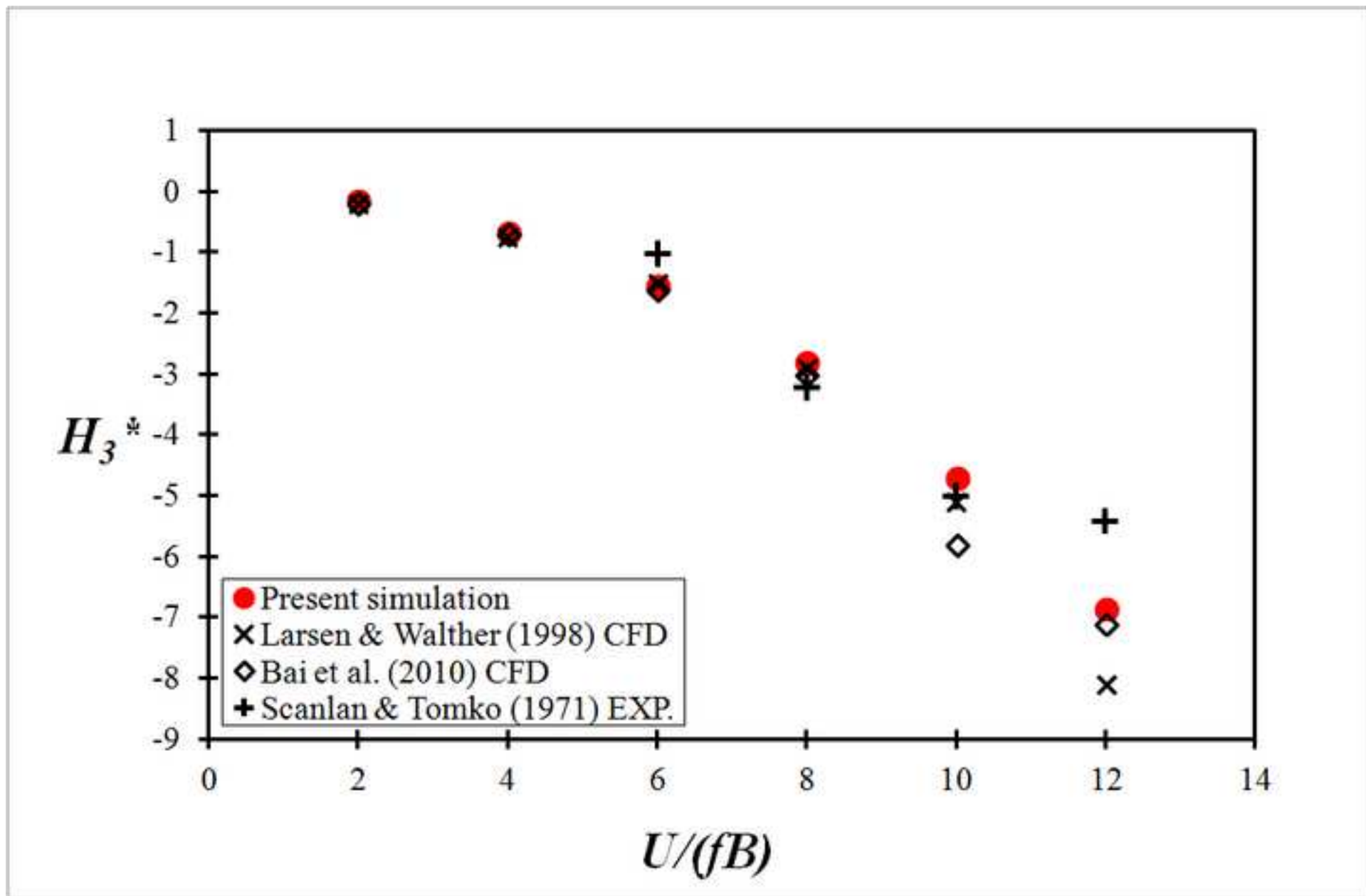


Figure 11 H4

[Click here to download high resolution image](#)

